DISSERTATION

THE DYNAMIC NATURE OF SNOW SURFACE ROUGHNESS

Submitted by

Jessica Sanow

Department of Ecosystem Science and Sustainability

In partial fulfillment of the requirements

For the Degree of Doctor of Philosophy

Colorado State University

Fort Collins, Colorado

Summer 2022

Doctoral Committee:

Advisor: Steven Fassnacht

Graham Sexstone
Dan McGrath
William L. Bauerle

Copyright by Jessica Sanow 2022

All Rights Reserved

ABSTRACT

THE DYNAMIC NATURE OF SNOW SURFACE ROUGHNESS

Throughout the winter season, the snowpack becomes the surface-atmosphere boundary for the energy balance within the hydrologic cycle and is key for understanding and modeling meltwater availability, streamflow, and groundwater recharge. The aerodynamic roughness length, z_0, is one metric to quantify the roughness characteristics of the snowpack surface. Roughness is a key component when analyzing the snowpack surface energy exchange because it exerts a strong influence on turbulent energy exchanges between the snowpack and atmosphere. Snow surface roughness fluctuates throughout the winter season due to snowpack accumulation and melt, redistribution, ecological, and meteorological influences. However, current hydrologic and energy balance models use a static z_0 value despite the snowpack surface, and resulting z_0 value, being spatially and temporally dynamic throughout the winter. Inclusion of a site specific, spatially, and temporally variable z_0 is expected to improve hydrologic and energy balance models. Therefore, the following research investigates 1) comparing the anemometric and geometric methods of measuring z_0, 2) the correlation between z_0 and snow depth, 3) spatial and temporal variability of z_0, 4) post-processing effects on z_0 measurements, and 5) application of a variable z_0 within the SNOWPACK model.

Results of this study indicate a strong correlation when comparing geometric versus anemometrical methods of calculation. 30 wind profiles were compared to 30 corresponding geometrically calculated surface measurements using a terrestrial based LiDAR. These combined profiles had a Nash-Sutcliffe Coefficient of Efficiency of 0.75, an r^2 of 0.96, a best fit slope of 0.98, and a

Root Mean Square Error of 8.9 millimeters. The correlation between snow depth and z_0 is variable depending on periods of melt, accumulation, and the initial snow-free roughness. The z_0 was shown to be spatially and temporally variable across study sites. Interpolation resolution during post processing of z_0 was found to modify z_0 by several orders of magnitude. Variable z_0 values were found to alter SNOWPACK model results within several of the output variables. The most sensitive output variables were sublimation, latent, and sensible heat due to the direct use of z_0 within the calculations. These key findings highlight the importance of a variable z_0. Inclusion of a variable z_0 parameterization within models should be site specific, spatially and temporally dynamic, with special attention to post-processing steps.

ACKNOWLEDGEMENTS

This research would not have been possible without the help and support of my advisor, Dr. Steven Fassnacht. His support and guidance throughout this entire process has changed my life in ways I can't begin to express, even during our 'roughest' moments. I would also like to thank my committee members, Dr. Graham Sexstone, Dr. Daniel McGrath, and Dr. Bill Bauerle, even though I was a 'non-traditional' student, their support was unwavering.

This research was in part made possible by the NIWR and Colorado Water Conservation Board 2018 grant. This funding helped to set up and monitor the snow sites used in the study. I would like to highlight the support from the USGS-Fort Collins, BLM – White River Field Office, and NOAA-NWS Alaska-Pacific River Forecast Center for allowing me to pursue my research while employed through their organizations. To the Trout Family of Meeker, CO, I want to thank you for allowing me to set up a primary study site in the winter of 2019-2020. To Sarah Wingard, SUPER student 2018-2019, your contributions to this research were imperative. And to Luke Smith, this research would not have been possible without your aid in fieldwork, editing, and all-around support.

DEDICATION

This dissertation is dedicated to my friends and family, who supported me throughout all these years. I could not have done any of this without your care. Especially my husband, Luke, whose constant help, patience, positivity, and love made my dreams come true.

And to my cats and dog, Mewport, Mr. Paw-Tato, and Rio Bark-o, your cuddles and positivity bring me more joy than I could ever describe, this work is to ensure I can give you the best life possible.

TABLE OF CONTENTS

ABSTRACT ii
ACKNOWLEDGEMENTS iv
DEDICATION v
1.0 INTRODUCTION 1
1.1 Background 1
1.1.1 Snow Dominated Systems 1
1.1.2 Atmospheric Interactions and Climate Driver 3
1.1.2.1 Q_E and Q_H in the Snowpack 4
1.1.2.2 Stability Terms 5
1.1.3 Aerodynamic Roughness Length Uncertainty 6
1.2 Research Motivation 7
1.2.1 Spatial and Temporal Implications of z_0 8
1.2.2 Variable versus Static z_0 9
1.2.3 Sublimation Case Study 10
1.2.4 Calculation Methods 11
1.2.5 Alternative Methods 12
1.3 Research Objectives 12
1.4 References 13
2.0 OBSERVING DIFFERENCES IN AERODYNAMIC ROUGHNESS LENGTH USING THE ANEMOMETRIC VERSUS GEOMETRIC ESTIMATION METHODS 30
2.1 Summary 30
2.2 Introduction 30
2.3 Methodology and Data 33
2.3.1 Site Descriptions 34
2.3.2 Stability Parameters 35
2.4 Results 35
2.5 Discussion 36
2.6 Conclusions 40
2.7 References 41
3.0 THE CORRELATION BETWEEN SNOW DEPTH AND A SPATIALLY AND TEMPORALLY DYNAMIC AERODYNAMIC ROUGHNESS LENGTH 51
3.1 Summary 51

3.2 Introduction 51
3.3 Methodology and Data 54
3.3.1 Field Data Collection 54
3.3.2 Site Descriptions 54
3.3.3 Data-Processing 54
3.3.4 Data Analysis 55
3.4 Results 56
3.5 Discussion 59
3.5.1 Limitations 63
3.6 Conclusions 65
3.7 References 66
4.0 RESOLUTION AND APPLICATION OF z_0 83
4.1 Summary 83
4.2 Introduction 83
4.3 Methods 85
4.3.1 Datasets 85
4.3.2 SNOWPACK Model 86
4.3.3 Meteorological Data 88
4.4 Results 88
4.5 Discussion 91
4.5.1 Limitations 94
4.6 Conclusions 96
4.7 References 97
5.0 DISCUSSION 110
5.1 Study Overview and Objectives 110
5.2 Implication of Findings 113
5.3 Limitations and Future Opportunities 116
5.4 References 119
6.0 REFLECTION 128

1.0 INTRODUCTION

The hydrological cycle dominates the Earth's climatic processes with 50% of the Northern Hemisphere being covered in shallow, seasonal snowpacks that create a natural water reservoir and creates a high albedo (Dutra *et al*., 2010; Kukko *et al*., 2013). The timing, depth, and duration of this seasonal snowpack determines the spring melt runoff which influences everything from the ecology to the economy (Lopez-Moreno *et al*., 2017; Wayand *et al*., 2018). In addition, the role of the snowpack within the hydrologic cycle impacts year-round soil moisture content, evaporation rates, precipitation (Magand *et al.*, 2014), annual recharge of groundwater and streamflow (Musselman *et al*., 2017), sediment and nutrient supply (Huss *et al*., 2017), biogeochemical fluxes, nitrate concentrations, soil respiration (Bales *et al*., 2006), freeze thaw cycles, erosion and weathering, permafrost, and ecological responses including phenology and animal mortality rates (Lopez-Moreno *et al*., 2017).

1.1 Background

1.1.1 Snow Dominated Systems

The snowpack is a key component in both global (Figure 1.1) and local (Figure 1.2) climate systems (Bales *et al*., 2006). Throughout the winter season, the snowpack becomes the primary interface for the earth-atmosphere boundary (Fassnacht *et al*., 2009a; Kukko *et al*., 2013). This interface is a key driver in atmospheric and climate processes and is affected by meteorological (Anttila *et al*., 2014; Lopez-Moreno *et al*., 2011; Magand *et al*., 2014), ecological (Magand *et al*., 2014), topographical (Lopez-Moreno *et al*., 2011), and spatial and temporal snowpack fluctuation (Magand *et al*., 2014; Raleigh *et al*., 2013).

On a global scale, the timing of snow accumulation and melt regulates the amount of shortwave radiation that the earth absorbs, therefore, snow albedo has a substantial impact on climate in the northern hemisphere (Figure 1.1; Wang *et al*., 2015). An expansive snow-covered area has a much higher reflectance capacity (0.40 - 0.95) compared to bare ground (0.05 - 0.40) or open water (0.03 - 0.10),

resulting in less absorption into the atmosphere (Oke, 1987; Sato, 2001; Raleigh *et al*., 2013). Over the past century, over half of the earth's continental surface was covered by a seasonal snow (Anttila *et al*., 2014), however due to climate change the expanse of that snowpack is diminishing, causing an overall increase in global air temperature (Langlois and Barber, 2008; Park *et al*., 2013; Wang *et al*., 2015).

Locally, snowmelt is the primary source of runoff in mountainous regions (Luce *et al*., 1999), and the influence of the timing and magnitude of the peak runoff is essential to local phenology (Harpold *et al*., 2012; Lopez-Moreno *et al*., 2017), freeze thaw cycles (Lopez-Moreno *et al*., 2017), length of the growing season (Harpold *et al*., 2012), vegetation distribution, water storage for drinking water supply, and irrigation (Bales *et al*., 2006; Barnett *et al*., 2005). Due to climate change, by the end of the 21st century it has been predicted that peak flow in the northern hemisphere will occur 30-40 days earlier than it currently does (Musselman *et al*., 2017), consequently measuring and quantifying the snowpack and snow water equivalent is vital, especially in areas with over allocated watersheds (Painter *et al.,* 2010).

Snow water equivalent (SWE), the measure of snow water volume within the snowpack, is the primary variable when considering snowpack storage for water supply (Anttila *et al*., 2014). The snowpack, and the resulting SWE, is used by over 1 billion people worldwide for drinking water (Clow, 2010; Sturm *et al*., 2017; Jennings *et al*., 2018), however, all populations benefit from the snow based on reservoir water storage which determines the water supply for crop irrigation, residential use, agriculture, industry, and even the timing of water release for salmon runs (Barnett *et al*., 2005).

Since 1915, there has been an observed 21% decrease in western US snowpack storage (Mote *et al*., 2017) with a decrease in 3-9 snow covered days per year (Harpold *et al*., 2012). Each region of the US has noticed a variation in timing and magnitude of SWE (Trujillo and Molotch, 2014). For example, maritime climates have been influenced by earlier rain on snow events due to the warming climate, which have caused earlier melt, especially at lower elevations (Trujillo and Molotch, 2014). In 2015, the maritime region saw an April 1 record low SWE resulting from high temperatures, not lack of precipitation (Mote *et al*., 2017). These climate-based changes are becoming so commonplace that terms

like ‘snow drought’ or ‘anthropogenic drought’ are being used to refer to situations where drought is occurring based on increasing demand on water resources (Harpold *et al*., 2017b).

1.1.2 Atmospheric Interactions and Climate Driver

In snow covered regions, the hydrologic cycle during the winter is driven by the energy balance of the snowpack. The energy balance equation in terms of available energy for melt (Q_M) is given as:

$$Q_M = Q_K^* + Q_L^* + Q_H + Q_E + Q_P + Q_G + Q_{CC} \quad (1.1),$$

where Q^*_K is net shortwave radiation, Q^*_L is net longwave radiation, Q_H is sensible heat flux (Equation 1.2), Q_E is latent heat (Equation 1.3), Q_P is heat associated with the precipitation flux, Q_G is the ground heat flux at the snow-soil interface, and Q_{CC} is snowpack cold content. Within the context of this study, we are focused on the spatial and temporal sensible and latent heat fluxes. Sensible heat (Q_H) is the gain or loss of energy within a system due to an increase or decrease in temperature (Oke, 1987), as follows:

$$Q_H = \rho_a c_p C_H U_z (T_0 - T_z) \quad (1.2),$$

where ρ_a is density of air, c_p is specific heat of air at a constant pressure, U_z is the wind velocity at a reference height, T_0 is surface temperature and T_z is the potential temperature at a reference height (z). C_H is bulk transfer coefficient for sensible heat at neutral stability. Sensible heat is driven by momentum due to wind and conductivity due to temperature gradients, while latent heat (Equation 1.3) is driven by momentum and diffusivity due to vapor gradients (Oke, 1987). Latent heat is the flux of energy due to a change of phase associated with no change in temperature, and is expressed by the equation:

$$Q_E = \rho L_s C_E \zeta (q_0 - q_z) \quad (1.3),$$

where L_s is latent heat of sublimation of ice, ζ is the atmospheric stability parameter, q_0 is water vapor density at the surface, q_z is water vapor density at an arbitrary reference height, and C_E is the bulk transfer coefficient for latent heat. Both the sensible and latent heat fluxes include roughness for the momentum; sensible and latent heat fluxes also include roughness for conductivity and diffusivity, respectively.

1.1.2.1 Q_E and Q_H in the Snowpack

As the climate warms, shifting patterns in precipitation type and quantity have been observed (Harpold *et al*., 2017a), influencing snow accumulation rates and timing, average height of the annual snowline (Bales *et al*., 2006; Kapnick and Hall, 2012), internal snowpack metamorphism, frequency of rain on snow events, and timing of melt rates (Anttila *et al*., 2014). Turbulence on the surface of the snowpack is a function of the size, shape, and distribution of roughness features which influence the rates of conduction, diffusion, and momentum. The latent heat flux (equation 1.3) can be re-written using the sublimation term (E):

$$Q_E = -L_S E \qquad (1.4),$$

where L_s is the latent heat of sublimation (2835 kJ/kg at 0°C). Thus, sublimation is often estimated by the latent mass flux:

$$E = \frac{0.622 * \rho_a * k^2}{Pr_a * \varphi_m * \varphi_e} * \frac{U_z}{\ln(\frac{z_a - z_d}{z_{0M}})} * \frac{q_a - q_0}{\ln(\frac{z_a - z_d}{z_{0q}})^2} \qquad (1.5),$$

where ρ_a is air density (kg/m^3), Pr_a is air pressure (mb), φ_m and φ_e are the stability terms, U_z is wind speed (m/s) at height z (m), q_a is the specific humidity at height z (mb), q_0 is the specific humidity at the snow surface (mb), z_a is the measurement height (1.72 m), z_d is the zero-plane displacement (m), and z_0 is the roughness (m).

Latent heat exchanges over the surface of the snowpack are heavily influenced by the z_0 via energy exchange in the form of sublimation (Hultstrand and Fassnacht, 2018). As the saturated vapor pressure, turbulence, and/or air temperature increases, an increase in sublimation will occur which will

decrease the amount of snow available to melt resulting in increased turbulent energy fluxes (Harpold *et al*., 2012). Harpold *et al*. (2012) found that an air temperature change of 1.3° C between two winter seasons led to an increase in sensible and latent heat flux from 25% to 54%.

1.1.2.2 Stability Terms

Oke (1987) defines atmospheric stability as the relative tendency of an air parcel to move vertically. There are three potential conditions that can occur within the atmosphere: stable, neutral, and unstable. Stable conditions indicate that the parcel is cooler than the air, and it sinks and compresses. Neutral conditions indicate the parcel and air are the same, and it remains in place. Unstable conditions indicate the parcel is warmer than the air, so it rises and expands. The latent and sensible heat fluxes at the surface will then directly affect the parcel's ability to find equilibrium after the vertical displacement (Oke, 1987). The latent and sensible heat fluxes create eddies within the wind profile that are controlled by the surface boundary layer and the frictional drag caused by the underlying roughness features on the surface (Oke, 1987). During the winter, the snowpack becomes this surface boundary interface, and the state of atmospheric stability is important for estimating latent and sensible heat fluxes from the snowpack (Fassnacht, 2010). There are several methods and variables used to determine the stability of the atmosphere within a wind profile.

The Reynolds Number is a dimensionless coefficient used to predict flow patterns; it is the ratio of inertial forces to the fluid or viscous forces (Oke, 1987; Manes *et al*., 2008). Aerodynamic roughness length and atmospheric stability is dependent on the roughness of the surface (Oke, 1987; Manes *et al.* 2008). In terms of the Reynolds Number, rougher surfaces have a higher Reynolds Number (turbulent flow) and lower values are for smoother surfaces (laminar flow) (Oke, 1987).

The Richardson Number categorizes atmospheric stability and the amount of turbulence caused by a surface; it is the ratio of the buoyancy to the flow shear stress (Oke, 1987).

$$Ri = \frac{g}{\overline{T}} * \frac{(\frac{\Delta \overline{T}}{\Delta z})^2}{(\frac{\Delta \overline{u}}{\Delta z})^2} \qquad (1.6),$$

where g is the acceleration due to gravity, $\overline{T}$ is the mean temperature in layer Δz, $\overline{u}$ is the mean wind speed in layer Δz. In stable conditions, the flow is considered laminar until it reaches a Richardson number critical value (assumed to be 0.2 to 0.25), in which case flow becomes turbulent and therefore unstable (Andreas, 2002). In this study, when determining atmospheric stability, only wind profiles with a Richardson Number between -0.01 and 0.01 were used.

The von Karman constant is used to relate the momentum profile to turbulent fluid flow using fluid density, shear stress, and friction velocity (Andreas et al., 2006). This value is height dependent. However, a value of 0.4 is typically used (Andreas et al., 2006). The von Karman constant is used in the equation 1.2, 1.3 and 1.5 (sublimation equation).

1.1.3 Aerodynamic Roughness Length Uncertainty

The term roughness is applied to many earth science topics with specific definitions and measurement techniques based on the type of study (Smith, 2014). Roughness is used to understand and quantify many natural processes, and Smith (2014) provides a comprehensive review of the different approaches and models developed to analyze the various types of surface roughness. The roughness of naturally occurring surfaces are not homogenous, creating difficulty in measuring and quantifying them (Andreas, 1987; Smith, 2014). Roughness is controlled by many meteorological, topographical, and environmental influences ranging from the macro (>1-meter) to micro (<1-meter) scales. The current research focuses on topographic surface roughness and its effect on snowpack surface roughness.

The aerodynamic roughness length, z_0, is a measure of the height above the surface at which wind velocity is equal to zero (Lettau, 1969; Manes *et al*., 2008; Smith, 2014). Aerodynamic roughness length is a key component in the estimation of the sensible and latent heat fluxes between the ground surface and the atmosphere (Fassnacht *et al*., 2009a; Hultstrand and Fassnacht, 2018), and these roughness characteristics influence the air-surface momentum transfer on the snowpack due to wind (Amory *et al*., 2016). The variation of rough and smooth surfaces directly affects the amount of turbulent exchanges of

sensible and latent heat as well as the resulting transfer rates over the surface (Andreas, 1987; Miles *et al*., 2017). The turbulent heat fluxes over the snowpack are influenced by the seasonal snow accumulation, wind and resulting snow redistribution, incoming radiation, melt patterns, internal snowpack metamorphism (Musselman *et al*., 2015), and changes in snow-covered area (SCA) throughout the season (Luce and Tarboton, 2004). To estimate these fluxes and understand the movement of air over the surface-atmosphere boundary, it is necessary to know or calculate z_0 (Fassnacht *et al*., 2009a; Manes *et al*., 2008).

1.2 Research Motivation

The seasonal, shallow snowpack are a critical factor for anthropogenic use (Barnett *et al*., 2005; Grunewald *et al*., 2010; Jacobson, 2010; Sturm et al., 2017), natural ecological processes (Barnett *et al*., 2005; Huss *et al*., 2017; Magand *et al*., 2014; Musselman *et al*., 2017), and meteorological processes (Barnett *et al*., 2005; Magand *et al*., 2014; Musselman *et al*., 2017). There is a desperate need in science to understand, quantify, and implement spatial and temporal variations in the snowpack for water quantity estimations (Sturm et al., 2017).

Surface roughness decreases during accumulation as the snow follows the underlying terrain in the initial stages of accumulation until the roughness features have been enveloped by a certain snow depth (Sanow *et al*., 2018). Vegetation height from small shrubs and grasses to dense forests create spatial heterogeneities and heavily influence the z_0 (Niu and Yang, 2007). Small grasses and shrubs will typically be covered by the seasonal snowpack, whereas large vegetation, such as sagebrush, will create larger scale roughness features and usually be visible throughout the winter season (Tedesche *et al*., 2017).

Throughout the winter season, the snowpack depth and surface roughness can change due to redistribution from wind-swept areas (Musselman et al., 2015; Fassnacht *et al*., 2009a). Snowpack surface roughness variability throughout the winter is caused by various types of elevation, aspect, canopy cover,

and ground cover within a single watershed (Jost *et al*., 2007; Watson *et al*., 2006). Jost *et al*. (2007) found that these factors contributed to 80-90% variability of snow accumulation within a watershed. Watson *et al*. (2006) found that various ground and canopy covered landscapes (i.e. burned forests, meadows, etc.) resulted in up to a 61% variation within the snowpack. Lastly, heterogeneities in snowmelt are common based on topography, slope, aspect, meteorological conditions, and land cover (Niu, 2007).

Hydrological, snowpack, and climate models have typically used snow surface roughness as a static parameter (Manes *et al*., 2008; Gromke *et al*., 2011), with z_0 only varying as a function of land cover type. For example, the Community Land Model version 4.0 (CLM4) applies a single z_0 value of 2.4 x 10^{-4} m to all snow-covered surfaces (further examples are shown in Table 1.1). However, z_0 varies both spatially (Brock *et al*., 2006) and temporally (Andreas, 2002) resulting in variable estimates of turbulent heat fluxes within models (Fassnacht, 2010). Thus, in models it is proposed that for snow, z_0 should be considered a variable and not a parameter.

1.2.1 Spatial and Temporal Implications of z_0

Spatial and temporal variability of the snowpack is a difficult measurement to capture (Deems *et al*., 2013). A single roughness element affects and is affected by the arrangement of all other roughness features around it (Fassnacht, 2010; Smith, 2014). The variability leads to a non-uniform snowpack surface from the micro to macro scale (Niu, 2007) that is also influenced by meteorological conditions, snow movement, and metamorphism (Fassnacht, 2010). The z_0 variability is especially drastic during snowmelt, which is greatly affected by incoming solar radiation, longwave radiation, snowpack metamorphism, and wind redistribution (Bales *et al*., 2006; Fassnacht, 2010; Liston, 2004; Luce, 2004). Brock *et al.,* (2006) found that the z_0 associated with spatial variability on glaciers pre and post ablation season changed considerably based on the smoother snow cover to the hummocky, ice surface.

Meteorological conditions, especially in the spring time during snowmelt, have a large effect on the spatial and temporal variability. Rain on snow events are becoming more frequent, earlier in the season (Anttila *et al*., 2014; Trujillo and Molotch, 2014), this can increase melt and refreeze on and within the snowpack which can alter the overall snowpack surface roughness (Anttila *et al*., 2014). Wind direction and speed can drastically redistribute the snowpack which regulates snowmelt timing, duration and rates (Fassnacht *et al*., 2009a; Wayand *et al*., 2018). The direction of the wind over the primary roughness features can increase the turbulence and therefore sublimation (Fassnacht *et al*., 2009a; Harpold *et al*., 2012; Hock *et* al., 2017).

1.2.2 Variable versus Static z_0

Surface roughness hardly consist of uniform, evenly distributed roughness features (Smith, 2014). The spatial and temporal variability of z_0 is often represented in hydrologic and meteorological models as a static value instead of a dynamic variable based on site specific observations (Quincey *et al*., 2017). Heights of only <10 centimeters can change the calculated z_0 value by an order of magnitude, meaning values calculated over highly heterogeneous surfaces will not be accurately represented by a static value (Quincey *et al*., 2017). Similar studies have shown a decrease in z_0 following 1-2 snowfall events, and an increase in z_0 due to melting as a function of time since last snowfall (Brock *et al*., 2006; Fassnacht *et al*., 2009a; Fassnacht, 2010; Smeets and van den Broeke, 2008). Just one snowfall event of 0.1 meters of fresh snow has the potential to alter the z_0 by a factor of 20 to 50 (Smeets and van den Broeke, 2008). An example of snowpack variability is highlighted in Figures 1.3 and 1.4, where the differences between the initial surface roughness with and without snow are shown. Vegetation causes variability (Figure 1.3a, 1.4a) which is then covered by the entirety of the snowpack (Figure 1.3b, 1.4b), depending on the height of the vegetation. As the snowpack depth increases, it is able to encapsulate larger roughness features (Figure 1.3c, 1.4c). A general, conceptual model of this concept is shown in Figure 1.5.

1.2.3 Sublimation Case Study

In order to illustrate the importance of z_0 within the energy balance, specifically focusing on sublimation, two case studies were performed. Data was download from the NRCS SNOTEL Site #457 Dry Lake, located in Dry Lake, CO for the 2017-2018 winter season (https://wcc.sc.egov.usda.gov/nwcc/site?sitenum=457). Sublimation rates were calculated as a monthly total using Equation 1.5 and a static z_0 value of 2.4 millimeters. The static z_0 value was chosen because of its use in the CLM. Sublimation was then calculated again, but instead of a static value, a dynamic value was used for z_0. These dynamic values were based on z_0 values found for fresh snow and melting snow from Brock *et al*. (2006). When snow depth was between 0-40 millimeters, the z_0 of 2.4 millimeters was used, when snow depth between 41-90 millimeters, the z_0 of 1.0 millimeters was used, etc. This entire process was repeated for the Trout Farm site, however, instead of using dynamic values from the Brock *et al*. (2006) table, terrestrial LiDAR based scans were taken throughout the season and the geometric z_0 was found (explained further in Chapter 2), and a static z_0 value of 35 millimeters was used (calculated as the initial value of the site based on terrestrial LiDAR calculations).

The results of the first case study from the Dry Lake SNOTEL Site #457 are shown in Figure 1.6a. The results show a decrease in sublimation rates with the inclusion of a dynamic z_0 value, excluding October. Snow first accumulated during October. Consequently, z_0 values changed considerably due to snow depth compared to the rest of the season. Since the majority of the snow throughout the season was greater than 100 millimeters deep, the z_0 value of 0.2 millimeters was used most often. The total sublimation for the entire winter season with a dynamic z_0 is 100 mm compared to a static z_0 total of 120 millimeters. The application of only three dynamic z_0 values changed the sublimation rates by 19.0%. If the z_0 is measured and changed throughout the season, sublimation as well as energy balance estimations can be substantially improved. The results of the second case study from the Trout Farm study site, located near Meeker, CO are shown in Figure 1.6b. The total amount of static z_0 sublimation was 140 millimeters and the dynamic z_0 sublimation was 120 millimeters. The overall sublimation values were similar throughout the winter season with the exception of January and February.

1.2.4 Calculation Methods

LiDAR scans taken throughout the study were processed using a combination of Cloud Compare, Surfer, and MATLAB in order to compute the geometric z_0. The MATLAB code written by Ron Pasquini (Colorado State University, Senior Mathematics Project, 2017). The code uses the formula for z_0 based on the geometry of the surface for irregular arrays of reasonably homogenous elements developed by Lettau (1969):

$$z_0 = z_h \lambda F \quad (1.7),$$

where z_h is the mean height of the roughness elements in meters, and λF is equal to,

$$\lambda F = Ly\, z_h \rho el \quad (1.8),$$

where Ly is the mean breadth of the roughness elements perpendicular to the wind direction, and ρel is the density or number of roughness units per unit area (Lettau, 1969; Sanow *et al.*, 2018). Typically, this equation includes the experimentally-derived average drag coefficient of 0.5, however, this has been shown to produce geometric z_0 estimates that are half of their corresponding anemometric estimates (Sanow *et al*., 2018), and therefore were disregarded in this study. An example of this formulation using synthetic roughness features is shown in Figure 1.7. First, the mean obstacle height, z_h, is calculated by finding the local maximums and minimums relative to their neighbors across the surface. The lot area, ρel, is calculated by the total area divided by the total number of maximums. Silhouette area, Ly, is similar to a cross section of each obstacle and is computed within the north-south and east-west directions. The final result is a z_0 value in N-S and E-W direction, for this study the z_0 value was chosen based on the dominate wind direction of the site. Snow depths were calculated using Cloud Compare by subtracting the initial snow-free scan from a snow-covered scan. The mean snow depth was computed across the AOI. This LiDAR based snow depth was compared to depth measurements using the t-posts and taken from each site visit.

1.2.5 Alternative Methods

Other methods include using millimeter-scale variations in snow-surface roughness features to estimate from a black plate pushed partially into the snow (Rott, 1984; Fassnacht *et al*., 2009a; Lacroix *et al*., 2008) obtained from two-dimensional photography followed by digital processing, and automated post-processing software (Fassnacht *et al*., 2009a; Fassnacht *et al*., 2009b; Fassnacht, 2010; Manninen *et al*., 2012). Three-dimensional snow surface elevation data are now available over large areas at the resolution of airborne LiDAR (< 1 meter^2 over >100 kilometer^2 horizontal resolution with <30 centimeters vertical resolution) (Deems *et al*., 2006; Harpold *et al*., 2014), terrestrial laser scanners (TLS) (resolution of +/-5 millimeters) (Hood and Hayashi, 2010; Prokop, 2008; Revuelto *et al*., 2014; Lopez-Moreno *et al*., 2016; Lopez-Moreno *et al*., 2017; Nolan *et al*., 2015; Deems *et al*., 2013), and photogrammetry (Nolan *et al*., 2015). Most LiDAR and photogrammetry efforts have only focused on snow depth (Deems *et al*., 2013), therefore very few datasets have been used to evaluate snow surface roughness at the meter-scale or sub-meter scale (Fassnacht *et al*., 2014; Fassnacht *et al*., 2015). However, even fewer of these datasets have been applied to interpolate z_0 and create a digital elevation model of the snowpack surface for evaluating surface roughness (Fassnacht *et al*., 2014).

1.3 Research Objectives

Currently, hydrologic, snowpack, and climate models have typically used z_0 as a static parameter (Manes *et al*., 2008; Gromke *et al.*, 2011). However, hydrologic processes vary spatially and temporally, and it is imperative to determine an adequate measurement method to incorporate this variable z_0. This dissertation first examines two methods of measuring z_0, anemometric and geometric to provide insight of advantages and limitations for each. Second, we observe the spatial and temporal characteristics of the snowpack and the effects on the roughness value. This was captured by using a terrestrial based LiDAR during a series of site visits to locations spread throughout Northwest Colorado. Finally, the resolution and scaling of z_0 is examined based on post-processing methodology. These resulting z_0 values are then used within the SNOWPACK model to determine the sensitivity of a variable versus static z_0.

1.4 References

Amory, C., Naaim-Bouvet, F., Gallee, H., Vignon, E., 2016. Brief communication: Two well-marked cases of aerodynamic adjustment of sastrugi. The Cryosphere, 10 [doi: 10.5194/tc-10-743-2016].

Anderson, B.T., McNamara, J.P., Marshall, H.P., Flores, A., 2014. Insights into the physical processes controlling correlations between snow distribution and terrain properties. Water Resources Research, 50(6), 4545-4563 [doi: 10.1002/2013wr013714].

Andreas, E.L., 1987. A theory for the scalar roughness and the scalar transfer coefficients over snow and sea ice. Boundary-Layer Meteorology, 38(1–2), 159–184 [doi: 10.1007/BF00121562].

Andreas, E., 2002. Parameterizing scalar transfer over snow and ice: a review. Journal of Hydrometeorology, 3(4), 417-432 [doi: 10.1175/1525-7541(2002)003<0417:pstosa>2.0.co;2].

Anttila, K., Manninen, T., Karjalainen, T., Lahtinen, P., Riihela, A., Siljamo, N., 2014. The temporal and spatial variability in sub-meter scale surface roughness of seasonal snow in Sodankyla Finnish Lapland in 2009-2010. Journal of Geophysical Research: Atmospheres, 119, 9236-9252 [doi: 10.1002/2014JD021597].

Artan, G.A., Verdin, J.P., Lietzow, R., 2013. Large scale snow water equivalent status monitoring: comparison of different snow water products in the upper Colorado Basin. Hydrology and Earth System Sciences, 17(12), 5127–5139 [doi: 10.5194/hess-17- 5127-2013].

Bales, R.C., Molotch, N.P., Painter, T.H., Dettinger, R.R., Dozier, J., 2006. Mountain hydrology of the western United States. Water Resources Research, 42(8) [doi: 10.1029/2005WR004387].

Barnett, T.P., Adam, J.C., Lettenmaier, D.P., 2005. Potential impacts of a warming climate on water availability in snow dominated regions. Nature, 438(7066), 303-309 [doi: 10.1038/nature04141].

Brock, B., Willis, I., Sharp, M., 2006. Measurement and parameterization of aerodynamic roughness length variations at Haut Glacier d'Arolla, Switzerland. Journal of Glaciology, 52(177), 281–297 [doi: 10.3189/172756506781828746].

Cho, J., Miyazaki, S., Yeh, P.J-F., Kim, W., Kanae, S., Oki, T., 2012. Testing the hypothesis on the relationship between aerodynamic roughness length and albedo using vegetation structure parameters. International Journal of Biometeorology, 56(2), 411-418 [doi: 10.1007/s00484-011-0445-2].

Clow, D.W., 2010. Changes in the timing of snowmelt and streamflow in Colorado: a response to recent warming. Journal of Climate, 23(9), 2293-2306 [doi: 10.1175/2009JCLI2951.1].

Datt, P., Srivastava, P.K., Negi, P.S., Satyawali, P.K., 2008. Surface energy balance of seasonal snow cover for snow-melt estimation in N-W Himalaya. Journal of Earth System Science, 117(5), 567–573. [doi: 10.1007/s12040-008-0053-7].

DeBeer, C. M., Pomeroy, J.W., 2017. Influence of snowpack and melt energy heterogeneity on snow cover depletion and snowmelt runoff simulation in a cold mountain environment. Journal of Hydrology, 553, 199–213 [doi: 10.1016/j.jhydrol.2017.07.051].

Dutra, E., Balsamo, G., Viterbo, P., Miranda, P. M. A., Beljaars, A., Schar, C., Elder, K., 2010. An improved snow scheme for the ECMWF land surface model: description and offline validation. Journal of Hydrometeorology, 11(4), 899–916 [doi: 10.1175/2010jhm1249.1].

Hock, R., Hutchings, J.K., Lehning, M., 2017. Grand challenges in cryospheric sciences: toward better predictability of glaciers, snow, and sea ice. Frontiers in Earth Science, 5(64), 1-14 [doi: 10.3389/feart.2017.00064].

Hultstrand, D.M., Fassnacht, S.R., 2018. The sensitivity of snowpack sublimation estimates to instrument and measurement uncertainty perturbed in a Monte Carlo framework. Frontiers of Earth Science, 12(4), 728-738 [doi: 10.1007/s11707-018-0721-0].

Huss, M., Bookhagen, B., Huggel, C., Jacobsen, D., Bradley, R.S., Clague, J.J., Vuille, M., Buytaert, W., Cayan, D.R., Greenwood, G., Mark, B.G., Milner, A.M., Weingartner, R., Winder, M., 2017. Toward mountains without permanent snow and ice. Earth's Future, 5(5), 418-435 [doi: 10.1002/2016ef000514].

Fassnacht, S.R., Williams, M.W., Corrao, M.V., 2009a. Changes in the surface roughness of snow from millimetre to metre scales. Ecological Complexity, 6(3), 221–229 [doi: 10.1016/j.ecocom.2009.05.003].

Fassnacht, S.R., Stednick, J.D., Deems, J.S., Corrao, M.V., 2009b. Metrics for assessing snow surface roughness from digital imagery. Water Resources Research, 45, W00D31 [doi: 10.1029/2008WR006986].

Fassnacht, S. R., 2010. Temporal changes in small scale snowpack surface roughness length for sublimation estimates in hydrological modelling. Cuadernos De Investigación Geográfica, 36(1), 43 [doi: 10.18172/cig.1226].

Fassnacht, S.R., 2017. A hydrological perspective on snow processes. Course Notes, Colorado State University.

Gromke, C., Manes, C., Walter, B., Lehning, M., Guala, M., 2011. Aerodynamic roughness length of fresh snow. Boundary-Layer Meteorology, 141(1), 21–34 [doi: 10.1007/s10546-011-9623-3].

Grunewald, T, Schrimer, M., Mott, R., Lehning, M., 2010. Spatial and temporal variability of snow depth and SWE in a small mountain catchment. Cryosphere Discussion, 4(1), 1-30 [doi: 10.5194/tcd-4-1-2010].

Hammond, J.C., Saavedra, F.A., Kampf, S.K., 2018. How does snow persistence relate to annual streamflow in mountain watersheds of the Western U.S. with wet maritime and dry continental climates? Water Resources Research, 2605-2623 [doi: 10.1002/2017WR021899].

Harpold, A., Brooks, P., Rajagopal, S., Heidbuchel, I., Jardine, A., Stielstra, C., 2012. Changes in snowpack accumulation and ablation in the intermountain west. Water Resources Research, 48 [doi: 10.1029/2012WR011949].

Harpold, A., Kaplanm M.L., Klos, P.Z., Link, T., McNamara, J.P., Rajagopal, S., Shumer, R., Caitriana, M.S., 2017a. Rain or snow: hydrologic processes, observations, prediction, and research needs. Hydrology and Earth Systems Science, 21, 1-22 [doi: 10.5194/hess-21-1-2017].

Harpold, A.A., Dettinger, M., Rajagopal, S., 2017b. Defining snow drought and why it matters. EOS, 98 [doi: 10.1029/2017EO068775].

Huss, M., Bookhagen, B., Huggel, C., Jacobsen, D., Bradley, R.S., Clague, J.J., Vuille, M., Buytaert, W., Cayan, D.R., Greenwood, G., Mark, B.G., Milner, A.M., Weingartner, R., Winder, M., 2017. Toward mountains without permanent snow and ice. Earth's Future, 5(5), 418-435 [doi: 10.1002/2016ef000514].

Jacobson, M.Z. Fundamentals of atmospheric modeling. 2nd Edition.; Cambridge University Press: Cambridge, Great Britain, 2005; 978-0-521-54865-6.

Jennings, K.S., Winchell, T.S., Livneh, B., Molotch, N.P., 2018. Spatial variation of the rain-snow temperature threshold across the Northern Hemisphere. Nature Communications, 9(1148), 1-9 [doi: 10.1038/s41467-018-03629-7].

Jost, G., Weiler, M., Gluns, D. R., & Alila, Y., 2007. The influence of forest and topography on snow accumulation and melt at the watershed-scale. Journal of Hydrology, 347(1–2), 101–115 [doi: 10.1016/j.jhydrol.2007.09.006].

Kapnick, S., Hall, A., 2012. Causes of recent changes in western North American snowpack. Climate Dynamics, 38(9-10), 1885-1899 [doi: 10.1007/s00382-011-1089-y].

Kukko, A., Anttila, K., Manninen, T., Kaasalainen, S., Kaartinen, H., 2013. Snow surface roughness from mobile laser scanning data. Cold Regions Science and Technology, 96, 23–35 [doi: 10.1016/j.coldregions.2013.09.001].

Lacroix, P., Legrésy, B., Langley, K., Hamran, S. E., Kohler, J., Roques, S., Dechambre, M. 2008. In situ measurements of snow surface roughness using a laser profiler. Journal of Glaciology, 54(187), 753-762 [doi: 10.3189/002214308786570863].

Langlois, A., Barber, D.G., 2008. Advances in seasonal snow water equivalent (SWE) retrieval using in situ passive microwave measurements over first-year sea ice. International Journal of Remote Sensing, 29(16), 4781–4802 [doi: 10.1080/01431160801908145].

Lettau, H., 1969. Note on aerodynamic roughness-parameter estimation on the basis of roughness-element description. Journal of Applied Meteorology, 8, 828-832 [doi: 10.1175/1520-0450(1969)008<0828:NOARPE>2.0.CO;2]

Liston, G.E., 1995. Local advection of momentum, heat, and moisture during the melt of patchy snow covers. Journal of Applied Meteorology, 34(7), 1705-1715 [doi: 10.1175/1520-0450-34.7.1705].

Liston, G.E., 2004. Representing sub-grid snow cover heterogeneities in regional and global models. Journal of Climate, 17(6), 1381–1397 [doi: 10.1175/1520-0442(2004)0172.0.co;2].

Lopez-Moreno, J.I., Fassnacht, S.R., Begueria, S., Latron, J.B.P., 2011. Variability of snow depth at the plot scale: Implications for mean depth estimation and sampling strategies. Cryosphere, 5(3), 617–629 [doi: 10.5194/tc-5-617-2011].

Lopez-Moreno, J.I., Revuelto, J., Alonso-Gonzalez, E., Sanmiguel-Vallelado, A., Fassnacht, S.R., Deems, J., Moran-Tejeda, E., 2017. Using very long range terrestrial laser scanner to analyze the temporal consistency of the snowpack distribution in a high mountain environment. Journal of Mountain Science, 14(5), 823-842 [doi: 10.1007/s11629-016-4086-0].

Luce, C.H., Tarboton, D.G., Cooley, K.R., 1999. Sub-grid parameterization of snow distribution for an energy and mass balance snow cover model. Hydrological Processes, 13(12-13), 1921–1933 [doi: 10.1002/(sici)1099-1085(199909)13:12/133.0.co;2-s].

Magand, C., Ducharne, A., Le Moine, N., 2014. Introducing hysteresis in snow depletion curves to improve the water budget of a land surface model in alpine catchment. Journal of Hydrometeorology, 15(2), 631–649 [doi: 10.1175/jhm-d-13-091.1].

Manes, C., Guala, M., Löwe, H., Bartlett, S., Egli, L., Lehning, M., 2008. Statistical properties of fresh snow roughness. Water Resources Research, 44(11), 1–9 [doi: 10.1029/2007WR006689].

Miles, E.S., Steiner, J.F., Brun, F., 2017. Highly variable aerodynamic roughness length for a hummocky debris-covered glacier. Journal of Geophysical Research: Atmospheres, 122, 8447-8466 [doi: 10.1002/2017JD026510].

Mock, C. J., Birkeland, K. W., 2000. Snow avalanche climatology of the Western United States mountain ranges. Bulletin of the American Meteorological Society, 81(10), 2367– 2392 [doi: 10.1175/1520-0477(2000)081<2367:SACOTW>2.3.CO;2].

Mote, P.W., Li, S., Lettenmaier, D.P., Xiao, M., Engel, R., 2017. Dramatic declines in snowpack in the Western US. Climate and Atmospheric Science, 1-6 [doi: 10.1038/s41612-018-0012-1].

Musselman, K.N., Pomeroy, J.W., Essery, R.L., Leroux, N., 2015. Impact of wind flow calculations on simulations of alpine snow accumulation, redistribution, and ablation. Hydrological Processes, 29, 3983-3999 [doi: 10.1002/hyp.10595].

Musselman, K.N., Clark, M.P., Liu, C., Ikeda, C., Rasmussen, R., 2017. Slower snowmelt in a warmer world. Nature Climate Change, 7, 214-220 [doi: 10.1038/NCLIMATE3225].

Nield, J. M., King, J., Wiggs, G. F. S., Leyland, J., Bryant, R. G., Chiverrell, R. C., Washington, R., 2013. Estimating aerodynamic roughness over complex surface terrain. Journal of Geophysical Research Atmospheres, 118(23), 12948–12961 [doi: 10.1002/2013JD020632].

Niu, G., Yang, Z.-L., 2007. An observation-based formulation of snow cover fraction and its evaluation over large North American river basins. Journal of Geophysical Research, 112(D21) [doi: 10.1029/2007jd008674].

Oke, T.R. Boundary layer climates. 2nd Edition, University Press, Cambridge, Great Britain, 1987; 0-415-04319-0.

Park, H., Walsh, J.E., Kim, Y., Nakai, T., Ohata, T., 2013. The role of declining Arctic sea ice in recent decreasing terrestrial Arctic snow depths. Polar Science, 7(2), 174-187 [doi: 10.1016/j.polar.2012.10.002].

Quincey, D., Smith, M., Rounce, D., Ross, A., King, O., Watson, C., 2017. Evaluating morphological estimates of the aerodynamic roughness of debris covered glacier ice. Earth Surface Processes and Landforms, 42, 2541-2553 [doi: 10.1002/esp.4198].

Raleigh, M.S., Landry, C.C., Hayashi, M., Quinton, W.L., Lundquist, J.D., 2013. Approximating snow surface temperature from standard temperature and humidity data: New possibilities for snow model

and remote sensing evaluation. Water Resources Research, 49(12), 8053–8069 [doi: 10.1002/2013wr013958].

Sato, T., 2001. Spatial and temporal variations of frozen ground and snow cover in the eastern part of the Tibetan Plateau. Journal of the Meteorological Society of Japan, 79(1B), 519-534 [doi: 10.2151/jmsj.79.519].

Smeets, C.J.P.P., van den Broeke, M.R., 2008. Temporal and spatial variations of the aerodynamic roughness length in the ablation zone of the Greenland ice sheet. Boundary Layer Meteorology, 128, 315-338 [doi: 10.1007/s10546-008-9291-0].

Smith, M.W., 2014. Roughness in the earth sciences. Earth Science Reviews, 136, 202-225 [doi: 10.1016/j.earscirev.2014.05.016].

Sturm, M., Holmgren, J., 1995. A seasonal snow cover classification system for local to global applications. American Meteorological Society, 8(5), 1261-1283 [doi: 10.1175/1520-0442(1995)008<1261:ASSCCS>2.0.CO;2].

Sturm, M., Goldstein, M.A., Parr, C., 2017. Water and life from snow: A trillion dollar science question. Water Resources Research, 53(5), 3534-3544 [doi: 10.1002/2017WR020840].

Sturm, M., and Liston, G.E., 2021. Revisting the global seasonal snow classification: an updated dataset for the Earth systems applications. Journal of Hydrometeorology, 22(11), 2917-2938 [doi: https://doi.org/10.1175/JHM-D-21-0070.1].

Tedesche, M., Fassnacht, S.R., Meiman, P.J., 2017. Scales of snow depth variability in high elevation rangeland sagebrush. Frontiers of Earth Science, 11, 469-481 [doi: 10.1007/s11707-017-0662-z].

Trujillo, E., Molotch, N.P., 2014. Snowpack regimes of the Western United States. Water Resources Research, 50, 5611-5623 [doi: 10.1002/2013WR014753].

Wang, T., Peng, S., Krinner, G., Ryder, J., Li, Y., Dantec, S., 2015. Impacts of satellite- based snow albedo assimilation on offline and coupled land surface model simulations. PloS ONE, 10(9) [doi: 10.1371/journal.pone.0137275].

Watson, F.G, Anderson, T.N., Newman, W.B., Alexander, S.E., Garrott, R.A., 2006. Optimal sampling schemes for estimating mean snow water equivalents in stratified heterogeneous landscapes. Journal of Hydrology, 328(3-4), 432-452 [doi: 10.1016/j.jhydrol.2005.12.032].

Wayand, N.E., Marsh, C.B., Shea, J.M., Pomeroy, J.W., 2018. Globally scalable alpine snow metrics. Remote Sensing of Environment, 213, 61-72 [doi: 10.1016/j.rse.2018.05.012].

Tables

Table 1.1. Aerodynamic roughness values found within the literature for several land cover and topographic areas.

z_0 (mm)	Surface Type	Citation
0.01 - 20	Fresh Snow	Brock *et al*, 2006; Poggi, 1977; Clifton *et al*, 2006 and 2008; Poggi 1976; Gromke, 2011
0.05 – 9.2	Snow	Brock *et al*, 2006; Lacroix *et al*., 2008; Price, 1977; Jackson and Carroll, 1978; Pluss and Mazzoni, 1994; Moore and Owens, 1984; Wagnon *et al*, 1999
0.1 – 13.5	Melting Snow	Brock *et al*, 2006; Plus and Mazzoni, 1994
0.65 - 0.88	Slush	Brock *et al*, 2006
0.01 - 70	Flat, Antarctic terrain	Jackson and Carroll, 1978
0.07 – 6.89	Ice sheet, bare ice	Brock *et al*, 2006
0.01 - 50	Glacier Ice	Brock *et al*, 2006; Rees and Arnold, 2006; Irvine-Fynn *et al*, 2014; Grainger and Lister, 1966; Smeets *et al*, 1998; Munro, 1989; Poggi, 1977; Denby and Snellen, 2002; Skieb, 1962; Hogg *et al*, 1982; Greuell and Smeets, 2001; Van de Wal *et al*, 1992; Denby and Smeets, 2000; Hoinkes and Untersteiner, 1952; Hoinkes, 1953; Strenten and Wendler, 1968; Untersteiner, 1957; Wendler and Weller, 1974; Ishikawa *et al*, 1992; Martin, 1975; Smeets *et al*, 1999; Obleitner, 2000
0.9 - 30	Glacier Snow	Wagnon *et al*, 1999; Munro, 1989; Wendler and Strenten, 1969; Wendler and Weller, 1974; Greuell and Smeets, 2001; Obleitner, 2000; Sverdrup, 1936; Fohn, 1973
5 - 50	Debris Covered Glacier	Miles *et al*, 2017; Takeuchi, 2000; Brock *et al*, 2010; Rounce *et al*, 2015

Table 1.2. Dynamic z_0 values used for changing snow depths.

z_0 (mm)	Snow Depth (mm)
4.4	0-40
1.0	41-90
0.2	91+

Figures

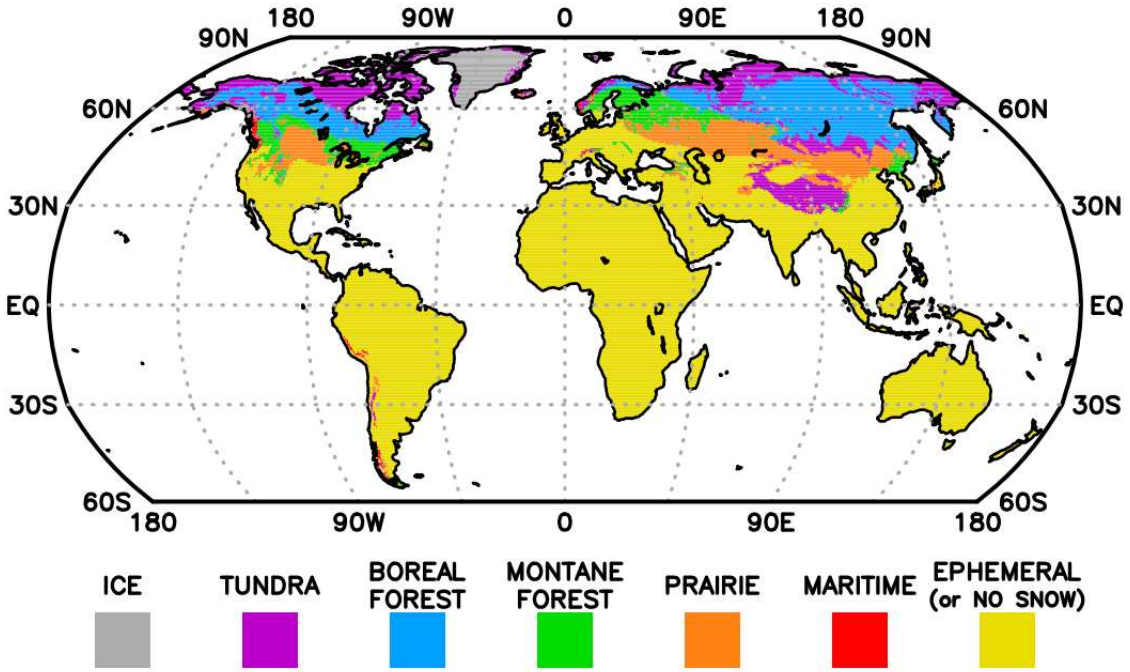

Figure 1.1. Snow regimes in the taken from Sturm and Liston, 2021.

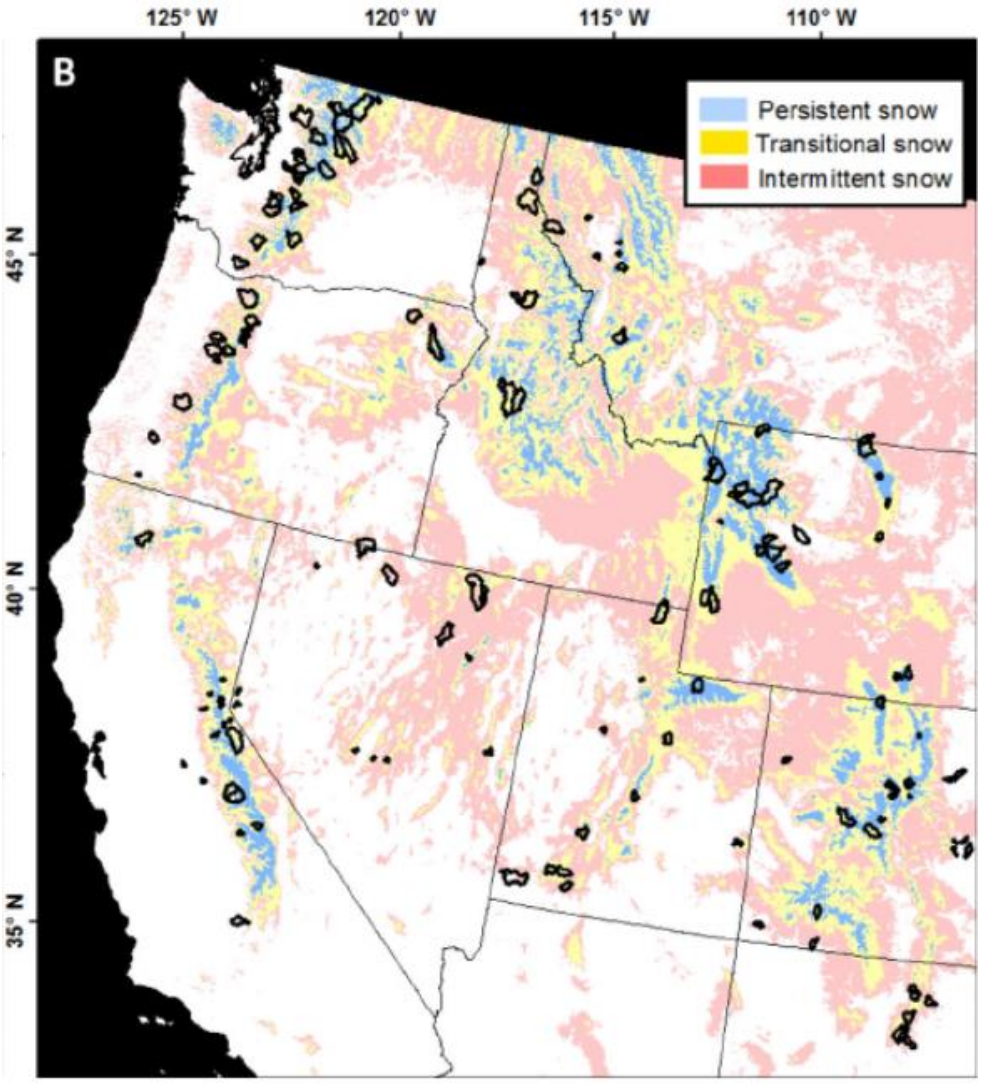

Figure 1.2. Snow regimes across the Western United States, highlighted with watersheds. Taken from Hammond *et al.,* 2018.

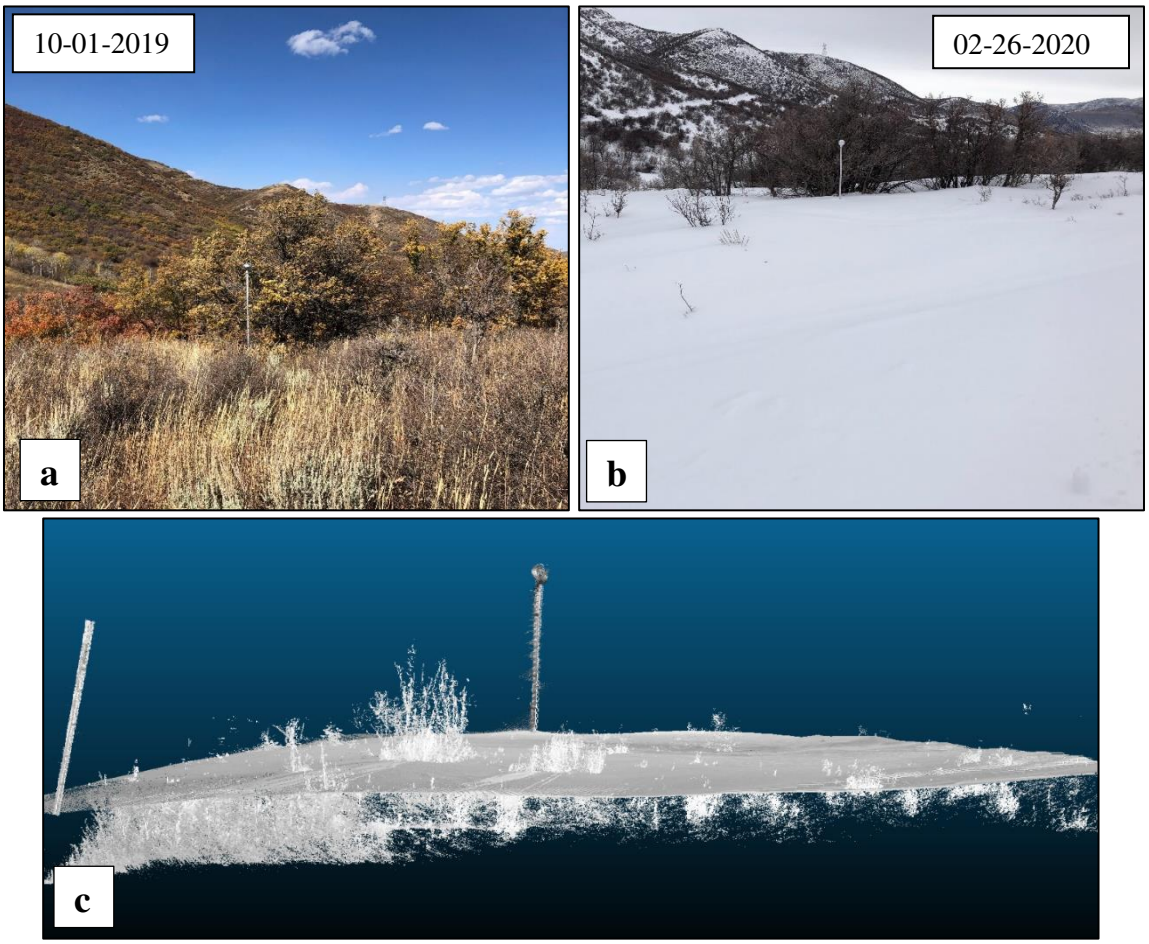

Figure 1.3. Yellow Jacket Pass site location a) photo of the initial site set up facing north, the snow stake with white sphere on top is the same throughout all photos. b) Photo of the peak snow depth (101 centimeters) on 02-26-2020, taken from a slightly different angle than A, however the snow stake with sphere can be seen against the vegetation. c) Screen shot of a Cloud Compare point cloud taken from terrestrial LiDAR scans taken at the site, the vegetation and ground cover was taken on 10-01-2019 (a) and the snow surface scan was taken on 02-26-2020 (b), these two scans were overlaid to demonstrate the difference of surface roughness with and without snow.

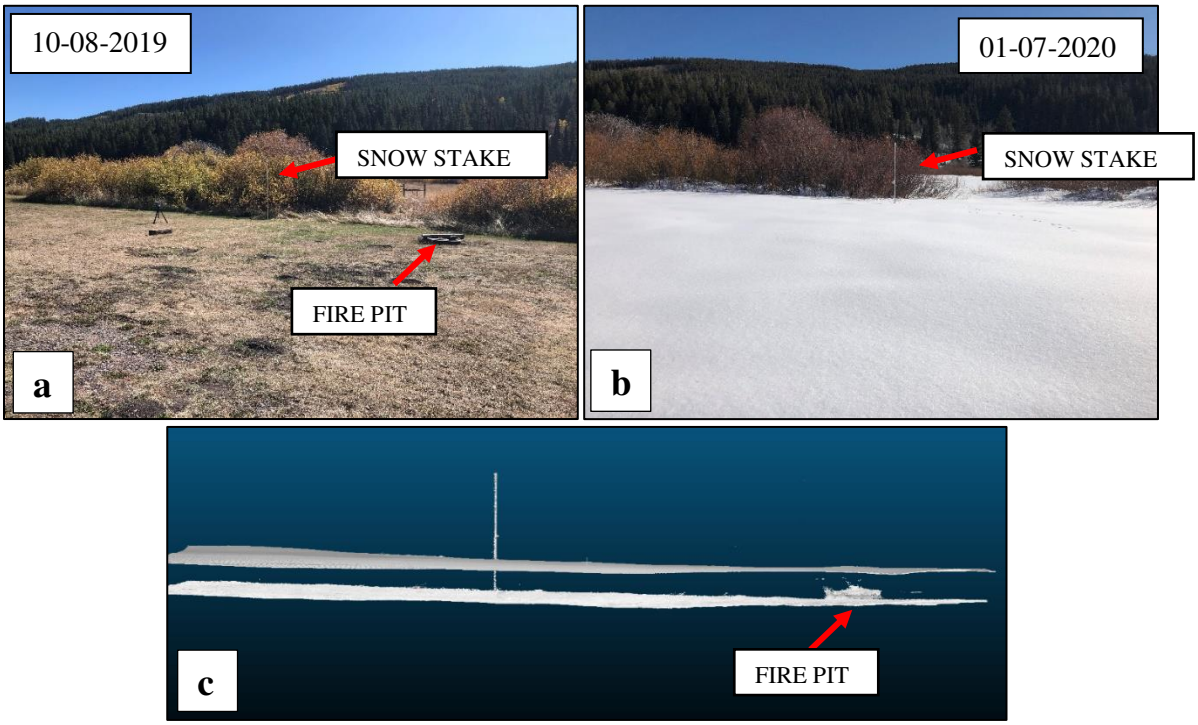

Figure 1.4. Lost Creek site, photo of the initial site set up facing south, the snow stake on top is the same throughout all photos, this is noted in the photo as well as the fire pit. b) Photo of the peak snow depth (76 centimeters) on 01-07-2020, taken from a slightly different angle than A, however the snow stake can be seen against the vegetation this is noted in the photo. c) Screen shot of a Cloud Compare point cloud taken from terrestrial LiDAR scans taken at the site, the vegetation and ground cover was taken on 10-08-2019 (a) and the snow surface scan was taken on 01-07-2020 (b), these two scans were overlaid to demonstrate the difference of surface roughness with and without snow. Note the fire pit in both A and C and how a slight variation in the snow surface is noticed above the pit in the point cloud.

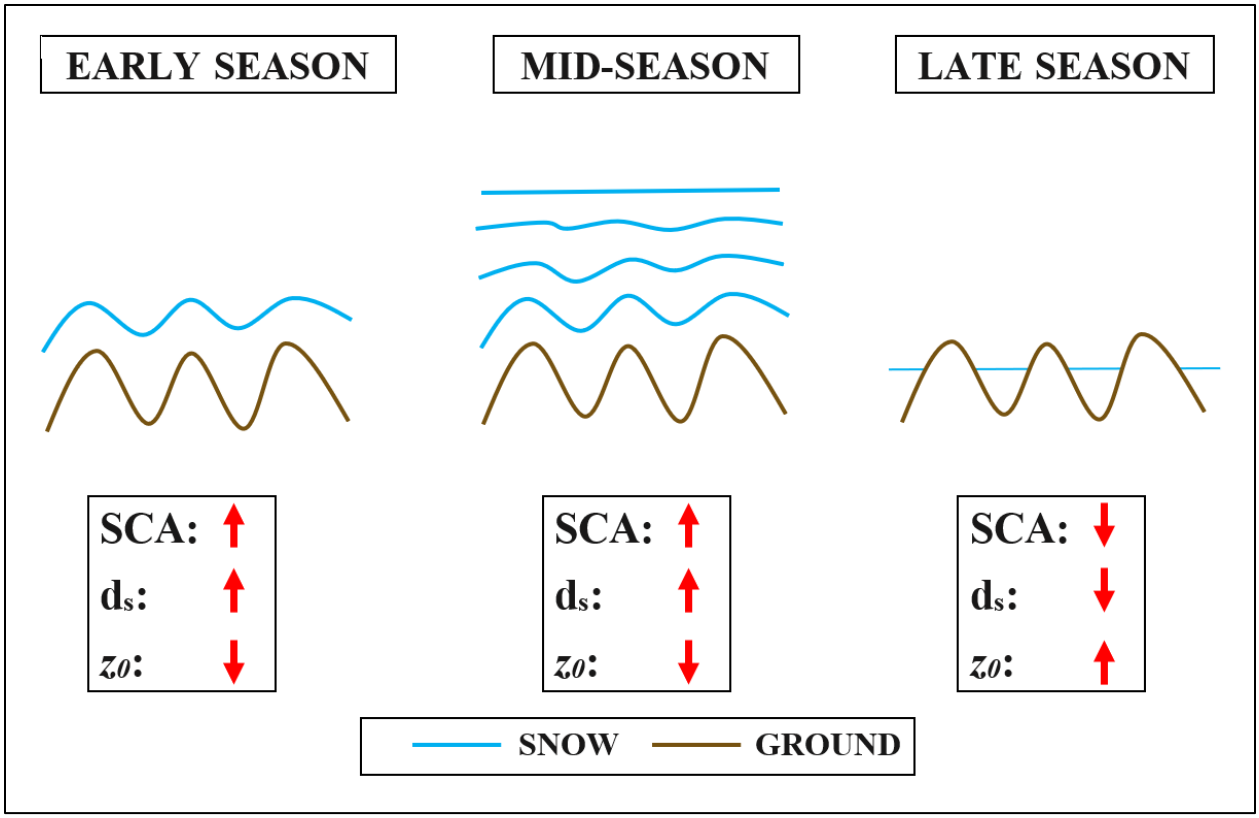

Figure 1.5. Conceptualization of the changes in snow-covered area (SCA), snow depth (d_s), and snow surface roughness (z_0) throughout the winter season and their relation with the underlying surface topography.

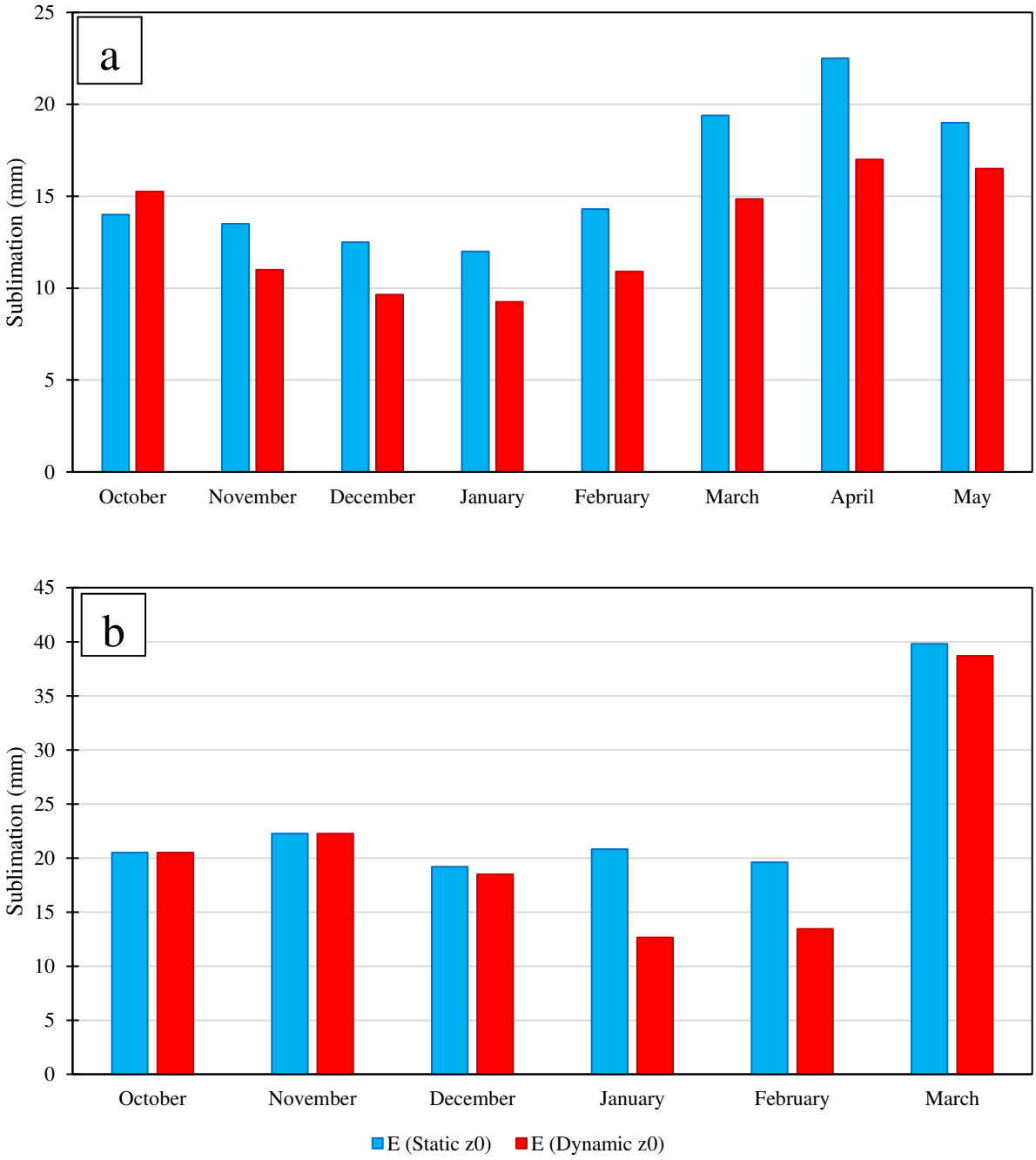

Figure 1.6. a) Monthly totals of sublimation rates over the 2017-2018 winter season at Dry Lake SNOTEL #457. The blue columns represent calculated sublimation using a static z_0 value of 2.4 millimeters. The red column uses a dynamic z_0 based on snow depths shown in Table 1.2. The total amount of sublimation for the static and dynamic z_0 values were 127 and 104 millimeters, respectively. b) Monthly totals of sublimation rates over the 2019-2020 winter season at the Trout Farm snow study site. The blue columns represent the calculated sublimation using a static z_0 value of 3.5 x 10^{-2} meters (this value was the calculated initial roughness value at the site). The red column uses a dynamic z_0 based on terrestrial LiDAR scans taken throughout the winter season at the site.

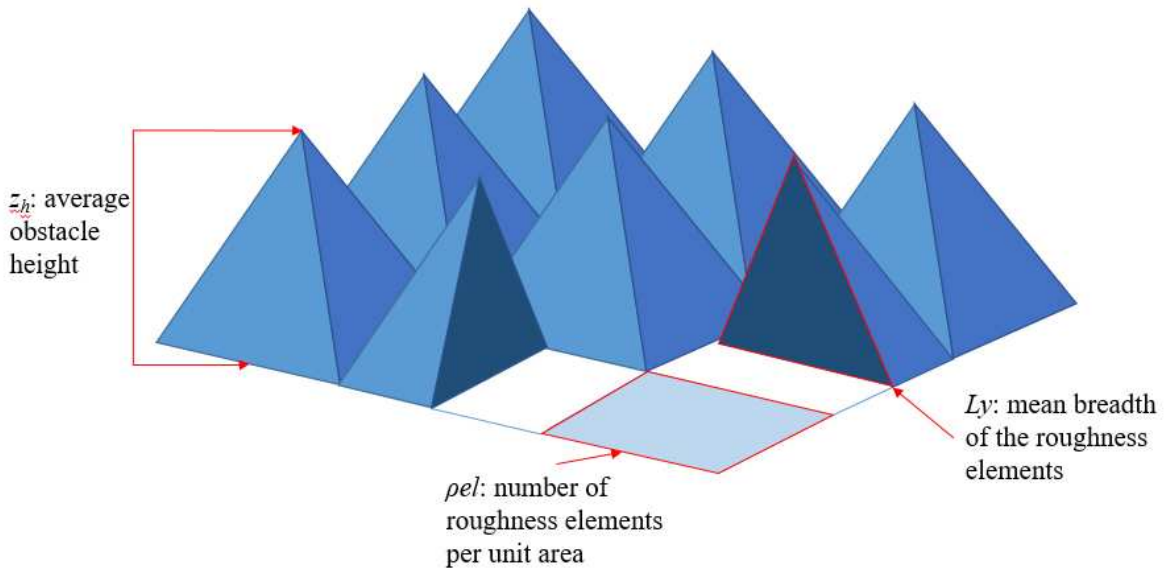

Figure 1.7. Visual representation of the MATLAB code used to calculate the geometric surface roughness.

2.0 OBSERVING DIFFERENCES IN AERODYNAMIC ROUGHNESS LENGTH USING THE ANEMOMETRIC VERSUS GEOMETRIC ESTIMATION METHODS

2.1 Summary

Aerodynamic roughness length, z_0, is a key feature in the energy balance and is an important parameter in hydrologic and atmospheric models. There are two primary methods of determining z_0 for a study site: anemometric, $z_{0\text{-}A}$, and geometric, $z_{0\text{-}G}$. Wind sensors on a meteorological tower are used to measure a wind profile which is used to compute $z_{0\text{-}A}$, and the surface topography is measured, here with a terrestrial light detection and ranging (LiDAR) system to compute for $z_{0\text{-}G}$. The $z_{0\text{-}A}$ and $z_{0\text{-}G}$ values were compared for three study areas in Colorado. There were 30 wind profiles that correlated with TLS scans. These combined profiles had a Nash-Sutcliffe Coefficient of Efficiency of 0.76, an r^2 of 0.98, a best fit slope of 0.98, and a Root Mean Square Error of 9.7 millimeters. There were four notable outliers that were attributed to low wind values during the time of the TLS scan. Overall, results indicate the anemometric, $z_{0\text{-}A}$, and geometric, $z_{0\text{-}G}$ had similar values, and the geometric calculation method proved suitable in determining z_0.

2.2 Introduction

The snowpack is the primary interface between the atmosphere and ground surface during the winter season, thus making it the control on surface energy fluxes (Bales *et* al., 2006; Fassnacht *et al.* 2009a; Gromke, 2011; Harpold *et* al., 2012; Raleigh *et al.*, 2013). The snowpack surface undergoes alterations spatially and temporally based on meteorological, ecological, and thermodynamic processes within the snowpack (Andreas, 1987; Fassnacht *et al*., 2009a; Musselman *et al*., 2015; Lopez-Moreno et al., 2017). The exchange of turbulent fluxes is dictated by the characteristics of the surface which is

represented by the aerodynamic roughness length (z_0), defined as the length scale above the ground surface when the wind velocity is equal to zero (Smith, 2014).This evolution of the snowpack surface throughout a winter season changes the value of the z_0, and thus, alters the exchange of turbulent fluxes, including latent and sensible heat exchange, and the resulting sublimation (Fassnacht *et al.*, 2009a; Raleigh *et al.*, 2013; Musselman *et al.*, 2015). However, spatial and temporal measurements of z_0 are difficult to obtain due to inaccessibility, cost, and severe weather (Deems *et al.*, 2008). Currently, the most accepted method of measuring z_0 is the anemometric method, which generates a logarithmic z_0 wind profile estimate (Jacobson, 2005). The anemometric method can be used for any surface with any arrangement of roughness elements but requires a meteorological tower with at least two vertically spaced wind, temperature, and humidity measurements that can be used to approximate the respective gradients. The measurement is integrated over a defined area rather than the single-point location of the sensors based on the distance from measurement source, elevation of sensor relative to the surface, meteorological conditions, turbulent boundary layer, and atmospheric stability (Andreas *et al.*, 2006). Each of these components can potentially create turbulent fluctuations affecting the downwind measurements of the wind profile (Schuepp *et al.*, 1990; Sexstone *et al.*, 2016). The anemometric method is also very sensitive to reported wind measurement heights. Munro (1989) found that adding 0.1 meters to any of the heights can alter z_0 by an order of magnitude. This makes determining a reference plane of zero difficult in rough terrain (Munro, 1989). Hultstrand and Fassnacht (2018) found that the greatest source of uncertainty when calculating sublimation rates, was using a static z_0 based on distance from ground as opposed to a dynamic z_0 based on distance from the snow surface. Anemometric data are used to estimate z_0 from the logarithmic wind profile through an empirical relation that describes the vertical distribution of horizontal wind speeds within the lowest portion of the planetary boundary layer (Oke, 1987). The wind speed (U_z in meters per second) at height z (meters) above a surface is given by:

$$U_z = \frac{U_*}{k}\ln[\frac{z}{z_0} + \psi\left(z, \frac{z}{L}, L\right)] \tag{2.1}$$

where U_* is the friction velocity (m/s), and ψ is a stability term, and L is the Monin-Obukhov stability parameter. Under neutral stability conditions, z/L tends towards zero, and therefore ψ is often neglected (Oke, 1987; Sanow *et al.*, 2018). Wind velocity profiles are often used to calculate z_0 estimates, but there are a limited number of sites that measure a wind profile over a snowpack surface, making the spatio-temporal representation of z_0 challenging. Anemometric towers can be expensive to set up and maintain, and they represent a limited point at the snowpack surface (Sanow *et al*., 2018). A single-point measurement does not represent the spatial and temporal characteristics of a snowpack throughout the winter season and thus limits the representation accuracy of the snowpack influence on the hydrologic cycle (Bales *et al*., 2006).

Geometric measurements to derive aerodynamic roughness length values have shown to be an effective method to account for a larger area with centimeter scale resolution throughout a winter season (Sanow *et al*. 2018). The geometric method uses the relation of z_0 to characteristics of surface roughness elements and does not require tower instrumentation, but instead measures the surface geometry (Lettau, 1969). The most common and general geometric method for estimating z_0 is simply a function of the height of the elements:

$$z_0 = f_0 z_h \tag{2.2}$$

where z_h is the mean height of roughness elements in meters, and f_0 is an empirical coefficient derived from observation. Lettau also created a reference table outlining a generalized guide to surface roughness values ranging from 3.6 x 10^{-5} m for sand flats to 2.14 m for forests (Lettau, 1969). For snow surfaces Fassnacht (2010) and Fassnacht *et al.* (1999) estimated a z_0 value (from Lettau, 1969) of 0.005 m. Various relations have been developed to relate the geometry of roughness elements with z_0 (Lettau, 1969; Munro, 1989). For example, the dependence of z_0 on the size, shape, density, and distribution of surface elements has been studied using wind tunnels, analytical investigations, numerical modeling, and field observations (Grimmond and Oke, 1999; Foken, 2008).

This study focuses on the measurement techniques of z_0 by directly comparing the anemometric and geometric methods. LiDAR and other methods (e.g., Structure from Motion) for producing high-resolution surface topographic measurements are becoming more readily available (Deems *et al.*, 2013, Harpold *et al.*, 2014) and are considered a better representation of the snowpack spatially and temporally (Bales *et al*., 2006). Therefore, it is expected that the two methods should generate comparable results. The objective of this study is to answer the question: How well geometrically calculated ($z_{0\text{-}G}$) values compare to anemometrical calculated ($z_{0\text{-}A}$) values?

2.3 Methodology and Data

The snowpack surface was scanned using a FARO Focus3D X 130 model Terrestrial LiDAR Scanner (TLS). This LiDAR tool generates a point cloud scan with an error of +/- 2 millimeters and a resolution of approximately 7.5 millimeters. For each site visit, the TLS was set up in three different locations around the site in order to account for shadows caused by scan angles. The three LiDAR scans were cropped and merged in the open source program Cloud Compare (https://www.danielgm.net/cc/) and an Area of Interest (AOI) was determined. Within the AOI the point spacing was 1.2 points/mm^2. Then, the AOI was interpolated using the 0.01-meter kriging method in the Golden Software Surfer (https://www.goldensoftware.com/products/surfer). The final, gridded AOI was calculated using the modified Lettau method implemented in MATLAB (Lettau, 1969; Sanow *et el*., 2018; shown in Equation 2.3) to calculate the final $z_{0\text{-}G}$ value. The code takes the interpolated surface and finds the mean obstacle height (h^*) by finding all local maximums and minimums relative to each other across the surface. Then, the lot area (S) is calculated as the total area divided by the total number of maxima. Next, the silhouette area (s) is found as the profile of an obstacle, this is done at a pre-defined resolution step within the code. This study used a resolution step of 0.01 meters over the 10x10 meter study site. All of these steps applied within Equation 2.3, results in the average z_0 of the surface.

$$z_0 = h^* s/S \tag{2.3}$$

Further details of the MATLAB code can be found in Chapter 1.2.4.

2.3.1 Site Descriptions

A meteorological tower was set up at Colorado State University Agriculture Research, Development and Education Center (ARDEC) (https://aes-ardec.agsci.colostate.edu/, 2021), for the 2014-2015 (data collected by Kamin, 2015), 2017-2018, and 2018-2019 winter seasons. The site was flat with plowed furrows and troughs that had an amplitude of approximately 25 centimeters deep and 50 centimeters wide, oriented East-West. This area receives an average of 119 centimeters of snow per year (https://wrcc.dri.edu). The study area was 40 meters wide with the tower placed in the middle, leaving 100 unobstructed, homogenous meters upwind. Five anemometers and five temperature/relative humidity sensors were set up on the tower at heights ranging from 137-549 centimeters from the ground surface (Figure 2.1a). The temperature and relative humidity sensors were manufactured by METER (previously Decagon) VP-3. The temperature and relative humidity were variable across a range of +/-4% and +/-0.25-0.50°C, respectively. The METER Davis Cup Anemometers had a wind direction accuracy of +/- 7° at 1° increments, and speed accuracy within +/- 5 % from 1-58 m/s. Meteorological data was recorded continuously every 15 minutes throughout the winter season using a datalogger. The Davis Cup anemometers integrates wind speed for one minute. The average of the one-minute values becomes the average speed. The depth of the snow was also accounted for in the anemometric calculations for the distance from each anemometer from the surface.

The Trout Farm site consisted of a meteorological tower set up in an open, grassy, farm field about 3 kilometers west from Meeker, Colorado. The tower included the same anemometers as the ARDEC tower and was monitored during the 2019-2020 winter season (Figure 2.1b). The site was flat with no dominate roughness features. Meeker, Colorado averages 177 centimeters of snow per year (https://www.wrcc.dri.edu). A total of 30 correlating scans and wind profiles were used for the study. The

results are plotted in Figures 2.2 with a black 1:1 line. The Nash-Sutcliffe coefficient of efficiency statistic was calculated from data fit to the 1:1 line. For both sites, wind speeds of >2.5 m/s were used for analysis. Typically, wind speeds of 4 m/s are used (Andreas *et al.,* 2006), however, due to lack of corresponding scans and high wind speeds this threshold was lowered.

2.3.2 Stability Parameters

Stability parameters are used to determine the amount of turbulence within the study area. This can be calculated using the Richardson Number, a dimensionless ratio of buoyancy and gravitational force (Oke, 1987), which is given in the following equation:

$$Ri = \frac{R}{T_S+273.15}\frac{(T_S-(T_2+\gamma R))}{U_2^2} \tag{2.4}$$

where R is the reference height of the mid-point anemometer; T_2 is the air temperature (°C) at height R, T_S is the surface temperature (°C), γ is gravity multiplied by the specific heat of air at a constant pressure, and U_2 is the wind speed (m/s) at height R. Only values with a Richardson Number between -0.01 and 0.01 were used within this study to ensure neutral stability (Oke, 1987).

2.4 Results

Lettau's general surface roughness z_0 value estimates that bare soils have a value of 0.58 x 10^{-3} meters, assuming a flat study area with no variation (Lettau, 1969). Therefore, with the addition of the furrows, vegetation, and snow in the field, the calculated $z_{0\text{-}G}$ values ranged from 0.6 x 10^{-4} meters to 0.06 meters. The differences in these calculated values reflect variations in snow depth. For example, the smallest value was from January 24, 2020 at Trout Farm when the site had 0.21 meters of snow. For the entire grouping of results, the $z_{0\text{-}G}$ values underestimated in 12 out of 30 profiles, overestimated in 14 out of the 30 profiles and were almost exact in 4 out of the 30 profiles. These profiles had combined NSCE of

0.76, r^2 of 0.98, and a RMSE of 9.7 millimeters. Statistics for all data and individual groups is in Table 2.1.

The first group of data from ARDEC during the 2017-2018 and 2018-2019 winter seasons are shown in Figure 2.2 in red, this grouping had a best fit line slope of 0.96 and a NSCE of 0.35. This dataset showed a lot of variation around the 1:1 line, with one particular outlier on December 24, 2017 with a $z_{0\text{-}G}$ value of 0.0086 meters (log value of -4.76 meters) and $z_{0\text{-}A}$ is 0.00053 meters (log value of -7.54 meters), an entire order of magnitude difference. Another outlier on January 21, 2018 yielded a $z_{0\text{-}G}$ value of 0.00201 meters (log value of -6.21 meters) and 0.0221 meters (log value of -3.81 meters) for $z_{0\text{-}A}$. The second group of data from Trout Farm during the 2019-2020 winter season in illustrated in blue (Figure 2.2). This group had a slope of 1.05, and a NSCE of 0.69 with only four data points that met criteria for use. All four points all aligned closely to the 1:1 line. The third grouping is from Sanow *et al*. (2018) at ARDEC-South during the 2014-2015 winter season and this group had a slope of 0.96 and a NSCE of 0.89 (Figure 2.2). Overall, this grouped aligned the best with the 1:1 line, thus the low NSCE value. One outlier taken on February 13, 2014 had a $z_{0\text{-}A}$ value of 0.0007 meters (log value of -7.26 meters) and $z_{0\text{-}G}$ of 0.00012 (log value of -9.03 meters). However, all data was plotted together the trendline (yellow dashes) resulted in a slope of 1.001 and NSCE of 0.70 (Figure 2.2).

2.5 Discussion

Wind parameters are very sensitive to the measurement height, which makes it very difficult when measuring over a spatially diverse area (Miles *et* al., 2017; Quincey *et al.*, 2017). This problem is also reflected in the $z_{0\text{-}A}$ data as the calculation is based off of the height of the anemometers. The height was measured from the base of the meteorological tower and then modified based on snow depth; however, in the case of the Kamin dataset (Sanow *et* al., 2018) it did not account for the potential difference in height in the trough of the furrows, which may have influenced the anemometric calculation.

Since the raw data is not available, sensitivity cannot be calculated. This error was explored using two outliers from 12/24/2017 and 01/21/2017 in Figure 2.3a,b. The blue error bars were calculated using the standard deviation of a +/- 2 centimeter error for the height measurements associated with each outlier. This error analysis indicates there is a prominent error margin associated with wind measurement height and the resulting $z_{0\text{-}A}$ value. The coefficient of variation for these values were 1% for 12/24/2017 and 4% for 01/21/2018 outliers.

Other outliers not previously discussed are likely due to several factors, including low wind speeds, lack of data points, and equipment accuracy. The most apparent error is likely from the anemometers themselves. Davis Cup anemometers have an assumed error of +/- 5%, which is common, however, the generally lower wind speeds that were common throughout the study coupled with the older age of the equipment led to greater inaccuracies. Andreas *et al*. (2006) did similar work, however much higher wind speeds were present due to the location of the study and therefore Andreas *et al.* (2006) wind profiles of U(z) and ln(z) resulted in a correlation constant of r>0.99, whereas in this study a correlation of r>0.70 was deemed adequate due to the quality of Davis cup anemometer and the generally low winds speeds at the site. Ideally, the study could be repeated with sonic anemometers and over more terrain variation as well as deeper, longer lasting snow pack coverage. This error was explored using two outliers from 12/24/2017 and 01/21/2017 in Figure 2.3a,b. The red error bars were calculated using the standard deviation of the +/-5% error for the wind speeds associated with each outlier. This error analysis indicates there is a notable error margin associated with wind speeds and the resulting $z_{0\text{-}A}$ value. The coefficient of variation for these values were 6% for 12/24/2017 and 55% for 01/21/2018 outliers. This associated error was found to be the most sensitive error compared to the height measurement.

Because of the lack of higher wind speed data, all profiles had to be considered for the analysis. However, previous studies such as Andreas *et al.* (2006) typically only use speeds greater than 4 m/s. This study used wind speeds greater than 2.5 m/s due to the lack of correlating scan and high wind data. However, the low wind speeds do have the potential to create instability in the aerodynamics and

therefore may have led to inaccuracies in the calculations (Fassnacht, 2010; Oke, 1987). This situation occurred at the ARDEC site on December 24, 2017 where lower wind values were likely the cause of the large differences. The $z_{0\text{-}A}$ wind values were low during the time of the scan (0.1-0.9 m/s); so, the next closest time was used which was six hour later.

Observations throughout the study indicate a decrease in z_0 as the snow depth increased, this relation is further explored in Chapter 3 (Luce and Tarboton, 2004; Magand *et al.*, 2014; Sanow *et al.*, 2018). This relation is why both $z_{0\text{-}A}$ and $z_{0\text{-}G}$ values changed throughout the winter season based on the varying snow depths. As the snow depth increased, the ground surface was covered, thus encapsulating the small scale variability of the topography and/or vegetation leading to a smoother surface (Swenson and Lawrence, 2012; Magand *et al*., 2014; Sanow *et al.,* 2018). These less variable, smoother surfaces decrease the extremities of the maxima and minima. Since calculations of $z_{0\text{-}G}$ require averaging over several local maxima and minima (Chapter 1), this relation has an effect on the calculations which can lead to large distributions of values. For instance, Figure 2.4a and Figure 2.4b show the frequency density distribution histogram. The distribution of values is erratic with frequent maxima and minima. These values end up being averaged together in order to calculate the $z_{0\text{-}G}$ value. Conversely, Figure 2.4c and Figure 2.4d show a point that falls directly on the 1:1 line from Trout Farm taken on 2/10/2020. Typically, the other points have a distribution of values that create a general bell curve shape with dominate values clustered around the mean.

The current study followed the methodology outlined in Section 2.3, however since the Kamin dataset (Sanow *et al*., 2018) was supplementary data, the exact methodology of post-processing is unknown. There is also uncertainty in the snow depth measurements being applied to the measurement height for $z_{0\text{-}A}$, and the size and consistency of the AOI. Kamin only used two LiDAR scans per site visit and the current study used three to ensure no shadow was interfering with the scan integrity. This study cropped the AOI to the exact area for every scan. The AOI was chosen based on the distance from the tower (approximately 2 meters). The LiDAR was set up around the AOI (approximately 1.5 meters from

the edges of AOI) to ensure minor ellipsoids did not occur when scanning. Ellipsoids can occur due to the increased resolution (more points per square centimeter) closer to the scanner. Kamin stated at times there were notable shadows in the scans from the furrows and vegetation, as well as more 'point clusters' around the scanner location, which could lead to possible interpolation problems (Kamin, 2015). The use of Kamin's data also led to the inability to explore all outliers and meteorological information, snow depths, site photos, etc. to help explain any discrepancies that are noticed in the data, as we do not have access to the original data.

Errors within the $z_{0\text{-}G}$ calculation were also examined in Figure 2.3a,b. The final surface that was run within the MATLAB code was multiplied by a value of 2, this enhances the local maxima and minima in which the MATLAB code calculates $z_{0\text{-}G}$. This process was repeated using a multiplier of 0.5 as well. The mean, standard deviation, and coefficient of variance of the resulting $z_{0\text{-}G}$ values for all three runs were found. The standard deviation is plotted in Figure 2.3a,b by the purple, vertical error bar. The COV was 163% for the outlier on 12/24/2017 and 113% for the outlier on 01/21/2018. The 12/24/2017 outlier was affected more than the other outlier. This had to do with the initial surface being slightly rougher which was further enhanced by the multipliers.

Future studies exploring $z_{0\text{-}A}$ and $z_{0\text{-}G}$ data could investigate larger geometric areas measured by LiDAR, including the utility of airborne LiDAR, or other spatially derived surface measurements such as photogrammetry. Further, additional anemometric data with concurrent geometric measurements could be explored. Here, Ameriflux towers (https://ameriflux.lbl.gov/) were examined to find overlapping LiDAR scans available on (https://opentopography.com), but no overlap between the two datasets could be found. The rapid increase in availability of snow surface geometric data (Deems et al., 2013; Harpold et al., 2014; Nolan et al., 2015; Shaw et al., 2020) is another reason to favor the $z_{0\text{-}G}$ approach when calculating z_0. Another factor to be considered in future studies is the resolution of the geometric data. Airborne LiDAR may be too coarse to represent the small-scale surface features occurring on the snowpack throughout the winter (Fassnacht *et al.*, 2009).

2.6 Conclusions

In conclusion, the geometrically calculated z_0 values using the Lettau equation showed much more spatially and temporally dynamic estimations of the snowpack surface throughout the study period, while producing similar values when compared to $z_{0\text{-}A}$. Results show the $z_{0\text{-}G}$ values underestimated in 12 out of 30 profiles, overestimated in 14 out of the 30 profiles and were almost exact in 4 out of the 30 profiles. These profiles had combined NSCE of 0.76, r^2 of 0.98, and a RMSE of 9.7 millimeters. Although $z_{0\text{-}A}$ has been the traditional method of measuring z_0, LiDAR and other methods of spatial data are becoming more available. These other methods have the potential to capture the spatial and temporal roughness changes over a snowpack surface, whereas the anemometric tower is limited to smaller area of integration. The geometric method was able to capture these small-scale variations of the snowpack and was only limited by the TLS site measurement area. The variability captured throughout the study indicates that a site specific, variable $z_{0\text{-}G}$ is necessary to consider. Whereas, using a static value for z_0 within hydrologic and meteorological models will lead to inaccuracies resulting in either over or underestimating the snowpack.

2.7 References

Andreas, E. L., 1987. A theory for the scalar roughness and the scalar transfer coefficients over snow and sea ice. Boundary-Layer Meteorology, 38(1–2), 159–184 [doi: 10.1007/BF00121562].

Andreas, E.L., Claffey, K.J., Jordan, R.E., Fairall, C.W., Guest, P.S., Persson, P.O.G., Grachev, A.A., 2006. Evaluations of the von-Karman constant in the atmospheric surface layer. Journal of Fluid Mechanics, 559, 117-149 [doi: 10.1017/S0022112006000164].

Bales, R.C., Molotch, N.P., Painter, T.H., Dettinger, R.R., Dozier, J., 2006. Mountain hydrology of the western United States. Water Resources Research, 42(8) [doi: 10.1029/2005WR004387].

Bloschl, G., 1999. Scaling issues in snow hydrology. Hydrologic Process, 13, 2149-2175 [doi: 10.1.1.709.499].

Deems, J.S., Fassnacht, S.R., Elder, K.J., 2008. Inter-annual consistency in fractal snow depth patterns at two Colorado mountain sites. Journal of Hydrometeorology, 9(5), 977-988 [doi: 10.1175/2008jhm901.1].

Deems, J.S., Painter, T., Finnegan, D., 2013. LIDAR measurement of snow depth: a review. Journal of Glaciology, 59(215), 467–479 [doi: 10.3189/2013jog12j154].

Fassnacht, S.R., Soulis, E.D., Kouwen, N. Shape characteristics of freshly fallen snowflakes and their short-term changes. Interactions between the Cryosphere, Climate and Greenhouse Gases (Proceedings IUGG 99 Symposium HS2, Birmingham, July 1999), IAHS, 256, 111-122.

Fassnacht, S. R., Williams, M. W., Corrao, M. V., 2009. Changes in the surface roughness of snow from millimetre to metre scales. Ecological Complexity, 6(3), 221–229 [doi: 10.1016/j.ecocom.2009.05.003].

Fassnacht, S. R., 2010. Temporal changes in small scale snowpack surface roughness length for sublimation estimates in hydrological modelling. Cuadernos De Investigación Geográfica, 36(1), 43 [doi: 10.18172/cig.1226].

Fassnacht, S.R., Velasco, M.T., Meiman, P.J., Whitt, Z.C. The effect of aeolian deposition on the surface roughness of melting snow, Byers Peninsula, Antarctica. Hydrological Processes, 24(14). 2007-2013 [doi: https://doi.org/10.1002/hyp.7661].

Foken, T. Micrometeorology. Springer-Verlag: Berlin, Heidelberg, New York, USA. 2008; 978-3-540-74666-9.

Grimmond, C.S.B., Oke, T.R., 1999. Aerodynamic properties of urban areas derived from analysis of surface form. Journal of Applied Meteorology, 38, 1262-1292 [doi: 10.1175/1520-0450(1991)038<1262:APOUAD>2.0.CO;2].

Harpold, A., Brooks, P., Rajagopal, S., Heidbuchel, I., Jardine, A., Stielstra, C., 2012. Changes in snowpack accumulation and ablation in the intermountain west. Water Resources Research, 48 [doi: 10.1029/2012WR011949].

Harpold, A.A., Guo, Q., Molotch, N., Brooks, P.D., Bales, R., Fernandez-Diaz, J.C., Musselman, K.N., Swetnam, T.L., Kirchner, P., Meadows, M.W., Flanagan, J., Lucas, R., 2014. LIDAR-derived snowpack data sets from mixed conifer forests across the Western United States. Water Resources Research, 50, 2749-2755 [doi: 10.1002/2013WR013935].

Hultstrand, D.M., Fassnacht, S.R., 2018. The sensitivity of snowpack sublimation estimates to instrument and measurement uncertainty perturbed in a Monte Carlo framework. Frontiers of Earth Sciences, 12(4), 728-738 [doi: 10.1007/s11707-018-0721-0].

Jacobson, M.Z., 2005. Fundamentals of atmospheric modeling. 2nd ed.; Cambridge University Press: Cambridge, Great Britain, 2005; 978-0-521-54865-6.

Kamin, D.J., 2015. Exploration of a geometric approach for estimating snow surface roughness (Master's Thesis). Colorado State University, Fort Collins, Colorado. Unpublished [http://hdl.handle.net/10217/170391].

Lettau, H., 1969. Note on aerodynamic roughness-parameter estimation on the basis of roughness-element description. Journal of Applied Meteorology, 8, 828-832 [doi:10.1175/1520-0450(1969)008<0828:NOARPE>2.0.CO;2].

Lopez-Moreno, J.I., Revuelto, J., Alonso-Gonzalez, E., Sanmiguel-Vallelado, A., Fassnacht, S.R., Deems, J., Moran-Tejeda, E., 2017. Using very long range terrestrial laser scanner to analyze the temporal consistency of the snowpack distribution in a high mountain environment. Journal of Mountain Science, 14(5), 823-842 [doi: 10.1007/s11629-016-4086-0].

Luce, C. H., Tarboton, D.G., 2004. The application of depletion curves for parameterization of subgrid variability of snow. Hydrological Processes, 18(8), 1409–1422 [doi: 10.1002/hyp.1420].

Magand, C., Ducharne, A., Le Moine, N., 2014. Introducing hysteresis in snow depletion curves to improve the water budget of a land surface model in alpine catchment. Journal of Hydrometeorology, 15(2), 631–649 [doi: 10.1175/jhm-d-13-091.1].

Manes, C., Guala, M., Löwe, H., Bartlett, S., Egli, L., Lehning, M., 2008. Statistical properties of fresh snow roughness. Water Resources Research, 44(11), 1–9 [doi: 10.1029/2007WR006689].

Munro, D. S., 1989. Surface roughness and bulk heat transfer on a glacier: comparison with eddy correlation. Journal of Glaciology, 35(121), 343–348 [doi: 10.3189/s0022143000009266].

Musselman, K.N., Clark, M.P., Liu, C., Ikeda, C., Rasmussen, R., 2017. Slower snowmelt in a warmer world. Nature Climate Change, 7, 214-220 [doi: 10.1038/NCLIMATE3225].

Musselman, K.N., Pomeroy, J.W., Essery, R.L., Leroux, N., 2015. Impact of windflow calculations on simulations of alpine snow accumulation, redistribution, and ablation. Hydrological Processes, 29, 3983-3999 [doi: 10.1002/hyp.10595].

Nolan, M., Larsen, C., Sturm., M., 2015. Mapping snow depth from manned aircraft on landscape scales at centimeter resolution using structure-from-motion photogrammetry. The Cryosphere, 9, 1445-1463 [doi: 10.5194/tc-9-1445-2015].

Oke, T.R. Boundary layer climates. 2nd Edition, University Press, Cambridge, Great Britain, 1987; 0-415-04319-0.

Quincey, D., Smith, M., Rounce, D., Ross, A., King, O., Watson, C., 2017. Evaluating morphological estimates of the aerodynamic roughness of debris covered glacier ice. Earth Surface Processes and Landforms, 42, 2541-2553 [doi: 10.1002/esp.4198].

Raleigh, M.S., Landry, C.C., Hayashi, M., Quinton, W.L., Lundquist, J.D., 2013. Approximating snow surface temperature from standard temperature and humidity data: new possibilities for snow model and remote sensing evaluation. Water Resources Research, 49(12), 8053–8069 [doi: 10.1002/2013wr013958].

Raupach, M.R., 1992. Drag and drag partition on rough surfaces. Boundary-Layer Meteorology, 60(4), 375-395 [doi: 10.1007/BF00155203].

Sanow, J.E., Fassnacht, S.R., Kamin, D.J., Sexstone, G.A., Bauerle, W.L., Oprea, I., 2018. Geometric versus anemometric surface roughness for a shallow accumulating snowpack. Geosciences, 8(12), 463 [doi: 10.3390/geosciences8120463].

Schuepp, P.H., Leclerc, M.Y., Macpherson, J.I., Desjardins, R.L., 1990. Footprint prediction of scalar fluxes from analytical solutions of the diffusion equation. Applied Mechanics Review, 50(1-4), 355-373 [doi: 10.1007/bf00120530].

Sexstone, G.A., Clow, D.W., Stannard, D.I., Fassnacht, S.R., 2016. Comparison of methods for quantifying surface sublimation over seasonally snow-covered terrain. Hydrologic Processes, 30, 3373-3389 [doi: 10.1002/hyp.10864].

Shaw, T.E., Gascoin, S., Mendoza, P.A., Pellicciotti, F., McPhee, J., 2019. Snow depth patterns in a high mountain Andean catchment from satellite optical tristereoscopic remote sensing. Water Resources Research, 56(2) [doi: 10.1029/2019WR024880].

Swenson, S.C., Lawrence, D.M., 2012. A new fractional snow-covered area parameterization for the Community Land Model and its effect on the surface energy balance. Journal of Geophysical Research, 117(D21) [doi: 10.1029/2012JD018178].

Tables

Table 2.1. Table of all statistical parameters of the datasets.

Dataset	r^2	Slope of best fit line	RMSE (mm)	NSCE	Mean		σ	
					LN($z_{0\text{-}A}$)	LN($z_{0\text{-}G}$)	LN($z_{0\text{-}A}$)	LN($z_{0\text{-}G}$)
All	0.98	0.98	9.7	0.76	-	-	-	-
Kamin	0.89	1.05	7.7	0.89	-4.90	-5.16	1.65	1.68
ARDEC	0.96	0.92	8.1	0.35	-5.48	-5.20	1.36	1.20
Trout Farm	0.77	0.98	2.0	0.69	-8.40	-7.07	1.36	0.93

Figures

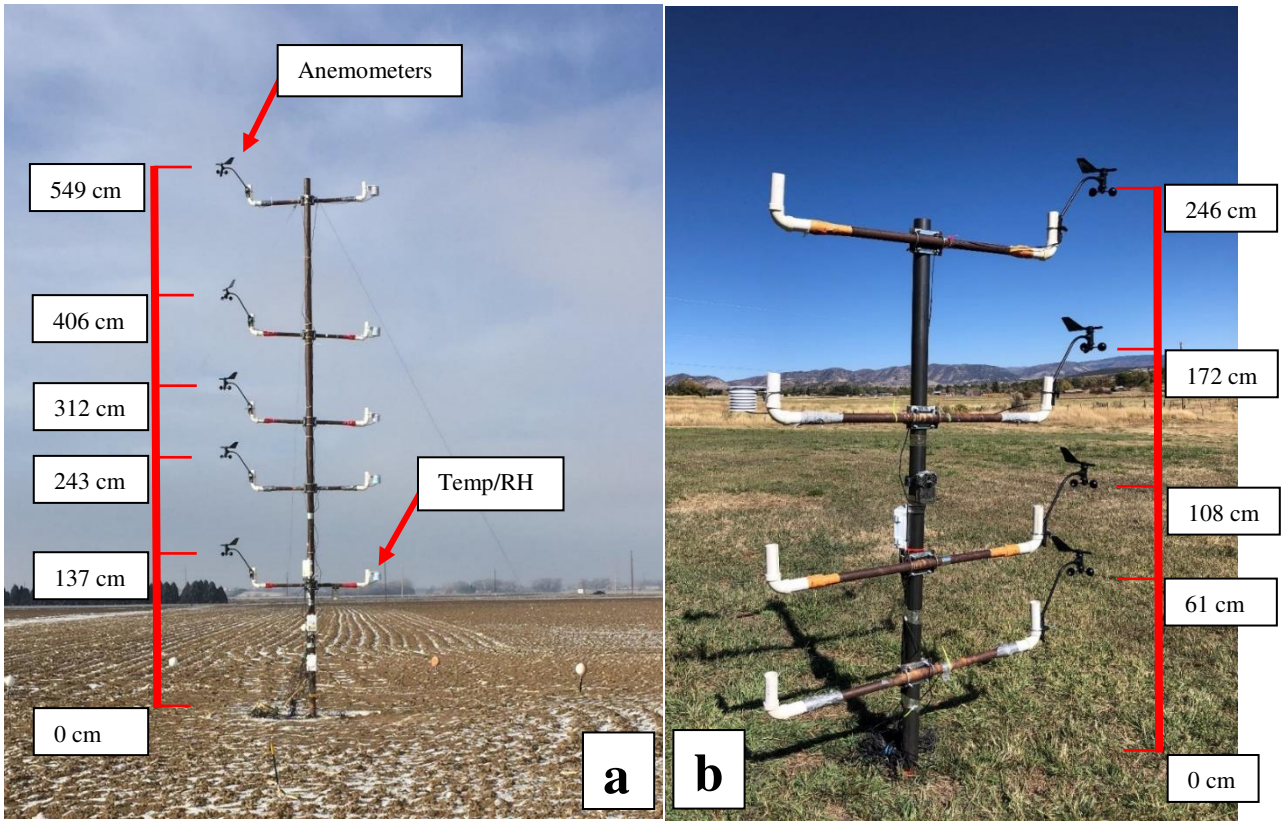

Figure 2.1. a) Meteorological tower at ARDEC study site for the 2017-2019 winter seasons. Photo is taken looking west. Furrows are in the East-West direction. b) Meteorological tower set up at the Trout Farm site for the 2019-2020 winter season. Photo is taken looking north.

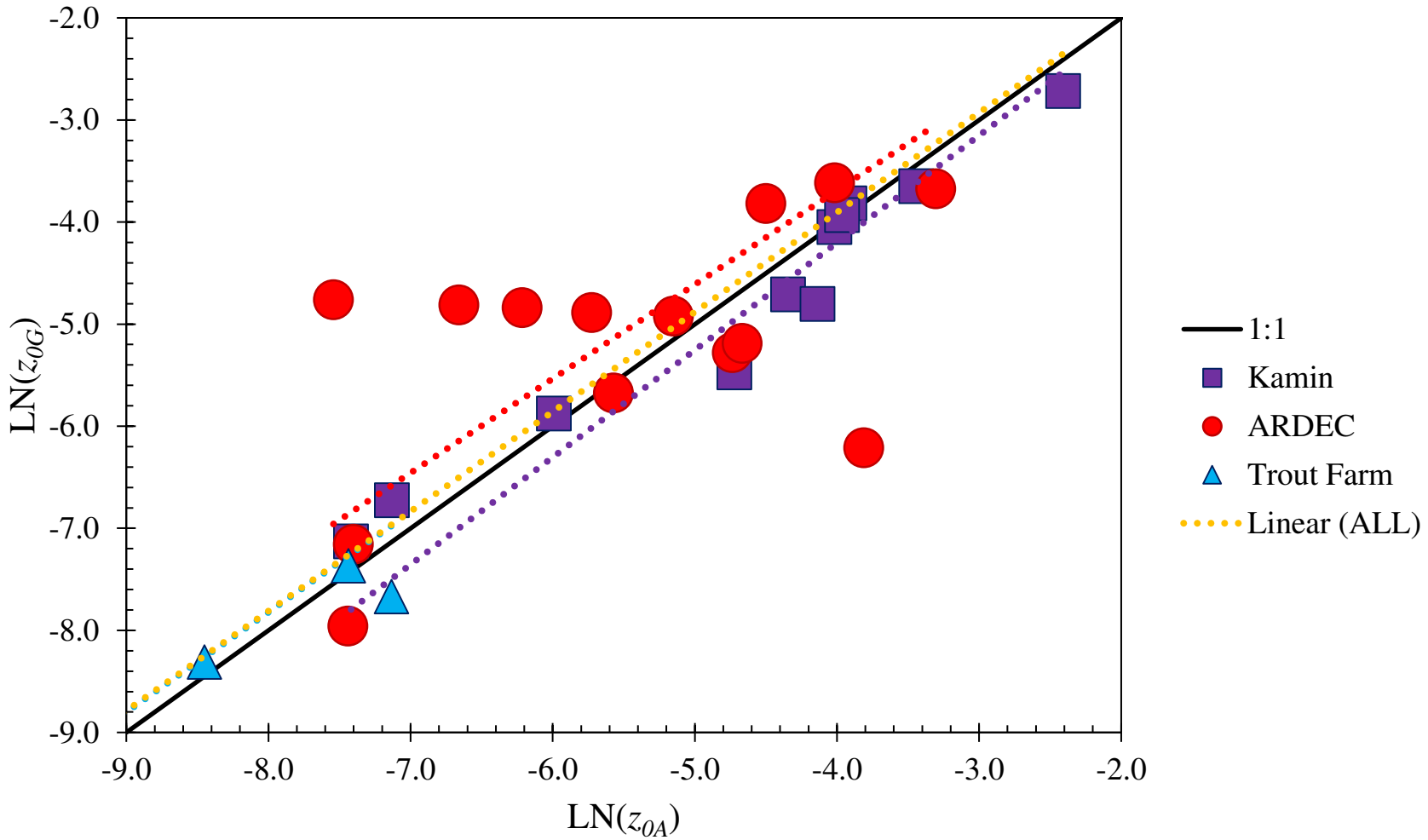

Figure 2.2. The natural log of anemometric versus geometric z_0 data from 2014-2015 winter season at ARDEC-South (Kamin, 2015), 2017-2019 winter seasons at ARDEC, and 2019-2020 winter season at Trout Farm.

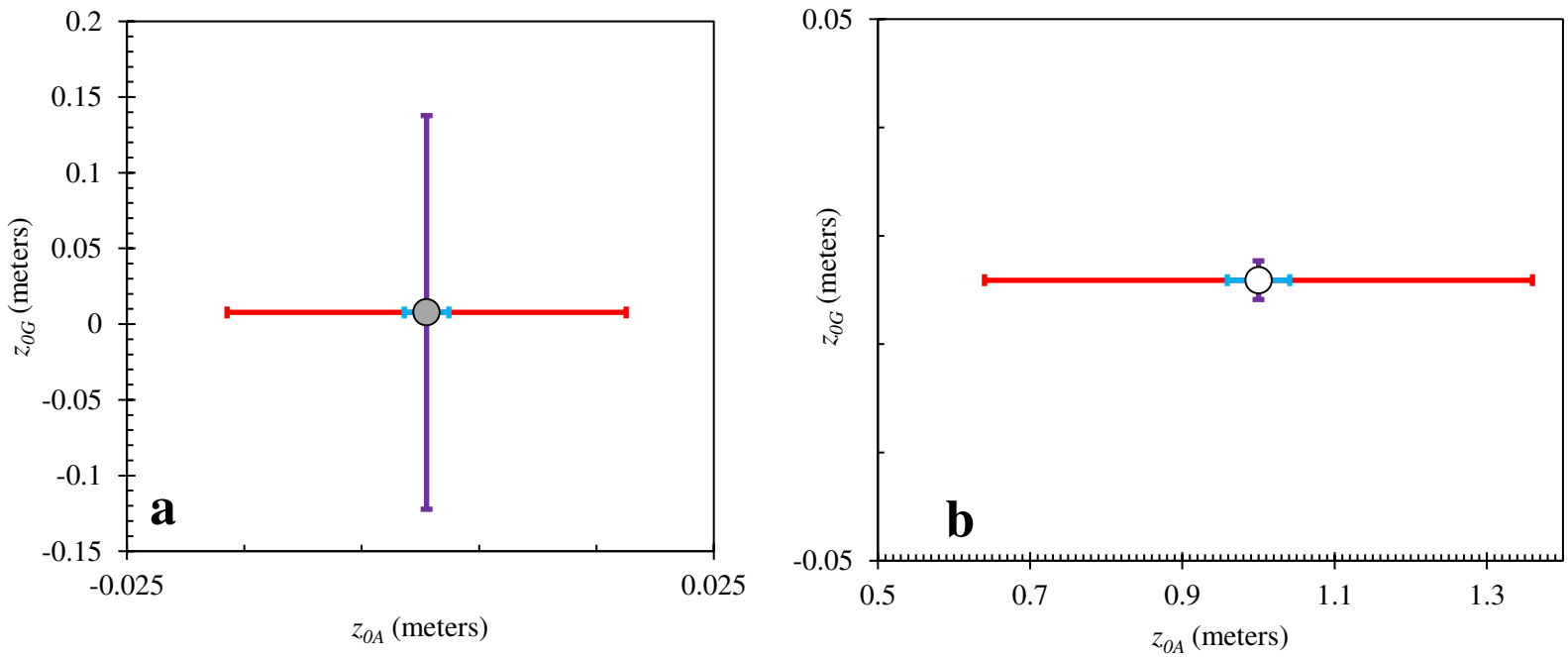

Figure 2.3. Error analysis of two dominate outliers, a) from 12/24/2017 and b) from 01/21/2018, both from ARDEC. The blue, horizontal error bars represent the error associated with a +/- 2 cm height difference with each of the anemometers, the red, horizontal error bars represent error associated with +/-5% difference in wind speeds, and the purple, vertical error bars represent the geometrically calculated z_0 error based on multiplying the scan are by 0.5 and 2.

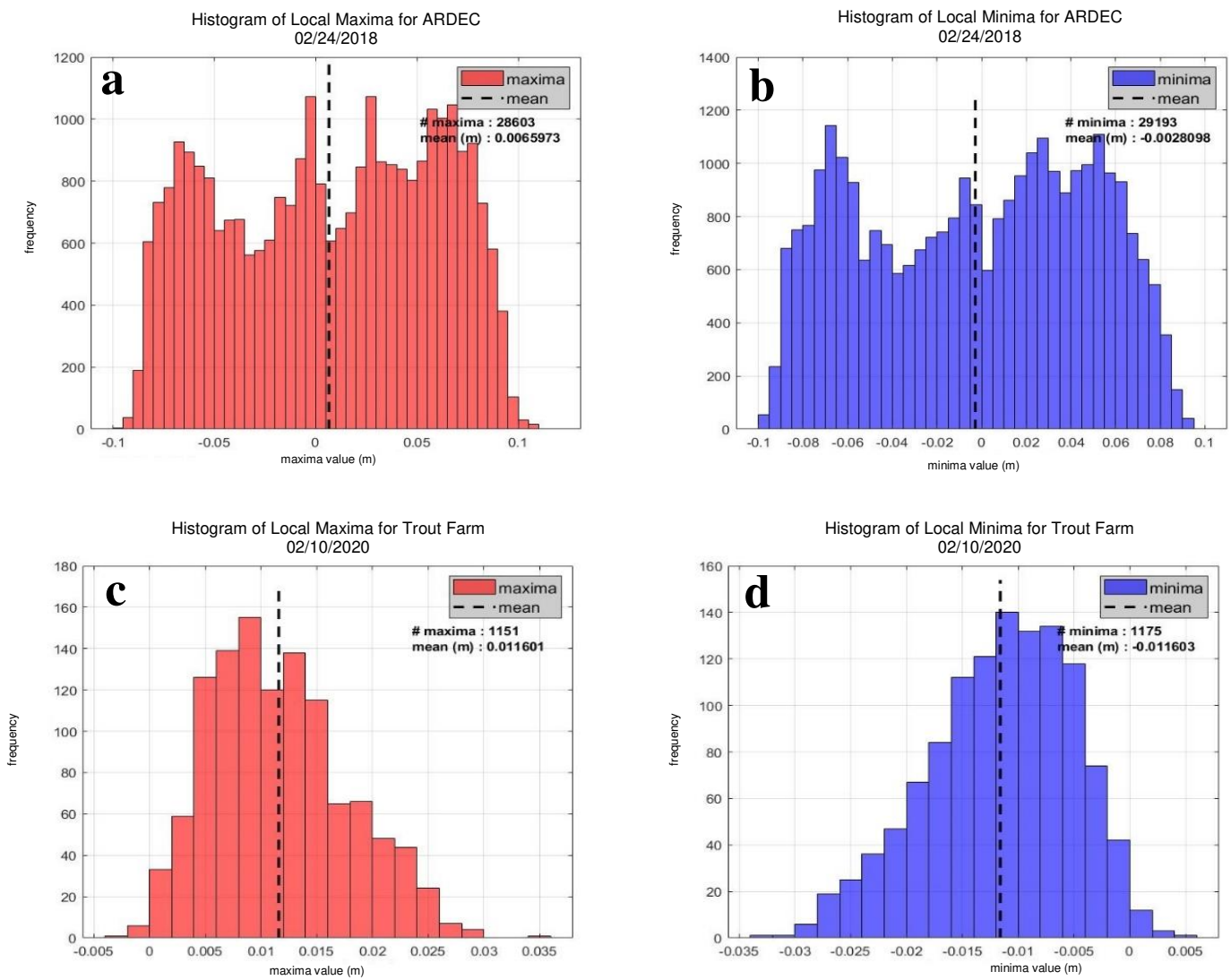

Figure 2.4. Histograms of a) the local maxima and b) local minima for an outlier point taken at ARDEC on 2/24/2018 with a $z_{0\text{-}G}$ value of 0.0001 meters and $z_{0\text{-}A}$ value of 0.0006 meters, and c) the local maxima and b) local minima for a point on the 1:1 line taken at Trout Farm on 2/10/2020 with a $z_{0\text{-}G}$ value of 0.00063 meters and $z_{0\text{-}A}$ value of 0.00060 meters.

3.0 THE RELATION BETWEEN SNOW DEPTH AND A SPATIALLY AND TEMPORALLY DYNAMIC AERODYNAMIC ROUGHNESS LENGTH

3.1 Summary

A shallow, seasonal snowpack is rarely homogeneous in depth, layer characteristics, or surface structure throughout an entire winter. Aerodynamic roughness length (z_0) is typically considered a static parameter within hydrologic and atmospheric models. However, observations have shown that z_0 is a dynamic variable. Therefore, accurate spatial and temporal measurements of z_0 are necessary. Terrestrial LiDAR data at nine different study sites from the 2019-2020 winter season in northwest Colorado were collected to observe variability of the snowpack surface. The z_0 and snow depth (d_s) were observed throughout 112 site visits, and all sites illustrated a change in z_0 as a function of d_s. The data show a decrease of z_0 during snow accumulation as the snow follows the underlying terrain in the initial stages of accumulation and an increase of z_0 during melt. The correlation varied spatially and temporally, though, it was obscured by modifications of the snowpack surface (presence of vegetation, anthropogenic or ecologic influence, etc.). The slope of the plotted z_0- d_s correlation was found to differ based on the initial roughness of the site and the x-intercept was influenced by the size of the initial roughness features.

3.2 Introduction

A seasonal, shallow snowpack covers approximately 50% of the Northern Hemisphere, making the snowpack surface the primary land-atmosphere interface during the winter season (Mialon *et al.*, 2005; Fassnacht *et al.* 2009a). Within Colorado, an important headwater state in the western United States, 60% of annual precipitation falls as snow (Barnett *et al.*, 2008; Fassnacht *et al.*, 2018). Accurately

observing and modeling snow water resources in the western United States is essential for water budgeting, recreation, wildfire management, and ecological resources (Fassnacht *et al*., 2018).

The snowpack varies spatially and temporally (Niu and Yang, 2007), and is controlled by local, regional, and global weather and climate (Anttila *et al*., 2014). Consequently, snowpack conditions will vary between maritime to continental climates (Trujillo and Molotch, 2014). Because of the variability of the snowpack across these regimes, a standard metric to quantify the snowpack is difficult to acquire. The aerodynamic roughness length, z_0, can be used as a measure of the snowpack surface (Luce and Tarboton, 2004; Smith, 2014). The z_0 captures the variability that is produced by land cover characteristics as well as the underlying topography (Niu and Yang, 2007; Fassnacht *et al*., 2009a; Fassnacht *et al*., 2009b). The variability is further enhanced by meteorological conditions (Niu and Yang, 2007), non-uniform distribution of snow cover during accumulation and melt (Luce and Tarboton, 2004; Niu and Yang, 2007), snow-canopy interactions (Moeser *et al*., 2015), and snow redistribution by wind (Liston, 2004). Small scale (<1 meter) and large scale (>1 meter) variations within the snowpack can alter the overall z_0 value (Blöschl, 1999; Smith, 2014). The effect of a single roughness feature coupled with non-uniform spatial arrangement among other elements affects all aspects of the snowpack surface (Luce and Tarboton, 2004; Smith, 2014). A dynamic z_0 characterizes heterogeneities in snow-water equivalent, melt rates (Luce and Tarboton, 2004), redistribution, snow deposition (Niu and Yang, 2007), and surface energy fluxes (Magand *et al.*, 2014).

The snow surface roughness will decrease during accumulation as the snow follows the underlying terrain in the initial stages of accumulation and roughness can increase during melt (Figure 3.1) (Magand *et al*., 2014). When the snow initially accumulates, it will match the underlying terrain until there is enough snow depth, d_s, to cause a decoupling from the underlying topography and form a mostly smooth surface (Luce and Tarboton, 2004; Brock *et al*., 2006; Magand *et al*., 2014). Quincey *et al*. (2017) found that one new snowfall decreased z_0 by ~75% since it covered small scale feature variability and only large features were left to increase the roughness. As d_s decreases, ground-based surface features and

underlying topographical features are recoupled with z_0, increasing the variability (Manes *et al.*, 2008; Magand *et al.*, 2014).

This relation of increasing d_s and decreasing z_0 in some form has been observed previously by Sanow *et al.* (2018), Luce and Tarboton (2004), Fassnacht *et al.* (2009a), and others. This correlation of d_s and z_0 is not considered within hydrologic, snowpack or land surface models. The relation of these two factors is also expected to differ between periods of melt and accumulation as periods of melt are typically less uniform (Magand *et al.,* 2014). Swenson and Lawrence (2012) found that topography and land cover features have the most influence on the hysteresis. Once the snow cover has reached full coverage over these features, the snowpack will accumulate homogeneously (Magand *et al.* 2014). These early, mid, and late-season snowpack surface changes have important impacts on estimating an accurate z_0 value within hydrologic models (Manes *et al.*, 2018).

To accurately understand and model the snowpack, variability needs to be considered at the local level. Otherwise, hydrologic models will either over or underestimate melt water availability (Luce *et al.* 1999; Manes *et al.*, 2008; DeBeer and Pomeroy, 2017). At present, the same z_0 is used for an entire watershed based on the assumption of 100% snow covered area, undeviating melt throughout an area, despite the topographic or vegetation influences (Niu and Yang, 2007; DeBeer and Pomeroy, 2017), and no other spatial or temporal variation representation (Hock *et al.*, 2017). However, we hypothesize that the incorporation of z_0 as a dynamic variable, rather than a static parameter, will improve hydrologic and meteorological models (Manes *et al.*, 2008; Fassnacht *et al.* 2009a; DeBeer and Pomeroy, 2017; Sanow *et al.*, 2018). To understand and observe the relation between z_0 and d_s, we ask the following questions, 1) Does the snow surface roughness, defined here as z_0, change as a function of d_s? 2) Does the correlation between z_0 and d_s vary spatially? 3) Is the decrease in z_0 as d_s increases consistent regardless of the initial ground roughness? 4) Is the correlation between increasing d_s and decreasing snow surface z_0 a function of the initial roughness feature, such as dominate vegetation and topographic features? and, 5) Is there a difference between the z_0-d_s correlation during periods of accumulation and melt, i.e., is it a hysteretic?

3.3 Methodology and Data

3.3.1 Field Data Collection

The snowpack surface was measured using a FARO Focus3D X 130 model Terrestrial LiDAR Scanner (TLS) (www.faro.com). This LiDAR instrument generates a point cloud scan of a given area with an error of +/- 2 millimeters and a resolution of approximately 7.5 millimeters. Three LiDAR scans from different locations were taken during each site visit to avoid shadowing from roughness features. Blue Maestro data downloads, air temperature on arrival and departure, current weather conditions (sunny, cloudy, windy, etc.), upcoming storm predictions, approximate new snow accumulation, snow depths at each T-post, and site photos were recorded during each site visit. These data and photos were used to explore any inconsistencies with z_0 calculations or processing errors. Meteorological data were used to explore any major increases or decreases in temperature that may alter melt rates.

3.3.2 Site Descriptions

We selected ten sites near Meeker, Colorado (Figure 3.2), with an elevation range of 1,885 to 2,468 meters, to evaluate these questions. Land cover ranged from open, grassy fields to large Pinyon-Juniper and shrub dominated sites. Sites were chosen for land cover variability (i.e. size of the primary roughness feature), elevation, and winter accessibility (Table 3.1). TLS scan frequency ranged from monthly to every two days. Annual precipitation ranged from 391 to 631 millimeters (https://wrcc.dri.edu/). Scan interruptions occasionally occurred due to extreme winter weather and/or inability to reach the site safely. Each site was equipped with a Bluetooth Blue Maestro Tempo Disc sensor (https://bluemaestro.com/) which recorded hourly temperature, humidity, and dew point temperature, 3-4 T-posts with measuring tape to record d_s during each site visit, and a silver sphere on the north facing T-post for direction orientation.

3.3.3 Data-Processing

The three LiDAR scans were cropped, merged, and aligned with each other in the corresponding cardinal direction (Figure 3.3) in the open source program Cloud Compare (https://www.danielgm.net/cc/). An area of interest (AOI) was chosen for each site within the middle of the t-posts that varied in size from 2x2 m to 8x8 m, and typically included a primary roughness feature such as a sagebrush, shrub, etc. The AOI had a nomial point density of 1-10 millimeters with a total of ~1.3 million points. The AOI was cropped out of each merged/aligned scan and interpolated using the kriging method at 0.01 meters in the Golden Software Surfer (https://www.goldensoftware.com/products/surfer). This created an interpolated, gridded AOI which was de-trended (Fassnacht *et al.*, 2009b) in the x-y plane to remove the bias from the slope of the field or the angle of the LiDAR scanner (Sanow *et al.*, 2018). The final geometric z_0 for the AOI was calculated using the same method as Sanow *et al.* (2018) and Lettau (1969). This method finds the mean obstacle height (h^*) by finding all local maximums and minimums relative to each other across the surface. Then, the lot area (S) is calculated as the total area divided by the total number of maxima. Next, the silhouette area (s) is found as the profile of an obstacle, this is done at a pre-defined resolution step. All of these steps, applied within Equation 3.1, results in the average z_0 of the surface.

$$z_0 = h^* s / S \tag{3.1}$$

The d_s were calculated using Cloud Compare by subtracting the initial snow-free scan from a snow-covered scan. The mean d_s was computed across the AOI. Snow depths from site visits were cross validated against LiDAR point clouds to ensure accuracy during post-processing.

3.3.4 Data Analysis

Initial roughness LiDAR scans were taken with no snow on the ground. Throughout the season when snow was present, the initial scans were subtracted from the snow-covered scans to find average snow depth. Corresponding z_0 values were calculated for each scan with and without snow, and compared across sites throughout the season. The sites were selected based on varying topography, vegetation cover

and abundance, elevation, and distribution throughout the watershed. This aided in determining spatial differences and the z_0-d_s correlation. Resulting snow depths were plotted again the natural logs of z_0 for each site, and grouped by slope. The coefficient of determination, r^2, was found for each site. One site, Julie Circle, was chosen to observe the hysteresis between periods of accumulation and melt due to the high temporal frequency of scans. Melt versus accumulation was determined by the d_s of the previous scan. If d_s had increased since the time of the last scan, it was an accumulation point. If it had decreased, it was a melt point. This was verified using site photos as well as recorded hand measurements.

3.4 Results

Over the 2019-2020 winter season, 112 total site visits were conducted between October and April. All sites, except one, showed that as d_s increased and enveloped roughness features, the corresponding z_0 decreased (Figure 3.4). Lost Creek, the exception, was disturbed during the spring and therefore did not follow this trend (Figure 3.5). For example, the Piceance site shows the d_s increasing and the corresponding z_0 value decreasing until 03/03/2020 when melt began (Table 3.2). Furthermore, as the d_s starts decreasing the z_0 values begin to increase. This relation developed quickly, and roughness feature size had an impact on the trend line slope.

In interest of identifying trends amongst all sites, the sites were placed into smaller groups using the resulting slopes from the least square regression fit; Trout Farm, Julie Circle, and CR11 (Figure 3.4a); Piceance, Spring Creek, Upper Piceance Creek, and Cathedral Creek (Figure 3.4b); Yellow Jacket (Figure 3.4c); and Lost Creek (Figure 3.4d). Figure 3.4a displays CR11 and Julie Circle having similar r^2, slope, roughness feature height, and initial z_0 values. The r^2 values of CR11 and Julie Circle are 0.73 and 0.68, respectively, which are similar r^2 values. This result occurred even with the drastic difference in data point quantities between the two sites, 5 compared to 31. The primary roughness feature height (height of the tallest feature found within the AOI, sagebrush, grass, etc.) at CR11 and Julie Circle are 0.46 meters

and 0.35 meters and with -0.048 and -0.043 slope, respectively. Julie Circle had one notable outlier on 2/6/2020, with a d_s of 0.521 meters and a z_0 value of 0.0035 meters (Figure 3.5). This occurred after a storm had deposited 0.18 meters of new snow overnight. Conversely, the lowest z_0 at the site occurred on 2/10/2020 with a total d_s of 0.41 meters and a z_0 of 0.00025 meters (Figure 3.7). Figure 3.7 also highlights the subtle snowpack surface differences which indicate that these small-scale features have a notable impact on the overall z_0 value. Similar to Julie Circle, CR11 had a maximum d_s of 0.488 meters with a z_0 of 0.00018 meters on 2/10/2020, yet, the lowest roughness value at the site occurred during the second highest d_s of 0.434 meters and a z_0 of 0.00007 meters on 01/29/2020. Trout Farm had a similar slope to this pair (Figure 3.4a). Yet, compared to CR11 and Julie Circle with initial z_0 values of 0.066 meters and 0.040 meters, Trout Farm had the lowest roughness feature height (0.01 meters for a grassy lawn) and initial z_0 of 0.00476 meters. These initial z_0 values are an order of magnitude different between CR11 and Julie Circle. However, Trout Farm produced a slope of -0.0233 which is only a difference of 0.02 from Julie Circle. Similar to the Julie Circle outlier on 02/10/2020, Trout Farm had a d_s value of 0.002 meters greater than the snowpack on 2/25/2020, but the z_0 values were 0.00063 and 0.00025, respectively (Figure 3.7).

The second grouping of sites by slope includes Cathedral Creek, Piceance, Spring Creek, and Upper Piceance Creek shown in Figure 3.4b. These sites had the lowest number of site visits (three to eight) due to distance and winter access difficulty. The slopes of all four sites were alike, Cathedral Creek -0.15, Piceance -0.11, Spring Creek -0.13, and Upper Piceance Creek -0.14. The main variation among these sites is the r^2, primary roughness feature height, and initial z_0 values. Spring Creek and Upper Piceance Creek have the highest r^2 of 0.71 and 0.79, respectively. We note, Spring Creek had the least amount of site visits and corresponding data. Upper Piceance has the highest amount of site visits in this grouping. Outliers from Cathedral Creek are from the two highest d_s with depths of 0.187 meters and 0.229 meters, and z_0 values 0.495 meters and 0.454 meters, respectively. Between the scan dates of 01/16/2020 and 02/10/2020 temperatures were often above freezing, with a maximum temperature of 18.7

°C. The interpolated surfaces of the 01/16/2020 (lowest z_0) and the 02/24/2020 (deepest snow) are shown in Figure 3.8.

This second group had the largest variation of roughness feature sizes ranging between 0.68 meters at Piceance and 1.65 meters at Upper Piceance Creek. It was initially thought that Piceance would fall into the category with the last group (Figure 3.4a) due to the size of the primary roughness feature height. Yet, the initial z_0 was 0.114 meters, which is much larger than the others within the last grouping. Spring Creek had a roughness feature height of 1.1 meters and initial z_0 of 0.22 meters which represents an average among the sites. The all-site average slope, roughness feature size, and initial z_0 was -0.10, 0.84 meters, and 0.19 meters, respectively. Cathedral Creek had the highest initial z_0 value of 0.56 meters, but it had only the third largest roughness feature (1.3 meters), indicating the site had the most roughness features compared to the others. Upper Piceance Creek had the second-largest initial z_0 value and roughness feature height at 0.39 meters and 1.65 meters, respectively. However, both sites fell below Yellow Jacket, which was placed into Figure 3.4c on its own. Yellow Jacket had the largest roughness feature of 1.85 meters (large sage and shrubbery). Though, it produced the third largest initial z_0 value of 0.33 meters. Additionally, it had the steepest slope of any of the sites at -0.32. Yellow Jacket had two outliers (Figure 3.4C) that resulted in a higher z_0 value than the initial. These instances occurred on 03/16/2020 and 04/07/2020, late in the season after peak d_s had occurred (Figure 3.9).

Lost Creek experienced heavy anthropogenic influence as shown in Figure 3.4d. Sometime between 01/28/2020 and 02/26/2020 a snowmobile drove through the site which altered the natural progression of the snow (Figure 3.5). Still, Lost Creek results show some similarities to the other sites. Prior to the snowmobile, Lost Creek was following the same hysteresis relation as the other sites. Lost Creek had the lowest r^2 (-0.279), attributed to the data being forced through the origin on the plot. When the data is not forced, the r^2 becomes 0.0798, still a very low correlation that can be explained by the snowmobile tracks.

Since Julie Circle had the most data points of any site, it was used to analyze melt and accumulation values (Figure 3.6). There are 12 accumulation points, 17 melt points, and two points with d_s of 0 m, taken as the initial surface roughness scan (fall) and the final surface roughness scan (spring). The results had a varying slope of -0.03 for melt, and -0.04 for accumulation. Melt resulted in an r^2 of 0.36, and accumulation resulted in an r^2 of 0.66.

3.5 Discussion

The calculated z_0 changed as a function of observed d_s, although outliers of the relation existed. The first outlier was at the Julie Circle location (Figure 3.4a). The initial point on the x-axis indicates the highest z_0 value due to the lack of snow, however two points fell on the x-axis. Upon investigation of the two points, they occurred during the first and last scan of the year. The initial z_0 was less than half compared to the terminal roughness, a large difference in z_0 at the exact same place. We attribute this to vegetation type, which is a regular lawn grass that was pushed down by the weight of the snow throughout the year. We note that this scenario could happen to flexible vegetation, fluctuating z_0 values throughout the year (Smith, 2014; Quincey *et al*., 2017).

Another discrepancy at the Julie Circle site is the lack of correlation between the highest d_s and lowest z_0 value. A likely explanation for this observation is the large Cottonwood tree that overhangs the Julie Circle site. For example, we note in the point clouds the pock-marks in the snowpack surface where accumulated canopy snow fell from the limbs and altered the roughness (Figure 3.6). No other sites in this study had canopy cover like Julie Circle. Although, most sites did have shrubbery vegetation present, so even small-scale canopy interception and deposition was possible (Quincey *et al*., 2017). Canopy interception and deposition is a potential issue when correlating between d_s and z_0. Therefore, to assume a uniform or linearly metamorphosing or melting snowpack would lead to potential errors (Luce and Tarboton, 2004; Gromke, 2011; Smith, 2014).

This lack of correlation is also noted at CR11 and Trout Farm. Similar to Julie Circle, the highest d_s value did not correspond with the lowest z_0 value at CR11. This can be attributed to a recent snowfall event of about 10 centimeters that had fallen the day before the 01/29/2020 scan. On 02/10/2020 there was less fresh snow (approximately 5 centimeters) and conditions were sunny and warmer. These differences in the snowpack were recorded in site notes and photos from the visits. Likewise, Trout Farm also experienced the same contradiction, the highest d_s value had a z_0 greater than double the lowest calculated z_0. This indicates that these small variations of the snowpack surface is key to addressing z_0 beyond simply considering the snow depth. These small variations are highlighted in Figure 3.7. Accounting for small surface variations is especially important on flat sites where initial z_0 may be surpassed by the development of surface features such as sun cups, sastrugi, surficial features, and wildlife and anthropogenic modifications (Fassnacht, 2010; Gromke, 2011; Quincey *et al.,* 2017; Fassnacht *et al*., 2018).

Cathedral Creek, shown in Figure 3.4b, followed the d_s and z_0 relation until the 02/10/2020 and 02/24/2020 surveys. Between the scan dates of 01/16/2020 and 02/10/2020 temperatures were often above freezing, with a maximum temperature of 19°C. The interpolated surfaces of 01/16/2020 (lowest z_0) and 02/24/2020 (deepest snow) are shown in Figure 3.10, highlighting pock-marks and uneven melting. These elevated temperatures resulted in an increased, non-uniform melt (Luce and Tarboton, 2004). Correspondingly, even though additional snow fell between the scans, it did not completely cover the snow surface characteristics (Luce and Tarboton, 2004; Brock *et al*., 2006; Magand *et al*., 2014).

Yellow Jacket had the highest initial z_0 of any of the sites (Figure 3.4c). Photos from the field visits late in the season show a lot of recent melt, which revealed larger shrubs as well as the development of sun cups within the AOI (Figure 3.9). The late season increase in roughness likely produced two irregular points with a higher z_0 than the initial after peak d_s had occurred (Fassnacht *et al.,* 2009a). Another influence on the site was the anthropogenic modifications of snowmobile tracks (Figure 3.4c and Figure 3.5). Combining these two factors led the roughness variations to be larger than the initial grassy,

shrub-filled plot. This same anthropogenic disruption occurred at the Lost Creek site. This led to an extreme increase in z_0 after the disturbance, even with the deep snowpack 0.85 meters (Figure 3.4d). The large increase in z_0 at the site was exacerbated by the very flat topography that contained one small controlled roughness feature railroad tie in the middle.

We hypothesized that slopes would remain the same and the x-intercept would change, however, initial ground roughness played a critical role in the slope of the data. The 0.13 meter railroad tie at the Lost Creek site is an example, of a feature responsible for the initial site z_0 value of 0.0094 meters. Without it, the z_0 would have been lower as the site was an open, grassy field. Due to this controlled roughness feature, none of the snowmobile-caused roughness values were larger than the initial. Lost Creek also had some of the highest d_s, which led to high z_0 values due to the snowmobile tracks. Snowmobiling and other recreational activities are common throughout public lands during the winter. Anthropogenic factors such as these are important to consider when evaluating a spatially and temporally dynamic z_0 (Fassnacht *et al*., 2018). Moreover, this could explain the data discrepancies like that in the Yellow Jacket site, another site influenced by snowmobiles. Together, land cover type and function be considered when applying z_0 (Fassnacht *et al*., 2018).

Figure 3.4b shows the grouping of Cathedral Creek, Piceance, Spring Creek, and Upper Piceance Creek. The slopes of all four sites were similar ranging from -0.11 to -0.15. The r^2 values, roughness features (ranging between 0.68-1.65 meters), and initial z_0 values (ranging from 0.11 to 0.57 meters) varied among the sites. Based on the primary roughness feature heights, Piceance aligns more with the CR11, Julie Circle, and Trout Farm group than the one in which it was placed. Upper Piceance was more similar in initial z_0 and roughness feature size to Yellow Jacket, but their slopes have a difference of 0.167. However, as discussed, there were some values that skewed the slopes in these sites. Potential reasoning for this was noted at several sites, such as overall changes of the surface of the snowpack throughout the season due to wind redistribution (Musselman *et al*., 2015); surface energy fluxes (Luce and Tarboton, 2004); formation of surface features (Fassnacht *et al*, 2009a); and non-uniform melt and

accumulation (Luce and Tarboton, 2004). These influences metamorphose the snowpack and are very difficult to quantify or predict. The development of surface features is one reason why the slopes of Trout Farm and Julie Circle have only a 0.02 difference despite the initial z_0 values being an order of magnitude different, 0.0048 meters and 0.0400 meters, respectively.

Julie Circle was used to compare melt and accumulation values in Figure 3.6. The accumulation values (blue) had a stronger r^2 value of 0.66, compared to the melt 0.36 r^2, indicating accumulation was more uniform (Magand *et al*., 2014). This was to be expected, since this relation was not observed to be linear in either case. The low correlation of the melt values can be attributed to several environmental processes, which is typical to occur within any snowpack. Potential melt factors are sensible and latent heat fluxes, dust deposition (Harpold *et al.,* 2012), spatial and temporal distribution of incoming solar radiation (Bales *et al*., 2006), wind redistribution (Gromke, 2011; Wayand *et al.*, 2018), longwave radiation, anthropogenic alterations (Liston, 2004), air temperature (Raleigh *et al*., 2013), spatial heterogeneity of the snowpack (Debeer and Pomeroy, 2017), and vegetation cover (Anttila *et al.,* 2014). Since melting occurred throughout the season, the environmental influences were also affecting accumulation rates, which supports the heterogeneity of the accumulation z_0 values. Melt rates influence atmospheric and hydrologic processes (Liston, 2004), and understanding the processes and rates that control melt water production is important for predicting the timing and magnitude of peak melt in a watershed (Liston, 1995; Luce *et al*., 1999; DeBeer and Pomeroy, 2017). Initially, this aspect of the study was to be conducted at Lost Creek and Yellow Jacket, however, these sites were anthropogenically altered and were unable to be used. It was hypothesized that the melt versus accumulation at Yellow Jacket would yield a higher difference between the melt and accumulation slopes. This is because of the higher initial roughness and quantity of roughness features to enhance melt. Since Lost Creek was a flat, open site it was hypothesized that the slopes would be similar to Julie Circle. The primary influence of melt at Julie Circle was the addition of ecological factors from the tree near the site, and the proximity to a residential house increasing the effects of longwave radiation induced melt. At Lost Creek, incoming

solar radiation and temperature would be considered the only dominate form of melt, therefore, slopes even more similar to each other were expected.

The method used to determine melt compared to accumulation values is also a source of potential error. Settling and metamorphism of the snowpack could have occurred resulting in snow depth decreases without any actual snowmelt taking place (Liston, 2004; Bales *et* al., 2006; Magand *et* al., 2014). Photos, atmospheric conditions, and visual assessments of the site were completed, however, without soil moisture sensors and other atmospheric/hydrologic monitoring equipment, exact periods of melt are difficult to assess.

3.5.1 Limitations

This study consisted of 112 site visits, which proved to produce an adequate amount of data to observe trends and correlations. However, an increase of temporal scan frequency is needed to explore this correlation further. Ideally, daily scans at each site would have been feasible because the surface of the snowpack is constantly changing due to surface processes (Niu and Yang, 2007; Anttila *et al*., 2014) and meteorological factors (Fassnacht *et al.*, 2009a; Raleigh *et* al., 2013). Scan areas per site are only a small fraction of the White River watershed, and although they provide insight on spatial and temporal changes, application to a watershed scale may not be possible due to the small idiosyncrasies with each plot. For example, the large cottonwood at Julie Circle substantially altered the surface, and therefore the addition of canopy cover. Such plot specific features enhance the assumed variability of the plots (Magand *et al*., 2014), though, plots with similar land cover characteristics could be similar. For example, Upper Piceance Creek and Cathedral had similar land covers and were both on an old river terrace surrounded by (50-100 meter) cliffs within ~0.3 kilometers. Upper Piceance Creek had a primary roughness feature height of 1.65 meters and initial roughness of 0.389 meters. Cathedral Creek had primary roughness feature height of 1.3 meters and initial roughness of 0.566 meters. These initial values are similar, and they both produced a slope of -0.15. This indicates that similar land covers in similar locations can produce comparable z_0 values. Once the correlation of z_0-d_s is established, it could be

applied to a larger area with similar characteristics. No sites were at any significant surface slope; however, incoming and outgoing shortwave and longwave radiation were not accounted for, which are another source of differential melt patterns (Bales *et* al., 2006; Harpold *et al*., 2012). The lack of radiation collection was due to lack of equipment and funding.

Future studies should include larger plots within a smaller watershed that can be LiDAR scanned for snow accumulation and melt more frequently (Magand *et al.*, 2014; Sanow *et al.* 2018). Inclusion of meteorological data beyond relative humidity and temperature could provide more insight to determining melt patterns and following accumulation patterns during mid-season melt (Davison, 2003). The results from this work will improve snowpack, hydrological and meteorological modeling (Manes *et al.*, 2008; Fassnacht *et al.* 2009a; DeBeer and Pomeroy, 2017; Sanow *et al.*, 2018), by better representing the aerodynamic roughness length for snow (Figures 3.4 and 3.6). Additional controlled experiments modifying the ground characteristics together with more meteorological monitoring and snowpack modeling would further quantify the relation between d_s and z_0 (Swenson and Lawrence, 2012; Magand *et al.*, 2014; Sanow *et al.* 2018).

Future studies could explore errors of uncertainty within the z_0 calculations. The current code (described in Chapter 1) calculates z_0 based on the local maxima and minima within the scan area. This method is acceptable when roughness elements are homogenously spaced and sized, however that is not always the case in nature. The code could be reformed to calculate z_0 on a certain sized area (every 0.01^2 meter, or 0.1^2 meter, etc. depending on the size of the scan). This would give a distribution of z_0 values that would encompass the variations in the terrain, vegetation, size, and/or distribution of roughness features. This methodology could enhance the estimation of z_0 for an area that is larger, as a larger area ($>10^2$ meters) will tend to have more variations than a small area, such as sites used within this study.

3.6 Conclusions

At all study locations, it was observed that as d_s increased z_0 decreased. This correlation varied spatially and was dependent on the initial roughness of the site. Initial roughness features played a large role in determining the slope and x-intercept of the z_0- d_s correlation. Although, when sites are disturbed during the course of data collection, the variability of z_0 can change by orders of magnitude, an observation made at several sites. Hence, the land use factor changes the correlation. We observed hysteresis between the z_0- d_s correlation from periods of melt and accumulation, however, further studies are necessary to explore this relationship further.

3.7 References

Anderson, B.T., McNamara, J.P., Marshall, H.P., Flores, A., 2014. Insights into the physical processes controlling correlations between snow distribution and terrain properties. Water Resources Research, 50(6), 4545-4563 [doi: 10.1002/2013wr013714].

Anttila, K., Manninen, T., Karjalainen, T., Lahtinen, P., Riihela, A., Siljamo, N., 2014. The temporal and spatial variability in submeter scale surface roughness of seasonal snow in Sodankyla Finnish Lapland in 2009-2010. Journal of Geophysical Research: Atmospheres, 119, 9236-9252 [doi: 10.1002/2014JD021597].

Bales, R.C., Molotch, N.P., Painter, T.H., Dettinger, R.R., Dozier, J., 2006. Mountain hydrology of the western United States. Water Resources Research, 42(8) [doi: 10.1029/2005WR004387].

Barnett, T.P., Pierce, D.W., Hidalgo, H.G., Bonfils, C., Santer, B.D., Das, T., Bala, G., Wood, A.W., Nozawa, T., Mirin, A.A., Cayan, D.R., Dettinger, M.D., 2008. Human induced changes in the hydrology of the western United States. Science, 319(5866), 1080-1083 [doi: 10.1126/science.1152538].

Blöschl, G., 1999. Scaling issues in snow hydrology. Hydrologic Process, 13, 2149-2175 [doi: 10.1.1.709.499].

Brock, B., Willis, I., Sharp, M., 2006. Measurement and parameterization of aerodynamic roughness length variations at Haut Glacier d'Arolla, Switzerland. Journal of Glaciology, 52(177), 281–297 [doi: 10.3189/172756506781828746].

Davidson, B., 2002. Snow accumulation in a distributed hydrological model. University of Waterloo [OCLC : (OCoLC)71493372].

DeBeer, C. M. and Pomeroy, J.W., 2017. Influence of snowpack and melt energy heterogeneity on snow cover depletion and snowmelt runoff simulation in a cold mountain environment. Journal of Hydrology, 553, 199–213 [doi: 10.1016/j.jhydrol.2017.07.051].

Fassnacht, S R., Williams, M.W., Corrao, M.V., 2009a. Changes in the surface roughness of snow from millimetre to metre scales. Ecological Complexity, 6(3), 221–229 [doi: 10.1016/j.ecocom.2009.05.003].

Fassnacht, S.R., Stednick, J.D., Deems, J.S., Corrao, M.V., 2009b. Metrics for assessing snow surface roughness from digital imagery. Water Resources Research, 45, W00D31 [doi: 10.1029/2008WR006986].

Fassnacht, S. R., 2010. Temporal changes in small scale snowpack surface roughness length for sublimation estimates in hydrological modelling. Cuadernos De Investigación Geográfica, 36(1), 43 [doi: 10.18172/cig.1226].

Fassnacht, S.R., Heath, J.T., Venable, N.B.H., Elder, K.J., 2018. Snowmobile impacts on snowpack physical and mechanical properties. The Cryosphere, 12, 1121-1135 [doi: 10.5194/tc-12-1121-2018].

Fassnacht, S.R., Venable, N.B.H., McGrath, D., Patterson, G.G., 2018. Sub-seasonal snowpack trends in the Rocky Mountain National Park area, Colorado, USA. Water, 10(5), 562 [doi: 10.3390/w10050562].

Gromke, C., Manes, C., Walter, B., Lehning, M., Guala, M., 2011. Aerodynamic roughness length of fresh snow. Boundary-Layer Meteorology, 141(1), 21–34, [doi: 10.1007/s10546-011-9623-3].

Grunewald, T., Schrimer, M., Mott, R., Lehning, M., 2010. Spatial and temporal variability of snow depth and SWE in a small mountain catchment. Cryosphere Discussion, 4(1), 1-30 [doi: 10.5194/tcd-4-1-2010].

Harpold, A., Brooks, P., Rajagopal, S., Heidbuchel, I., Jardine, A., Stielstra, C., 2012. Changes in snowpack accumulation and ablation in the intermountain west. Water Resources Research, 48 [doi: 10.1029/2012WR011949].

Lettau, H., 1969. Note on aerodynamic roughness-parameter estimation on the basis of roughness-element description. Journal of Applied Meteorology, 8, 828-832 [doi: 10.1175/1520-0450(1969)008<0828:NOARPE>2.0.CO;2].

Liston, G.E., 1995. Local advection of momentum, heat, and moisture during the melt of patchy snow covers. Journal of Applied Meteorology, 34(7), 1705-1715 [doi: 10.1175/1520-0450-34.7.1705].

Liston, G.E., 2004. Representing subgrid snow cover heterogeneities in regional and global models. Journal of Climate, 17(6), 1381–1397 [doi: 10.1175/1520-0442(2004)0172.0.co;2].

Liston, G.E., Hiemstra, C.H., 2007. A simple data assimilation system for complex snow distributions (SnowAssim). American Meteorological Society, Cold Land Processes Experiment, Special Edition, 989-1004 [doi: 10.1175/2008JHM871.1].

Luce, C.H., Tarboton, D.G., Cooley, K.R., 1999. Sub-grid parameterization of snow distribution for an energy and mass balance snow cover model. Hydrological Processes, 13(12-13), 1921–1933 [doi: 10.1002/(sici)1099-1085(199909)13:12/133.0.co;2-s].

Luce, C. H. and Tarboton, D.G., 2004. The application of depletion curves for parameterization of subgrid variability of snow. Hydrological Processes, 18(8), 1409–1422 [doi: 10.1002/hyp.1420].

Magand, C., Ducharne, A., Le Moine, N., 2014. Introducing hysteresis in snow depletion curves to improve the water budget of a land surface model in alpine catchment. Journal of Hydrometeorology, 15(2), 631–649 [doi: 10.1175/jhm-d-13-091.1].

Manes, C., Guala, M., Löwe, H., Bartlett, S., Egli, L., Lehning, M., 2008. Statistical properties of fresh snow roughness. Water Resources Research, 44(11), 1–9 [doi: 10.1029/2007WR006689].

Moeser, D., Stahli, M., Jonas, T., 2015. Improved snow interception modeling using canopy parameters derived from airborne LIDAR data. Water Resources Research, 51(7), 5041-5059 [doi: 10.1002/2014WR016724].

Mialon, A., Royer, A., Fily, M., 2005. Wetland seasonal dynamics and inter-annual variability over northern high latitudes, derived from microwave satellite data. Journal of Geophysical Research, 110, 1-10 [doi: 10.1029/2004JD005697].

Mote, P.W., Li, S., Lettenmaier, D.P., Xiao, M., Engel, R., 2017. Dramatic declines in snowpack in the western US. Climate and Atmospheric Science, 1-6 [doi: 10.1038/s41612-018-0012-1].

Musselman, K.N., Pomeroy, J.W., Essery, R.L., Leroux, N., 2015. Impact of windflow calculations on simulations of alpine snow accumulation, redistribution, and ablation. Hydrological Processes, 29, 3983-3999 [doi: 10.1002/hyp.10595].

Niu, G., and Yang, Z.L., 2007. An observation-based formulation of snow cover fraction and its evaluation over large North American river basins. Journal of Geophysical Research, 112(D21) [doi: 10.1029/2007jd008674].

Quincey, D., Smith, M., Rounce, D., Ross, A., King, O., Watson, C., 2017. Evaluating morphological estimates of the aerodynamic roughness of debris covered glacier ice. Earth Surface Processes and Landforms, 42, 2541-2553 [doi: 10.1002/esp.4198].

Raleigh, M.S., Landry, C.C., Hayashi, M., Quinton, W.L., Lundquist, J.D., 2013. Approximating snow surface temperature from standard temperature and humidity data: new possibilities for snow model and remote sensing evaluation. Water Resources Research, 49(12), 8053–8069 [doi: 10.1002/2013wr013958].

Sanow, J.E., Fassnacht, S.R., Kamin, D.J., Sexstone, G.A., Bauerle, W.L., Oprea, I., 2018. Geometric versus anemometric surface roughness for a shallow accumulating snowpack. Geosciences, 8(12), 463 [doi: 10.3390/geosciences8120463].

Smith, M.W., 2014. Roughness in the earth sciences. Earth Science Reviews, 136, 202-225 [doi: 10.1016/j.earscirev.2014.05.016].

Swenson, S.C., Lawrence, D.M., 2012. A new fractional snow-covered area parameterization for the Community Land Model and its effect on the surface energy balance. Journal of Geophysical Research, 117(D21) [doi: 10.1029/2012JD018178].

Trujillo, E., Molotch, N.P., 2014. Snowpack regimes of the Western United States. Water Resources Research, 50, 5611-5623 [doi: 10.1002/2013WR014753].

Wayand, N.E., Marsh, C.B., Shea, J.M., Pomeroy, J.W., 2018. Globally scalable alpine snow metrics. Remote Sensing of Environment, 213, 61-72 [doi: 10.1016/j.rse.2018.05.012].

Tables

Table 3.1. Site locations, elevations and land cover type, all sites are located within the White River watershed during the 2019-2020 winter season. The annual precipitation is found from the Western Regional Climate Center website (https://wrcc.dri.edu/).

Site Name	Latitude	Longitude	Elevation (m)	Land Cover	Scan Frequency	Annual Precipitation (mm)	Slope	r^2	Initial z_0 (m)	Primary Roughness Feature Height (m)
Trout Farm	40.0263	-107.9386	1885	Farm field, open	Weekly	426	-0.02	0.16	0.005	0.01
Cathedral Creek	39.7825	-108.6433	1917	Sagebrush	Bi-weekly	391	-0.15	0.05	0.566	1.30
Julie Circle	40.0453	-107.9136	1945	Grass	Every storm event or melt	416	-0.04	0.68	0.040	0.35
CR11	40.1194	-107.9161	2098	Sagebrush, slope of plateau	Bi-Weekly	545	-0.05	0.73	0.066	0.46
Upper Piceance	39.7296	-107.9847	2162	Sagebrush, within large canyon	Bi-Weekly	507	-0.14	0.79	0.389	1.65
Yellow Jacket	40.1481	-107.7389	2297	Conifers, Aspen, Sagebrush	Tri-Weeks	607	-0.32	0.61	0.328	1.85
Piceance	39.8939	-108.1625	2297	Sagebrush, on top of plateau	Bi-Weekly	489	-0.11	0.45	0.114	0.68
Lost Creek	40.0514	-107.4667	2320	Grassy field	Weekly	631	-0.05	-0.28	0.009	0.13

Spring Creek	40.0339	-108.5489	2468	Pinyon-Juniper forest, on top of plateau	Monthly	546	-0.13	0.71	0.223	1.10

Table 3.2. Mean d_s and corresponding z_0 values from Piceance snow study site.

Date	d_s (m)	z_0 (m)	LN(z_0)
11/15/2019	0.000	0.137	-1.991
12/02/2019	0.163	0.121	-2.116
12/30/2019	0.335	0.124	-2.085
01/24/2020	0.356	0.058	-2.842
02/11/2020	0.503	0.029	-3.546
03/03/2020	0.380	0.051	-2.977
03/12/2020	0.140	0.121	-2.113

Figures

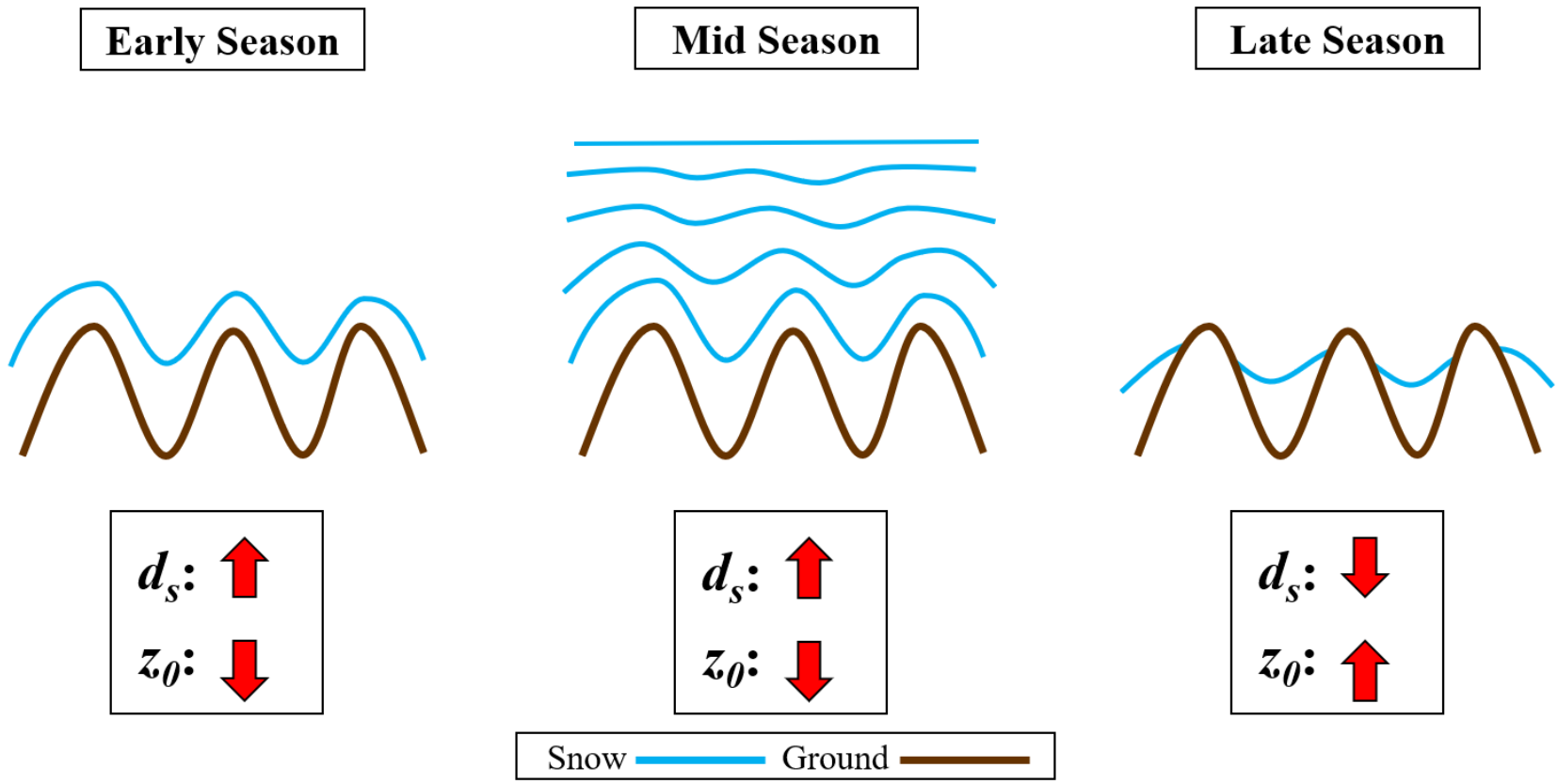

Figure 3.1. Hypothesized relation between snow depth and z_0. As the snow depth increases, the roughness feature will be enveloped and z_0 will decrease.

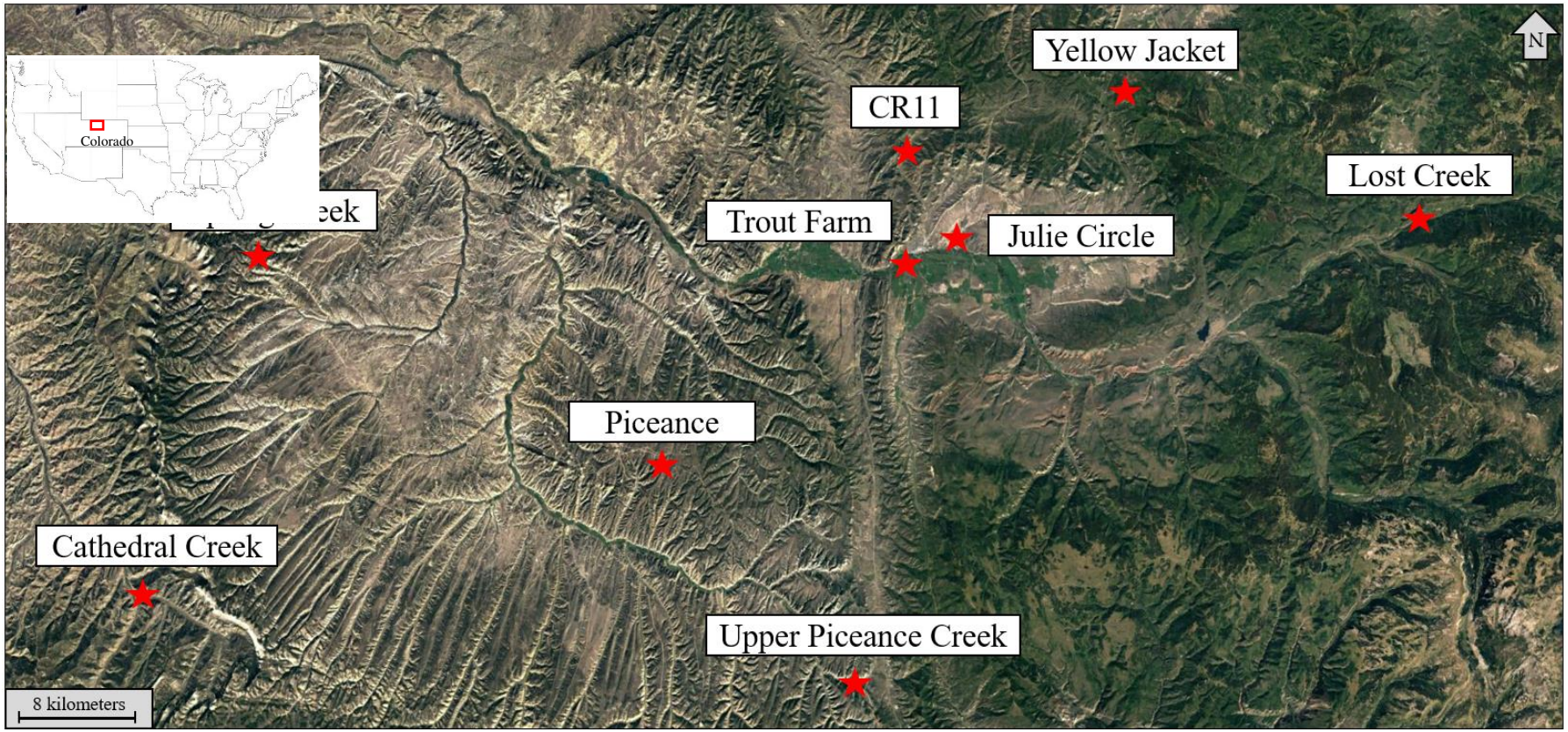

Figure 3.2. Study site locations around Northwest Colorado

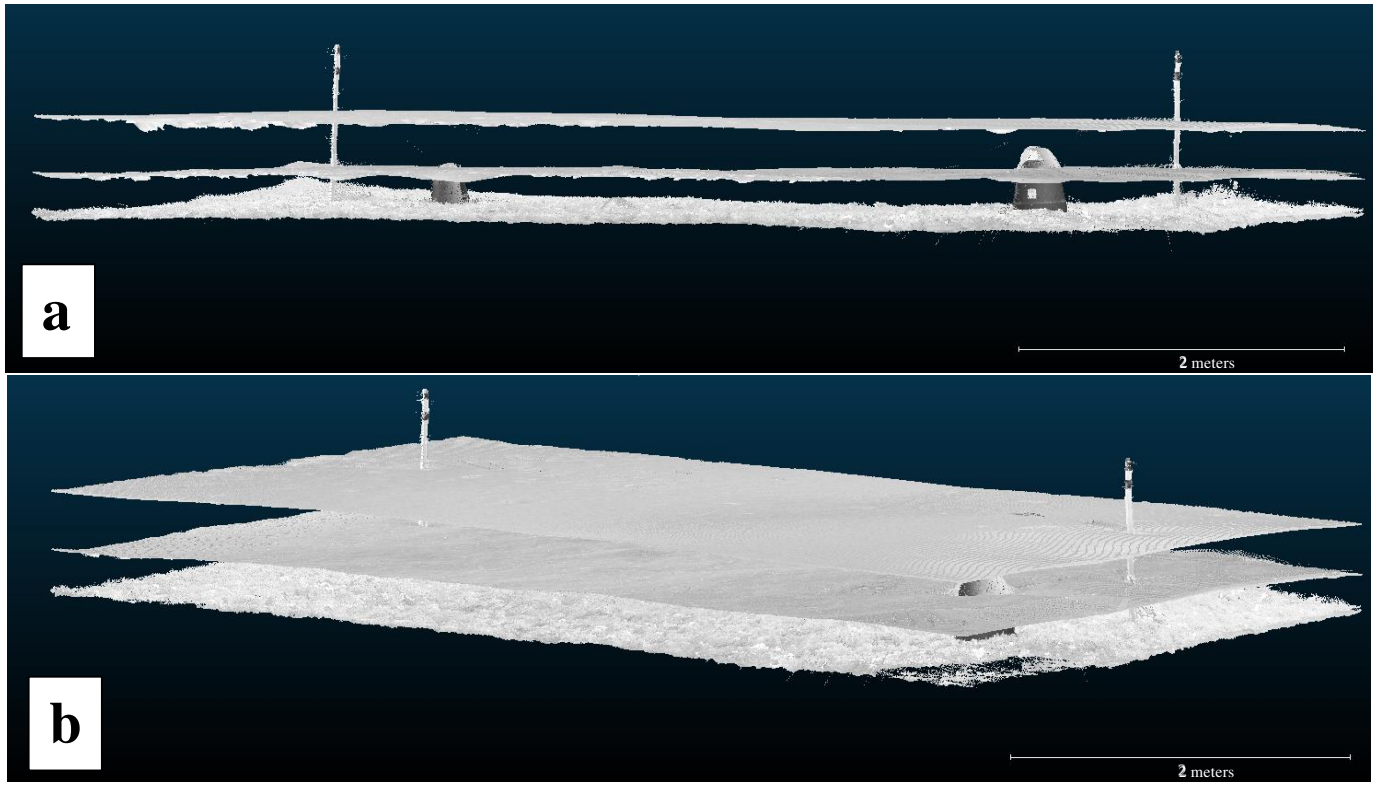

Figure 3.3. LiDAR scans from Julie Circle showing several different merged scans on top of each other demonstrating snowpack depth and decoupling from underlying surface roughness features within the AOI. a) a direct side profile view and b) a top-side view. The bottom scan (snow free) was taken on 11/25/2019 and has a z_0 value of 0.04001 meters. The middle scan is from 12/09/2019, with a depth of 0.21 meters and z_0 of 0.00419 meters. The top scan is from the largest d_s of the season, at 0.52 meters on 2/6/2020 with a z_0 of 0.00035 meters.

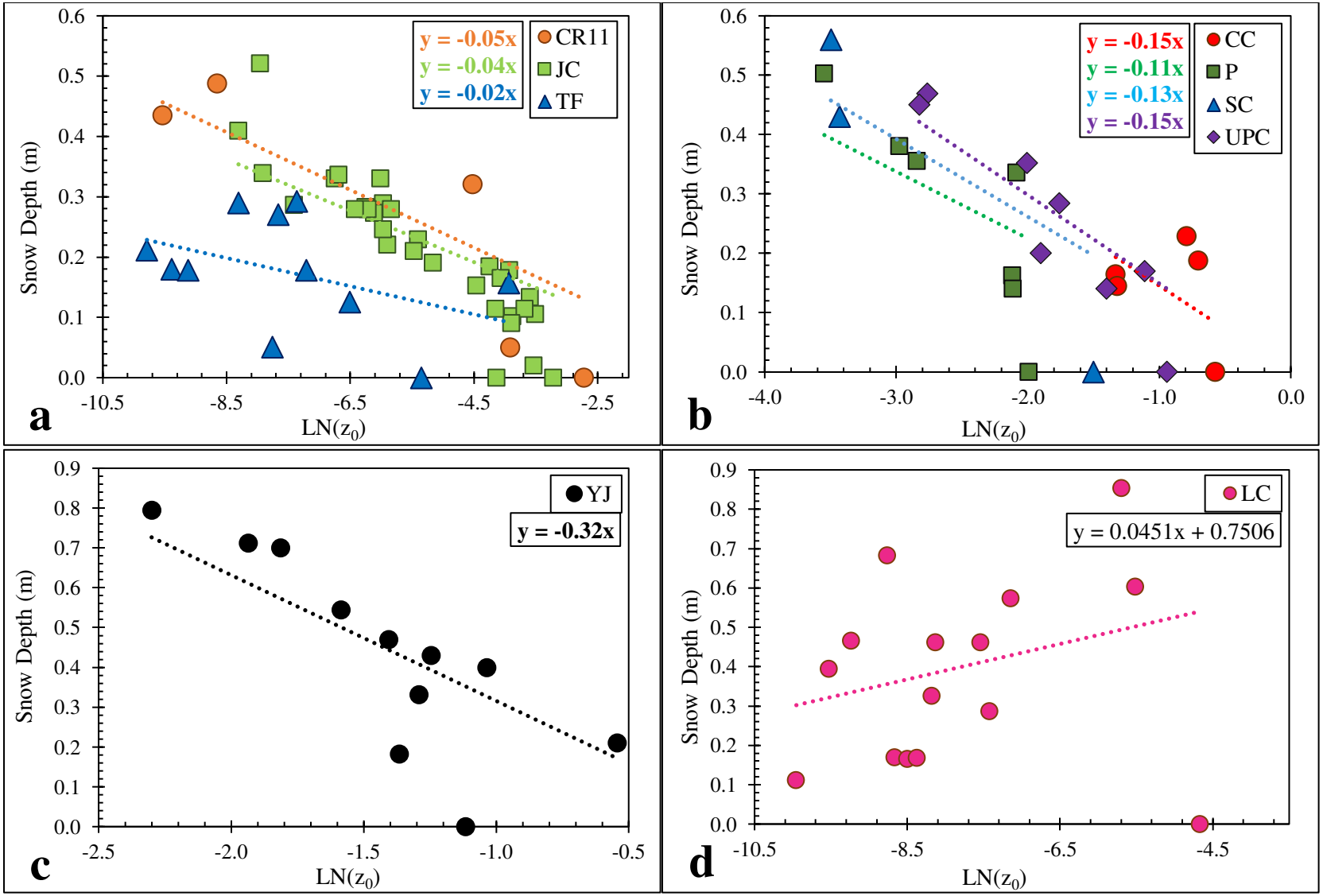

Figure 3.4. Sites grouped by similarities in the resulting slope of snow depth and ln(z_0). a) Shows CR11, Julie Circle (JC), and Trout Farm (TF). b) Shows Cathedral Creek (CC), Piceance (P), Spring Creek (SC), and Upper Piceance Creek (UPC). c) Shows Yellow Jacket (YJ). d) Shows Lost Creek (LC).

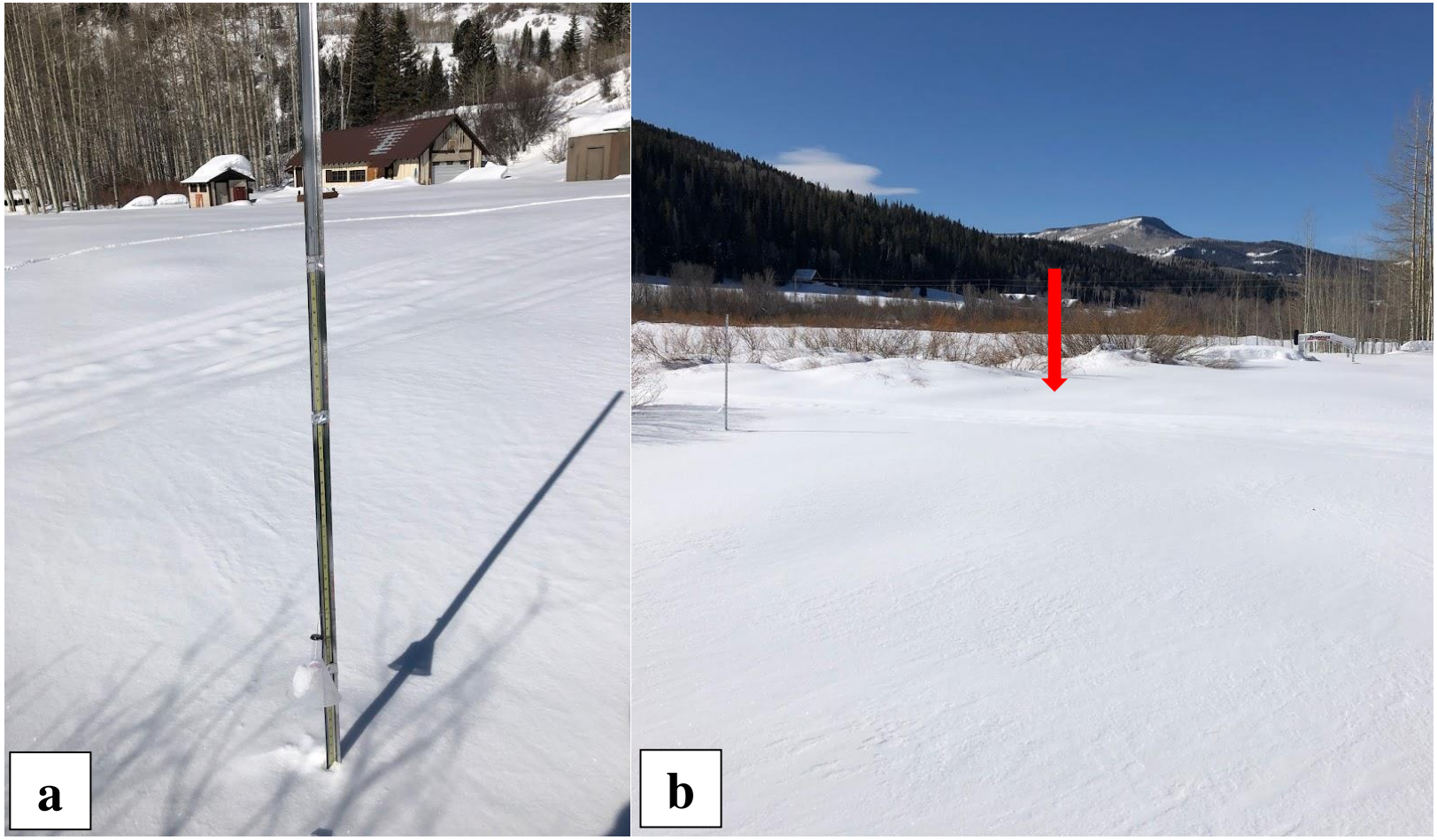

Figure 3.5. Lost Creek snow site on 02/26/2020, with a d_s of 0.85 meters and z_0 of 0.00338 meters. A) Shows a close up view of the snow stake with nearby snowmobile tracks and B) a general site view with a red arrow highlighting the snowmobile tracks.

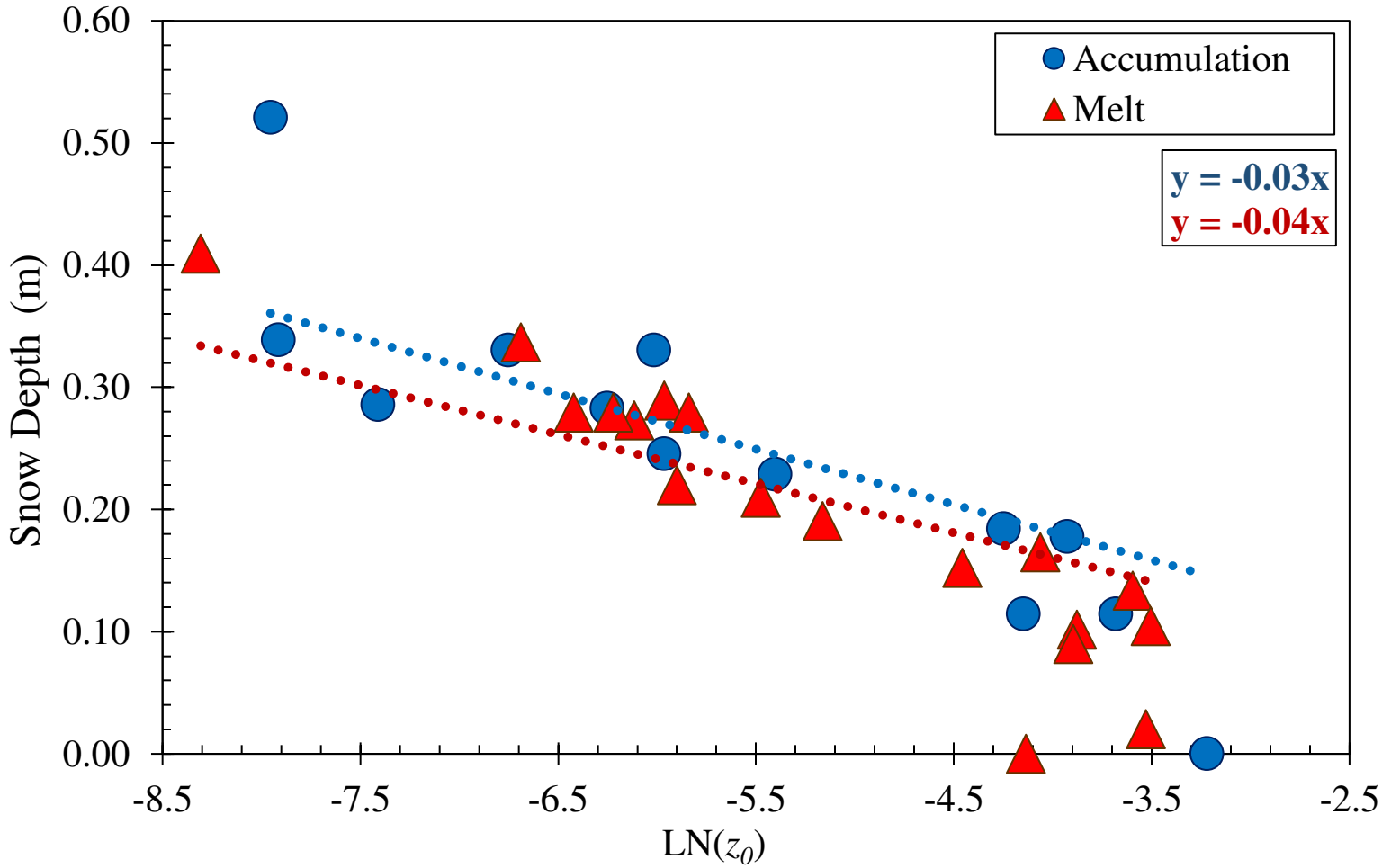

Figure 3.6. Accumulation (blue) and melt (red) values from Julie Circle. Accumulation was defined as any time where the snow depth was greater than the day before, and melt was defined as any time where snow depth was less than the day before.

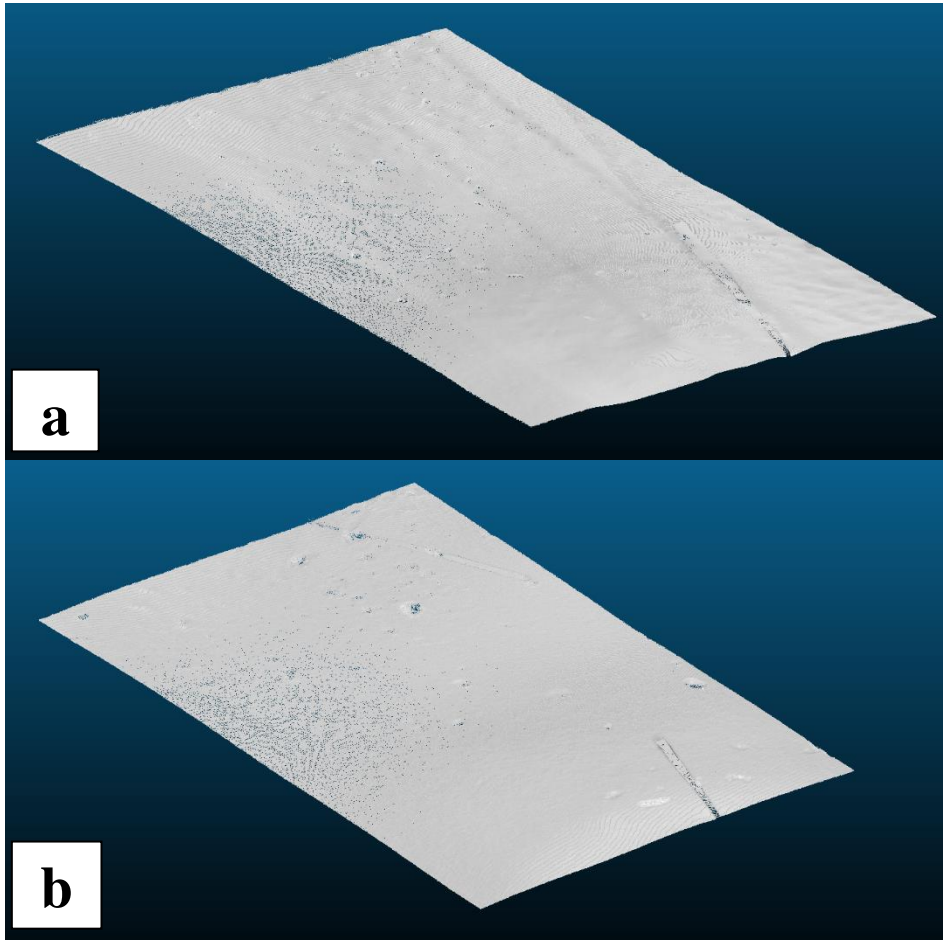

Figure 3.7. Cloud Compare images showing the Julie Circle AOI snowpack surface on a) 02/10/2020 the scan with the lowest z_0 (0.00025 meters), but the second deepest snowpack (0.41 meters), and b) 02/06/2020 the scan with the deepest snowpack (0.52 meters), but a higher z_0 (0.00035 meters).

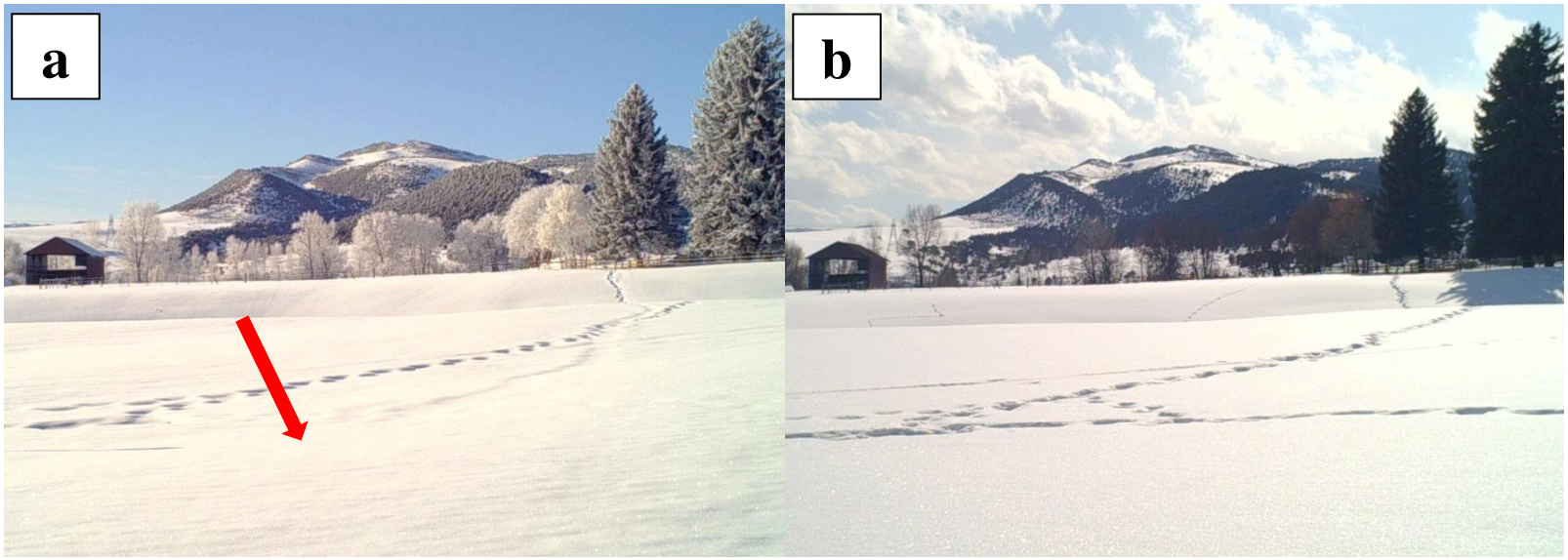

Figure 3.8. Trout Farm site game camera photos taken looking south a) on 02/10/2020 (d_s of 0.29 meters and z_0 of 0.00063 meters) showing minor variations of the snow surface topography highlighted by the red arrow and b) on 02/25/2020 (d_s of 0.29 meters and z_0 of 0.00025 meters) showing a smoother snowpack surface. Note that the footprints included in the site are not within the AOI.

Figure 3.9. Photos from two field visits to the Yellow Jacket site. a) Taken on 03/16/2020 (d_s of 0.40 meters and z_0 of 0.355 meters) recently after a snowmobile had driven through the site, plus the addition of sun cup development. b) Taken on 04/07/2020 (d_s of 0.21 meters and z_0 of 0.58083 meters) where the site had undergone extensive melt increasing the roughness. Both photos are taken from the north t-post facing south.

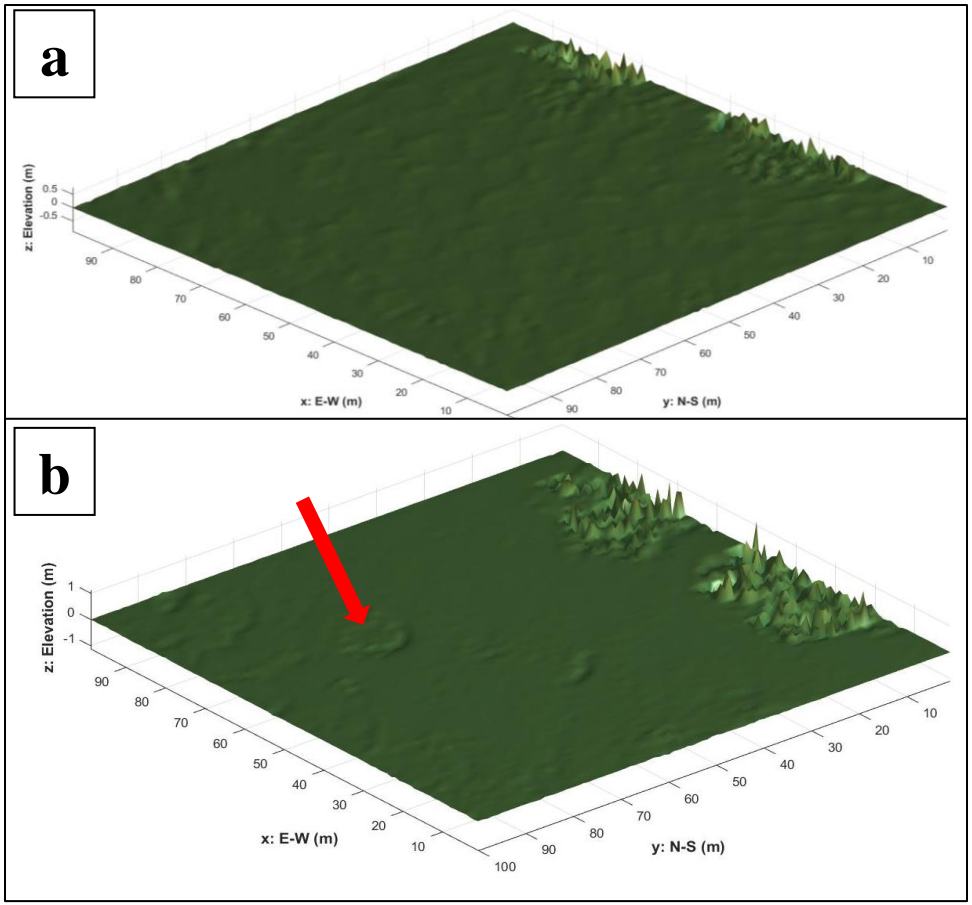

Figure 3.10. Interpolated surfaces from the Cathedral Creek site on a) 01/16/2020 with a lower d_s (0.145 meters) and a lower z_0 value (0.26797 meters), and b) on 02/24/2020 with the highest d_s recorded at the site (0.23 meters) but a very high z_0 value (0.45376 meters). The red arrow highlights the larger surface features.

4.0 RESOLUTION AND APPLICATION OF z_0

4.1 Summary

Terrestrial and airborne based LiDAR and other three-dimensional scans of the earth's surface are becoming more readily available. These data are across a range of resolutions and at varying scales, which can alter the value of aerodynamic roughness length, z_0. Inclusion of site specific z_0 values into hydrologic and meteorological models as a dynamic, instead of a static parameter, is critical to represent energy processes, and can be observed when simulating the snowpack surface using the SNOWPACK model. Results indicate that as the resolution increased, the z_0 value decreased. When these values were applied to the SNOWPACK model, smaller z_0 values (<0.002 meters) produced smaller sublimation and latent heat fluxes, and larger peak SWE, cumulative snow depths compared to larger (>0.02 meters) z_0 values. Similar trends were observed when a dynamic z_0 was applied to the SNOWPACK model, although output parameter values varied when comparing a static versus a dynamic z_0 value.

4.2 Introduction

Throughout the winter season, the snowpack becomes the interface for all atmospheric-ground interactions (Fassnacht *et al*., 2009; Gromke, 2011). Understanding and quantifying the small- and large-scale processes of the snowpack is important for hydrologic, climate, and ecological models (Blöschl, 1999; Luce *et al*., 1999; Manes *et al*., 2008; Quincey *et al*., 2017). One metric to increase understanding of the snowpack surface and improve models is the aerodynamic roughness length, z_0 (Andreas, 2002; Fassnacht, 2010; Hulstrand and Fassnacht, 2018; Sanow *et al*., 2018). The snowpack surface, and resulting z_0 value, is spatially and temporally variable due to accumulation and melt patterns, wind redistribution, land cover, aspect, meteorological conditions, and snowpack metamorphism (Niu and

Yang, 2007; Lacroix *et* al., 2008; Nield *et* al., 2013; Smith, 2014; Quincey *et al*., 2017; Sanow *et al*., 2018). This complex surface variability is present at any micro (<1-meter) or macro-scale (>1-meter) and changes based on that scale (Liston, 2004; Deems *et al*., 2006). This can lead to substantial effects on hydrologic and climate models when ignored (Liston, 2004). Current hydrologic models often do not represent the spatial and temporal variability of z_0 (Quincey *et al*., 2017), which is a significant problem when determining snow cover, snow water equivalent, and runoff quantities (Debeer and Pomeroy, 2017).

Scaling of z_0 has had limited investigation, and the scale at which z_0 can be collected is rarely similar to the scale at which hydrologic and meteorological models are run (Blöschl, 1999). This is problematic for any model resolution and/or extent, whether local, regional, or global, where an accurate depiction of snowpack surface roughness is necessary (Liston, 2004). Any data resampling or extrapolation, and along with collection methodology, can alter the resolution and scale of the data, and thus effect the model results (Blöschl, 1999). Current methods to estimate z_0 from surface geometry use terrestrial and airborne LiDAR (Lacroix *et al*., 2018; Sanow *et al*., 2018) which has data ranging in scales of ±80 mm and ±50-300 cm, respectively (Prokop, 2008; Deems *et al*., 2013; Harpold *et al*., 2014; López-Moreno *et al*., 2016; Painter *et al.,* 2016). Coarse resolutions over a larger scale may be lumped together to negate complex terrain features or combine accumulation and ablation zones leading to an incorrect representation of a study area (DeBeer and Pomeroy, 2017). Conversely, smaller scaled LiDAR data does not capture the large-scale process, which can lead to inconsistencies in the macroscale variability of the study area along with large quantities of data points (Munro, 1989; Blöschl, 1999; Fassnacht *et* al., 2014; Quincey *et al*., 2017). Small scale z_0 values are altered based on scale and resolution, potentially leading to overestimates (Quincey *et al*., 2017). The scale of the measured data needs to be considered in terms of the model scale, as this is defined as the spatial properties of the model itself, not the measurements (Blöschl, 1999).

As the availability of LiDAR and other three-dimensional scans of the earth's surface become more readily available (Deems *et al*., 2013; Nolan *et al.*, 2015; Gilbert and Fassnacht, 2017; Shaw *et al*., 2020),

the application to derive a site specific, spatially, and temporally variable z_0 is becoming more practical (Deems *et al*., 2006). As shown in Chapter 3, the snowpack surface is dynamic spatially and temporally. However, the sensitivity of varying resolutions of z_0 and its implication on models has had minimal investigation. The objectives of this study are 1) to determine how the geometrically calculated z_0 value changes with varying resolutions for typically available data (1mm, 1cm, and 1m), 2) to determine the implications of a different z_0 within the SNOWPACK model (2mm (default), 2cm, 20cm, 2m) and 3) to determine the implication of a variable z_0 within the SNOWPACK model using measured values throughout a winter season.

4.3 Methods

4.3.1 Datasets

The geometric z_0 was calculated at three different sites with different resolutions and extents (1, 10, and 1000 m) (Table 4.1). The first site, Niwot Saddle Airborne LiDAR dataset was collected on September 29, 2005 by University of Colorado at Boulder and can be found on Open Topography (https://www.opentopography.org) (ID: OTLAS.102012.26913.1). The data were downloaded as a 1000x1000 meter area with a resolution of 1 meter. The site is located south of Rocky Mountain National Park and is part of a long-term ecological study site. The Niwot Saddle ALS data were downloaded by Graham Sexstone and de-trended (Fassnacht et al., 2009) by Steven Fassnacht.

The Trout Farm terrestrial LiDAR scan was taken using a FARO Focus3D X 130 model Terrestrial LiDAR Scanner (TLS). This LiDAR tool generates a point cloud scan of a given area with an error of +/- 2 millimeters and a resolution of approximately 7.5 millimeters. The scan was taken on March 3, 2020 and consisted of an open, grassy, farm field about 3 kilometers from Meeker, Colorado city center. The site was flat with no dominate roughness features. Meeker, Colorado averages 177 centimeters of snow per year (https://www.wrcc.dri.edu). This site was the only one used for the

SNOWPACK model section of the study. There was a meteorological tower set up at the site, however, not all of the required input variables for SNOWPACK were collected. Nearby sites provided the additional data, as described in the SNOWPACK section.

Lastly, the Elm Street terrestrial LiDAR scan was taken April 16, 2021 by Steven Fassnacht. The scan area was in a residential yard of a grassy lawn surrounded by a 2 meter tall hedge. The location is within city limits of Fort Collins, Colorado which averages 119 centimeters of snow per year (https://www.wrcc.dri.edu). This particular snowfall event produced 20-30 centimeters of fresh snow in Fort Collins.

The intent is to examine coarsening resolutions of surface data, considering the initial size of the plot (Table 4.1). The LiDAR scans were processed and cropped in the open source program Cloud Compare (https://www.danielgm.net/cc/). An area of interest (AOI) was cropped out of the center area of the overlapping scans, which was a 10x10 meter plot at Trout Farm and a 1x1 meter plot at Elm Street. AOI's were then interpolated at different values using the kriging method in Golden Software Surfer (https://www.goldensoftware.com/products/surfer). The kriging method is dependent on the overall spatial arrangement of measured points. These surfaces were then run through a MATLAB code to calculate to the z_0 value. The code produces a figure of the surfaces shown in Figures 4.1 to 4.3 of Niwot Saddle, Trout Farm, and Elm Street, respectively. The figure highlights the maxima (red) and minima (blue), except for Figures 4.1a, 2a, and 3a that are too fine of a resolution to illustrate all the points.

4.3.2 SNOWPACK Model

The SNOWPACK model was developed at the Swiss Federal Institute for Snow and Avalanche Research as a response to an extreme avalanche period in February 1999 (Bartlet and Lehning, 2002). SNOWPACK is a one-dimensional physical snowpack model which numerically solves mass, energy, and momentum conservation partial differential equations (Bartlet and Lehning, 2002). Since the primary purpose of the model is for avalanche safety and research, the focus of the model is on layer formation

and evolution and surface heat exchanges (Lehning *et al*., 2000). The model uses meteorological input parameters to build a snowpack profile throughout a designated time-step (Lehning *et al*., 2002a; b).

The aerodynamic roughness length is incorporated into the surface heat flux calculations (Lehning *et al*., 2002b). Calculations for the surface heat fluxes assume a neutral atmospheric surface layer using the Monin-Obukhov similarity theory (Lehning *et al*., 2002b). To calculate the surface sensible heat flux, Q_H, the following equation is used:

$$Q_H = \frac{-ku_*}{0.74\ln\left(\frac{z}{z_0}\right)}\rho_a c_p(T(z) - T(0)) \tag{4.1}$$

where k is the von Karman constant (0.40), u_* is the friction velocity, z is the vertical coordinate where the surface of the snow is 0, ρ_a is the density of air, c_p is the heat capacity, T(z) is the temperature of the air at height z, and T(0) is the temperature of the snow surface. The latent heat equation is:

$$Q_E = -C\frac{0.622L^i\rho_a}{p_a}[e_s^w(T(z))rH - e_s^i(T(0))] \tag{4.2}$$

where L^i are the latent heat values for vaporizations and sublimation, respectively, $e_s^i$is the saturation vapor pressure (Pa) over water or ice, p_a is the air pressure, and C is the Kinematic Transfer coefficient:

$$C = \frac{ku_*}{0.74\ln(\frac{z}{z_0})} \tag{4.3}$$

The default z_0 within SNOWPACK is 0.002 meters. The second part of the study used z_0 values of 0.002, 0.02, 0.2, and 2 meters within SNOWPACK at the Trout Farm site. These values were chosen based on the default z_0 value and then increased by a factor of 10 to determine the differences of output variables from SNOWPACK. A final SNOWPACK value was run using a dynamic z_0 from measured values of the Trout Farm site. This consisted of z_0 values changing on a weekly time step within the model (Table 4.2). At present, z_0 is a parameter in SNOWPACK, i.e., the model cannot have a variable value for z_0. Therefore, to create this dynamic run, each measured z_0 value was run for the entire year.

Then, the z_0 values and resulting output values were combined for each corresponding week. For example, z_{0-1} was run for the entire year, but output values were only used for the allotted time frame of 12/01/2019-12/25/2019. Then, z_{0-2} was run for the entire year, but output parameters were only used between 12/26/2019-12/29/2019. This was done throughout the entire season, then, the output values were summed for the entire year.

4.3.3 Meteorological Data

The SNOWPACK model was used to gage the sensitivity of a static compared to a dynamic z_0 parameter over the 2019-2020 winter season at Trout Farm. The input data was from a combination of three weather stations (due to the lack of equipment available at the study site). Air temperature, relative humidity, air pressure, and verification snow heights (i.e. the manual snow depths taken) were all from the study site. Wind speed and precipitation were from the Meeker Airport ASOS station located 4 kilometers from the study site (https://mesonet.agron.iastate.edu). Incoming solar radiation data were from the Pinto RAWS station located approximately 30 kilometers from the study site (https://wrcc.dri.edu/cgi-bin/rawMAIN.pl?coCPIN). Ground temperature values were assumed to be 0°Celsius. Data were collected on an hourly time step and the model was run December 1, 2019 to March 31, 2020. Meteorological data from Trout Farm and Pinto RAWs were compared with other nearby sites in case of any erroneous data. The output variables used for comparison are sublimation, snow water equivalent, snow depth, sensible heat flux, and latent heat flux.

4.4 Results

As the resolution increased, the z_0 value decreased for all three sites (Table 4.1). The Niwot Saddle site, was the largest initial extent and therefore produced the largest z_0 values, ranging from 0.17-2.44 meters. Figure 4.1 highlights the small-scale topographic features in detail in the produced MATLAB surfaces based on the differing resolutions. There are small rocks and disparities in the

topography that are noticed in 4.1a compared to 4.1b, c. The other two sites, were predominantly grass and resulted in overall smaller z_0 values, ranging from 0.2 – 0.001 meters. Figure 4.2 and 4.3 display the three output surfaces for each Trout Farm and Elm Street from MATLAB.

The results of the first objective showed that varying resolutions can have impacts on the resulting z_0 value, however, will these difference in z_0 be substantial enough to alter results from the SNOWPACK model? Due to the lack of meteorological data at Niwot and the Elm Street site, this aspect of the study was conducted only at Trout Farm. The first grouping used z_0 values calculated for the previous section of the study based on the 0.01, 0.1, and 1 meter resolutions, which were found to be 0.26, 0.08, and 0.01 meters, respectively.

Four output values were used to observe differences, sublimation, peak SWE, latent heat, and sensible heat. Cumulative sublimation is plotted in Figure 4.4a. Overall, the runs follow the same trend until the end of January where they begin to fan out. The timing and magnitude of spikes in all runs are very similar. Peak SWE values for the 0.01 and 0.1 meter runs had very similar values of 12 and 13 mm, respectively. The 1 meter resolution run had a peak SWE value of 17 mm, which is noticeably different than the other two. Figure 4.4b shows the SWE values over the course of the study period. The 1 meter run shows much larger and longer values than the other two runs. The smaller spikes throughout the year are more similar in their magnitude and timing. Cumulative snow depth (Figure 4.4c) highlights that the 1 meter run had larger spikes than the other two runs. Overall, the cumulative snow depth values were similar to each, varying by only 3 centimeters per run. Cumulative latent heat values got progressively smaller as the resolution increased (Figure 4.4d). The timing and magnitude of the spikes are very similar between the runs. The largest difference between the runs are the periods of very small values for the 1 and 0.1 meter runs. Between 12/24/2019 – 1/15/2020 and 1/21/2020 – 2/3/2020 the 1 meter results are very small compared to the 0.01 run, which continued to have large spikes throughout this period. This is also noticed during 12/24/2019 – 1/5/2020 within the 0.1 meter run. Cumulative sensible heat values were also similar to each other across all three runs (Figure 4.4e). Similar to the latent heat in Figure 4.4d, the

sensible heat results in Figure 4.4e show the exact same low value trends for the 1 and 0.1 meter runs. All other spikes within the three runs are similar in magnitude and timing.

The next grouping of results used z_0 values ranging from 2 to 0.002 meters and a dynamic value (Table 4.2) (Figure 4.5). However, the z_0 value of 2 ended up stopping the model and therefore was not plotted with the other results. The dynamic value was calculated by incorporating measured z_0 values from throughout the 2019-2020 winter season during the appropriate times when measured. The SNOWPACK model was run from December 1, 2019 to March 31, 2020.

Cumulative sublimation rates were similar between the dynamic and 0.002 meter run with values of -16 and -14 mm, respectively. Since the 0.002 meter and the dynamic run values are in the same order of magnitude in most cases, it was expected that these values would be similar (Table 4.2). Figure 4.5a shows the cumulative sublimation plot over the year. The variable z_0 spiked early on and then leveled out, similar to the 0.002 run, except the latter spiked roughly one month later. The 0.2 and 0.002 runs started out opposite then merged together during the middle of January, a time when all values showed an overlap. From there, they followed a very similar trend with spikes of the same magnitude and timing. The peak SWE values had a similar grouping trend where the dynamic and 0.002 run had values of 0.66 and 50mm, and the 0.02 and 0.2 runs produced 17 and 13 mm, respectively. The groupings were consistent when plotted and Figure 4.5b highlight the trends. The first grouping (dynamic and 0.002) were much larger than the other two and with similar spikes, though the magnitude of these spikes were much smaller for the 0.002 values. The 0.02 run followed the same trends as the previous two, but with a much smaller magnitude. Lastly, the 0.2 run had the smallest magnitude of all and did not follow the trends of the other values.

Snow depths were the most similar between all runs, with the dynamic, ranging between 132 cm and 142 cm. The snow depth trends (Figure 4.5c) are similar to the ones discussed in SWE. Although, instead of the variable run being the largest, in this case, it was smallest and rarely followed and similarities to the other runs. Latent heat values varied considerably between all the runs. Even though the

values were very different, the overall trends were very similar between all runs (Figure 4.5d). This was because of the periods of smaller values in the data, for instance, the variable and the 0.002 run recorded very small values between 12/24/2019 – 3/4/2020. The 0.02 run had periods of small values between 12/25/2019 – 1/14/2020 and again 1/22/2020 – 2/3/2020. The 0.2 run had only a small period of small values between 1/21/2020 – 1/28/2020. Sensible heat values followed the grouping pattern similarly to SWE and sublimation. The periods of small values occurred exactly as they did for latent heat for every run (Figure 4.5e). When the data overlapped in periods of high or very low values, the trend and magnitude were often the same.

Table 4.4 highlights the percent change of each output variable compared to the default 0.002 meter run. Latent heat as most affected by a varying z_0 value and had an average change of 191%. Sublimation was the second most affected with an average of 111%, then SWE with -54%, and the least affected was sensible heat with an average of -42%. The most affected run was latent heat with a z_0 value of 0.2 meters which resulted in a percent change of 271%. The least affected run was sensible heat during the dynamic run with a percent change of only 8%.

4.5 Discussion

Each of the three sites resulted in differences between the varying resolution z_0 values. This was most apparent at the Niwot Saddle location (Figure 4.1). The 1 meter resolution (Figure 4.1a) run has a lot of fine detail within the surface, the 10 meter run shows much less fine detail (Figure 4.1b), and the 100 meter resolution run (Figure 4.1c) shows almost no details and all large topographic features have been leveled. This trend is reflected in the resulting computed z_0 values (Table 4.1). The other two sites, Trout Farm and Elm Street, produced the same trend of a decreasing z_0 with an increasing resolution. The initial z_0 values of these two study sites were much smaller due to the extent of the site being limited to one type of land cover, compared to Niwot Saddle which had complex terrain over a large area. This trend affirms

previous assumptions by Gromke et al. (2011) that if the initial resolution is coarser the z_0 value will be higher. The TLS is capable to vertically capture small scale features (vegetation, topography, rocks, land cover, etc.) for use within the z_0 geometric calculation method (Gilbert and Fassnacht, 2017). Coarse resolutions will not capture these small-scale features and therefore will not be reflected in the z_0 value (Quincey *et al*., 2017). This could cause an underestimation in resulting values; however, a finer resolution could cause overestimation (Quincey *et al*., 2017).

Even though the LiDAR from the Niwot Saddle site was able to produce a finely detailed surface of the area, the resulting z_0 value is not necessarily representative of the site. This is due to the calculation method within the MATLAB code (described in Chapter 1), in that the z_0 is averaged over the entire area. This is problematic due to the large area and variation in slope, topography, and elevation change. Instead, a z_0 derived over smaller areas within the scan (i.e. 10 square meter sections within the 1,000 square meter plot) may lead to a more likely overall z_0 value. Therefore, focusing on smaller representative plots within a study area can determine an overall z_0 to be used for the area. This could limit the capability of an ALS to areas that are more homogenous, compared to variable terrains. Overall, determining a z_0 is dependent on the site, arrangement and height of roughness features, and the goal of the study.

Post-processing of spatial data is also a factor leading to the differences in the results. For this study, the kriging method was applied for interpolation. Varying methods of interpolation or resampling could lead to potential changes in the resulting surface and change the estimated z_0 values (Blöschl, 1999). For example, Figure 4.3b shows the amount of variation within the site, with sharp peaks and troughs. In Figure 4.3c, these sharp features have been muted, therefore changing how drastic the resulting z_0 can potentially be. It is also important to consider the resolution of the measured data and the and interpolation method. For instance, a field of corn has very high roughness when considering the top of the plant to the soil surface, but the features are very skinny and tall. If the collected data is interpolated at a 1 meter scale, the definition of the corn stalks will be lost. The resulting surface will be a smoothed

average of the corn stalk height and the soil surface. In some studies, the smooth averaging technique may be acceptable, however, the end result of the study is an important factor to consider when deciding upon the post processing and data collection procedure (Blöschl, 1999; Smith 2014; Antonetti and Zappa, 2018). Another within post-processing is the detrending methodology. All sites were detrended in the x-y direction, but the Niwot Saddle data also had a cubic de-trend. The x-y detrending eliminates linear trends from the site and without it can result in larger z_0 values. The addition of a cubic detrend also removes non-linear trends, which was important in the Niwot Saddle site due to the variable topography, and without will results in a higher z_0 value. Overall, applying a site specific z_0, it must be understood the consequences of an over or under assumed z_0 value, and the scales at which it is being applied (Blöschl, 1999).

The applied z_0 values to SNOWPACK model produced very different results for each run, ranging from -42% to 191% average difference compared to the default output values (Table 4.4). This occurred even with all runs throughout the same time period and all other meteorological factor remaining constant. The first group of Trout Farm results were z_0 values that were found from differing resolution interpolations. The sublimation output was initially similar across all runs, until 1/26/2020 where they diverged. Upon investigation of field notes, it was around this time the snowpack was near its deepest value and there was a time of increased temperature along with direct sunlight. These meteorological factors heavily impact the sublimation equation used in SNOWPACK, which is one potential reason for the split. Since the 0.01 meter resolution run had the highest z_0, this resulted in the higher sublimation rates. The z_0 is incorporated into both the sensible (Equation 4.1) and latent heat (Equation 4.2). The low data values for the 1 meter and 0.1 meter resolution runs occurred at times with a generally low wind speed. It is concluded that the low values noticed in Figures 4.4d and 4.4e are due to the smaller z_0 values combined with the low winds speeds to produce smaller heat fluxes during these times. The size of z_0 has an obvious influence over these parameters, which then effect the modeled snow depth and SWE calculations. Peak SWE values and snow depths varied the least at the output parameters, though there

were still differences in results, especially with the 1 meter resolution run. This run had the lowest z_0 (0.01 meters) and resulted in the highest SWE and snow depths. A z_0 value of 0.01 meters is still much higher than the typical generalized, static z_0 value used within many models. For instance, the Community Land Model 4.0 (CLM4; https://www.cesm.ucar.edu/models/clm/) uses a z_0 of 0.0024 meters, which is a full order of magnitude higher.

The final grouping of results included z_0 values that ranged from 0.002-2 meters and a dynamic run. The 2 meter z_0 value stopped the SNOWPACK model on 1/27/2020, which was a little less than halfway through the allotted time steps. There was nothing mentioned in the literature by Lehning *et al*. (2002a; b) about a maximum z_0 value, however, 2 meters was too large. This is likely a boundary within the model that should be adjusted or removed. Especially when considering the two z_0 values found at Niwot Saddle were larger than 1 meter. The other values 0.002-0.2 meters ran within the model and produced similar results to the previous discussed trends. Sublimation values began very similar before diverging around 01/14/2020, a few days earlier than the previous group. The 0.002 meter z_0 had much lower sublimation values than the rest, although it followed very similar trends in terms of timing of spikes. In tandem with the previous grouping, the lowest z_0 values (0.002 meters and the dynamic run) produced the lowest sublimation rates. The latent and sensible heat values aligned very well with the results of the previous grouping. The periods of small values aligned with the lower z_0 values between each grouping as well. The snow depth and SWE plots matched with the previous grouping. The lower z_0 values resulted in a higher peak SWE and a cumulative snow depth value.

4.5.1 Limitations

Several limitations existed within the study as well within hydrologic models in general. Ideally, several scans over an entire area of various scales (watershed, mountain range, state, etc.) would be incorporated into the study. These larger scan areas could be coarsened to many different resolution values increasing the observations between them. Understanding the differences each resolution has and to what extent, is key in determining the correct site-specific z_0 value for a model. Without more data, it is

difficult to make a determination of the best practice in finding a site specific z_0. However, cost, time and availability of equipment are always the limiting factor for acquiring more LiDAR scans.

A very limited amount of runs within the SNOWPACK model were completed. Meteorological data collected at the Trout Farm study site was not adequate to run the model and so meteorological data from a location farther away had to be used. However, for the purpose of this study using the available data to illustrate the general patterns of a differing z_0 value was sufficient. The lack of equipment also resulted in failing to acknowledge the micrometeorology of the site, which is a potential source of error. The site was located near the base of rocky cliffs and hills which could create wind eddies, temperature reflectance, etc. The site was also near a river (within 120 meters) which will impact moisture content in the air. Similarly to Trout Farm, there were no nearby meteorological data available for the Niwot Ridge site, which would have been interesting to run through the SNOWPACK model as well to have verification in the observed trends. Even if meteorological data had been available for this site, the z_0 value of 2 meters run in the final grouping of SNOWPACK resulted in inconclusive results and so, the use of this site would not have been possible.

The variable SNOWPACK run posed a variety of limitations and was completed to highlight an overall potential outcome. A variable z_0 value is unable to be performed within the SNOWPACK model, which is why the piece-wise run was developed. However, this method breaks up the cumulative measure of the snowpack throughout the entire season, in which the energy balance is based on. This creates strange relics and outliers when plotting over the entire winter because of the fragmented nature of the run. Even though this run was not completely legitimate within the realm of mass balance, the overall story it represents highlights that a variable z_0 will produce different results.

Beyond the focus of this study are the limitation within hydrologic and meteorological models in general. These models are typically inadequate at representing the snowpack spatial and temporal variability (Liston, 2004) and one of the subsequent metrics of that limitation is the snowpack surface

roughness. These models are less physically based and rely on meteorological inputs (Fassnacht, 2010; Hock *et al*., 2017). Therefore, models will assume 100% snow coverage in a grid cell without taking topography, metamorphism, redistribution, melt uniformity and rate, or sub-grid variability into account (Liston, 2004; Niu and Yang, 2007; Fassnacht, 2010; DeBeer and Pomeroy, 2017). Snowpacks are dynamic in nature and are constantly evolving, which makes modelling z_0 extremely difficult (Liston, 2004; Gromke, 2011).

Future studies should include more sites with a more diverse range of collected LiDAR data. Models are run at different scales, climate models are 10-100 kilometers, meteorological and hydrologic models are 1-10 kilometers, and snowpack models are 10-100 meters, so running the site specific z_0 value through each type of model at different resolutions could prove to be useful. This study was limited to the ALS data that was available, though LiDAR across a larger area (10 kilometers, or more) would be useful. TLS data could be taken at a similar location to see how they may scale from each other.

4.6 Conclusions

The study explored how z_0 values change with varying resolutions and showed that there are differences between the different computed z_0 values at each resolution. It was found that as the resolution increased, the z_0 value got smaller. When these various values were applied to the SNOWPACK model, it was found that a varying z_0 value will have implications on the results of the model. The general trends showed that lower z_0 values produced smaller sublimation and latent heat values, and larger peak SWE, cumulative snow depths, and latent heat values compared to larger z_0 values.

4.7 References

Andreas, E., 2002. Parameterizing scalar transfer over snow and ice: a review. Journal of Hydrometeorology, 3(4), 417-432 [doi: 10.1175/1525-7541(2002)003<0417:pstosa>2.0.co;2].

Antonetti, M., Zappa, M., 2018. How can expert knowledge increase the realism of conceptual hydrological models? A case study based on the concept of dominant runoff process in the Swiss Pre-Alps. Hydrology and Earth Systems Sciences, 22, 4425-4447 [doi: 10.5194/hess-22-4425-2018].

Bartlet, P., Lehning, M., 2002. A physical SNOWPACK model for the Swiss avalanche warning Part I: Numerical model. Cold Regions Science and Technology, 35, 123-145 [doi: 10.1016/S0165-232X(02)00074-5].

Blöschl, G., 1999. Scaling issues in snow hydrology. Hydrologic Process, 13, 2149-2175 [doi: https://doi.org/10.1002/(SICI)1099-1085(199910)13:14/15<2149::AID-HYP847>3.0.CO;2-8].

Debeer, C. M., Pomeroy, J.W., 2017. Influence of snowpack and melt energy heterogeneity on snow cover depletion and snowmelt runoff simulation in a cold mountain environment. Journal of Hydrology, 553, 199–213 [doi: 10.1016/j.jhydrol.2017.07.051].

Deems, J.S., Fassnacht, S.R., Elder, K.J., 2006. Fractal distribution of snow depth from LIDAR data. Journal of Hydrometeorology, 7(2), 285–297 [doi:10.1175/jhm487.1].

Deems, J.S., Painter, T., Finnegan, D., 2013. LIDAR measurement of snow depth: a review. Journal of Glaciology, 59(215), 467–479 [doi: 10.3189/2013jog12j154].

Fassnacht, S.R., Williams, M.W., Corrao, M.V., 2009. Changes in the surface roughness of snow from millimetre to metre scales. Ecological Complexity, 6(3), 221–229 [doi: 10.1016/j.ecocom.2009.05.003].

Fassnacht, S. R., 2010. Temporal changes in small scale snowpack surface roughness length for sublimation estimates in hydrological modelling. Cuadernos De Investigación Geográfica, 36(1), 43 [doi: 10.18172/cig.1226].

Fassnacht, S.R., Oprea, I., Borleske, G., Kamin, D., 2014. Comparing snowpack surface roughness metrics with a geometric-based roughness length. Hydrology Days [doi: http://dx.doi.org/10.25675/10217/201064].

Gilbert, R. A., Fassnacht, S.R., 2017. Comparing fine scale snow depth measurements using LIDAR and photogrammetry. Colorado Water, May/June 2017, 2-5.

Gromke, C., Manes, C., Walter, B., Lehning, M., Guala, M., 2011. Aerodynamic roughness length of fresh snow. Boundary-Layer Meteorology, 141(1), 21–34, [doi: 10.1007/s10546-011-9623-3].

Hultstrand, D.M., Fassnacht, S.R., 2018. The sensitivity of snowpack sublimation estimates to instrument and measurement uncertainty perturbed in a Monte Carlo framework. Frontiers of Earth Sciences, 12(4), 728-738 [doi: 10.1007/s11707-018-0721-0].

Lacroix, P., Legrésy, B., Langley, K., Hamran, S. E., Kohler, J., Roques, S., Dechambre, M. 2008. In situ measurements of snow surface roughness using a laser profiler. Journal of Glaciology, 54(187), 753-762 [doi: 10.3189/002214308786570863].

Lehning, M., Bartlet, P., Brown, B., Fierz, C., Satyawali, P., 2002a. A physical SNOWPACK model for the Swiss avalanche warning Part II: Snow microstructure. Cold Regions Science and Technology, 35, 147-167 [doi: 10.1016/S0165-232X(02)00073-3].

Lehning, M., Bartlet, P., Brown, B., Fierz, C., 2002b. A physical SNOWPACK model for the Swiss avalanche warning Part III: Meteorological forcing thin layer formation and evaluation. Cold Regions Science and Technology, 35, 169-184 [doi: 10.1016/S0165-232X(02)00072-1].

Lehning, M., Doorschot, J., Bartlet, P., 2000. A snowdrift index based on SNOWPACK model calculations. Annals of Glaciology, 31, 382-386 [doi: 10.3189/172756400781819770].

Liston, G.E., 2004. Representing subgrid snow cover heterogeneities in regional and global models. Journal of Climate, 17(6), 1381–1397 [doi: 10.1175/1520-0442(2004)0172.0.co;2].

López-Moreno, J.I., Boike, J., Sanchez-Lorenzo, A., Pomeroy, J.W., 2016. Impact of climate warming on snow processes in Ny-Ålesund, a polar maritime site at Svalbard. Global and Planetary Change, 146, 10–21 [doi: 10.1016/j.gloplacha.2016.09.006].

Luce, C.H., Tarboton, D.G., Cooley, K.R., 1999. Sub-grid parameterization of snow distribution for an energy and mass balance snow cover model. Hydrological

Processes, 13(12-13), 1921–1933 [doi: 10.1002/(sici)1099-1085(199909)13:12/133.0.co;2-s].

Manes, C., Guala, M., Löwe, H., Bartlett, S., Egli, L., Lehning, M., 2008. Statistical properties of fresh snow roughness. Water Resources Research, 44(11), 1–9 [doi: 10.1029/2007WR006689].

Munro, D., 1989. Surface Roughness and Bulk Heat Transfer on a Glacier: Comparison with Eddy Correlation. Journal of Glaciology, 35(121), 343-348 [doi: 10.3189/S0022143000009266].

Nield, J. M., King, J., Wiggs, G. F. S., Leyland, J., Bryant, R. G., Chiverrell, R. C., Washington, R., 2013. Estimating aerodynamic roughness over complex surface terrain. Journal of Geophysical Research Atmospheres, 118(23), 12948–12961 [doi: 10.1002/2013JD020632].

Niu, G., Yang, Z.L., 2007. An observation-based formulation of snow cover fraction and its evaluation over large North American river basins. Journal of Geophysical Research, 112(D21) [doi: 10.1029/2007jd008674].

Nolan, M., Larsen, C.F., Strum, M., 2015. Mapping snow-depth from manned-aircraft on landscape scales at centimeter resolution using structure-from-motion photogrammetry. The Cryosphere Discussions, 9(1), 333–381 [doi: 10.5194/tcd-9-333-2015].

Painter, T., Berisford, D., Boardman, J., Bormann, K., Deems, J., Gehrke, F., Hedrick, A., Joyce, M., Laidlaw, R., Marks, D., Mattmann, C., Mcgurk, B., Ramirez, P., Richardson, M., Skiles, S.M., Seidel,

F., Winstral, A., 2016. The Airborne Snow Observatory: fusion of scanning lidar, imaging spectrometer, and physically-based modeling for mapping snow water equivalent and snow albedo. Remote Sensing of Environment, 184, 139-152 [doi:10.1016/j.rse.2016.06.018].

Quincey, D., Smith, M., Rounce, D., Ross, A., King, O., Watson, C., 2017. Evaluating morphological estimates of the aerodynamic roughness of debris covered glacier ice. Earth Surface Processes and Landforms, 42, 2541-2553 [doi: 10.1002/esp.4198].

Rees, W., Arnold, N., 2006. Scale-dependent roughness of a glacier surface: Implications for radar backscatter and aerodynamic roughness modelling. Journal of Glaciology, 52(177), 214-222 [doi: 10.3189/172756506781828665].

Sanow, J.E., Fassnacht, S.R., Kamin, D.J., Sexstone, G.A., Bauerle, W.L., Oprea, I., 2018. Geometric versus anemometric surface roughness for a shallow accumulating snowpack. Geosciences, 8(12), 463 [doi: 10.3390/geosciences8120463].

Shaw, T.E., Gascoin, S., Mendoza, P.A., Pellicciotti, F., McPhee, J., 2019. Snow depth patterns in a high mountain Andean catchment from satellite optical tristereoscopic remote sensing. Water Resources Research, 56(2) [doi: 10.1029/2019WR024880].

Smith, M.W., 2014. Roughness in the earth sciences. Earth Science Reviews, 136, 202-225 [doi: 10.1016/j.earscirev.2014.05.016].

Tables

Table 4.1. The z_0 values based on different resolution interpolations.

	Initial Extent (m)	Interpolation Resolution (m)	Grid Size	z_0 (m)
Niwot Saddle	1000x1000	1	1,000 x 1,000	2.4399
		10	100 x 100	0.4269
		100	10 x 10	0.1744
Trout Farm	10x10	0.01	1,000 x 1,000	0.2592
		0.1	100 x 100	0.0843
		1	10 x 10	0.0100
Elm Street	1x1	0.001	1,000 x 1,000	0.2055
		0.01	100 x 100	0.0817
		0.1	10 x 10	0.0026

Table 4.2. Table of measured z_0 values from the Trout Farm site over the 2019-2020 winter season. These z_0 values were used in the 'dynamic' run in the SNOWPACK model.

Dates Used	z_0 (m)
12/01/2019-12/25/2019	0.00476
12/26/2019-12/29/2019	0.00043
12/30/2019-01/01/2020	0.00149
01/02/2020-01/05/2020	0.00008
01/06/2020-01/18/2020	0.0074
01/19/2020-01/23/2020	0.00011
01/24/2020-02/03/2020	0.00006
02/04/2020-02/09/2020	0.00047
02/10/2020-02/24/2020	0.00063
02/25/2020-03/04/2020	0.00025
03/05/2020-03/10/2020	0.01948
03/11/2020-03/31/2020	0.00476

Table 4.3. SNOWPACK results from Trout Farm. The plot was interpolated with the same resolution (0.1 meters) unless otherwise noted by parentheses.

z_0 Value (m)	Sublimation (mm)	Peak SWE (mm)	Sensible Heat (MW/m^2)	Latent Heat (MW/m^2)
0.002 (Default)	-14	50	3.5	-1.7
0.010 (1m)	-28	17	1.9	-4.6
0.020	-30	17	2.1	-4.8
0.084	-33	13	1.9	-5.7
0.200	-35	13	1.5	-6.3
0.259 (0.01m)	-39	12	1.5	-6.4
2.000*	95	57	-1.3	-2.6
Dynamic	-16	67	3.2	-1.8

Table 4.4. Percent change of SNOWPACK results from the default (0.002 meter) value.

SNOWPACK Run	Sublimation	Peak SWE	Sensible Heat	Latent Heat
0.02	112%	-66%	-40%	184%
0.2	143%	-74%	-57%	271%
Dynamic	12%	32%	-8%	7%
0.01	174%	-76%	-58%	275%
0.1	129%	-74%	-44%	238%
1	97%	-66%	-44%	170%
Average	111%	-54%	-42%	191%
Standard Deviation	0.5524	0.4235	0.1833	1.0002

Figures

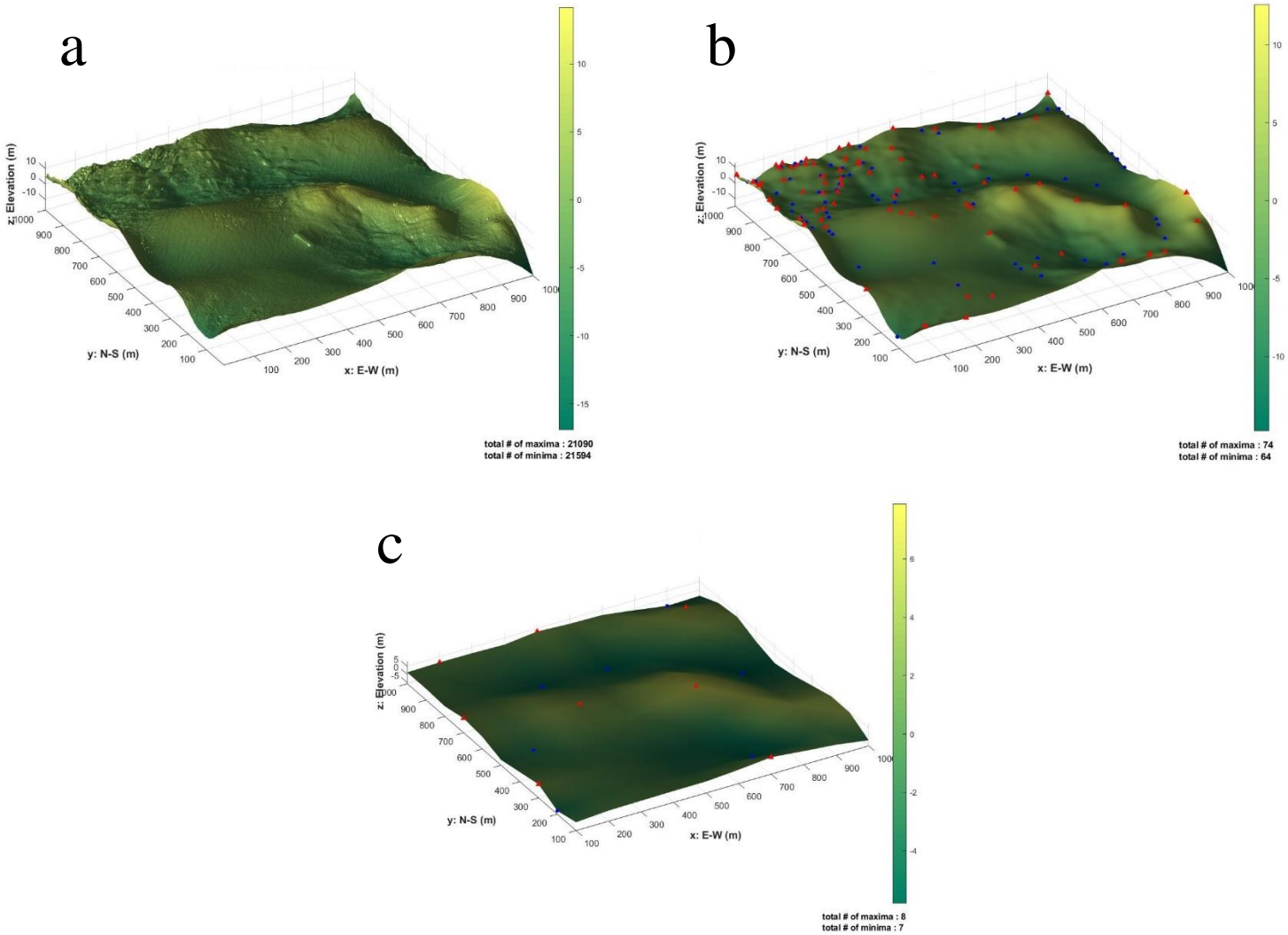

Figure 4.1. Interpolated surface of the Niwot site at three resolutions, a) 1 meter, b) 10 meter, and c) 100 meter.

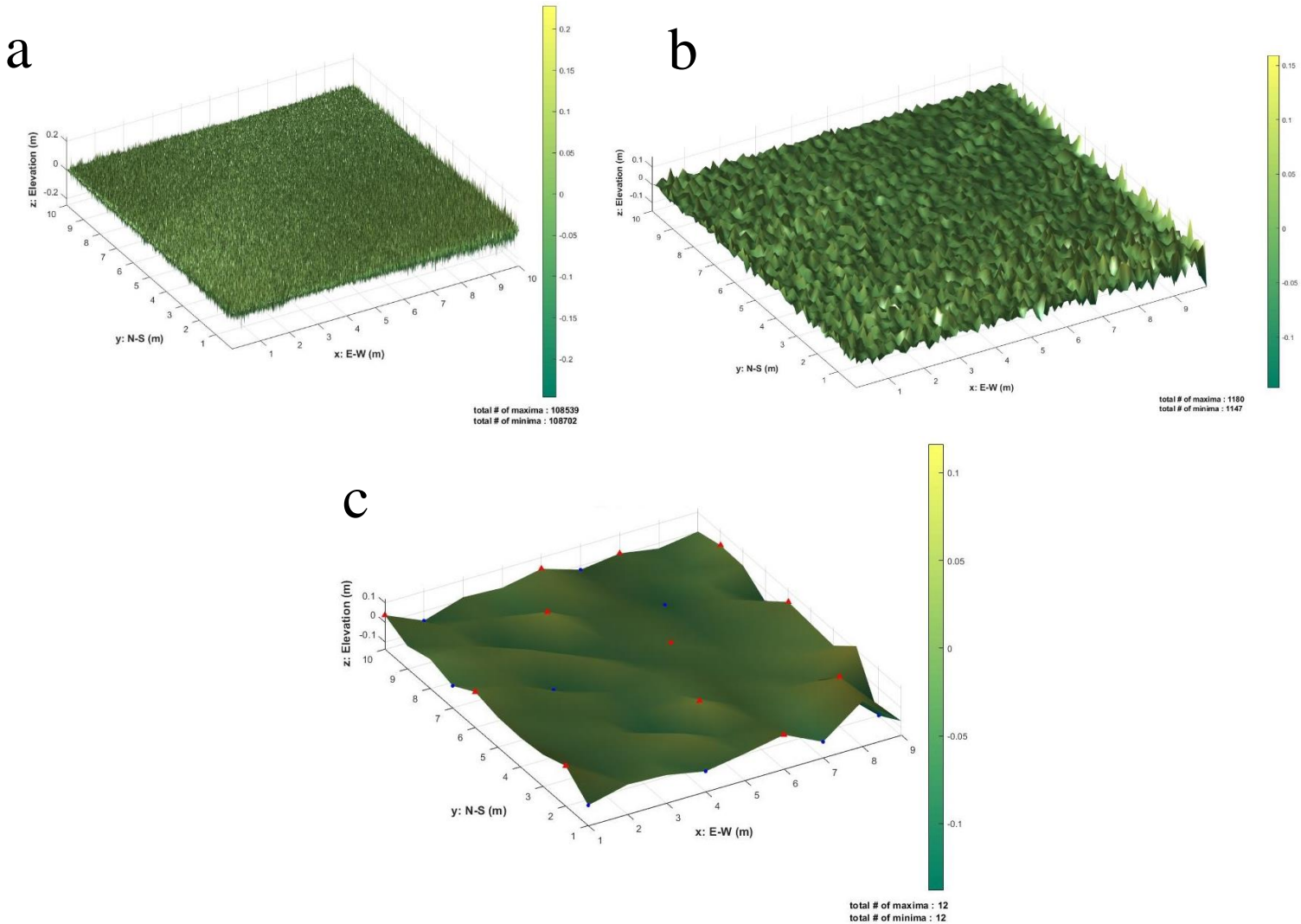

Figure 4.2. Interpolated surfaces of the Trout Farm site at three resolutions, a) 0.01 meters, b) 0.1 meters, and c) 1 meter.

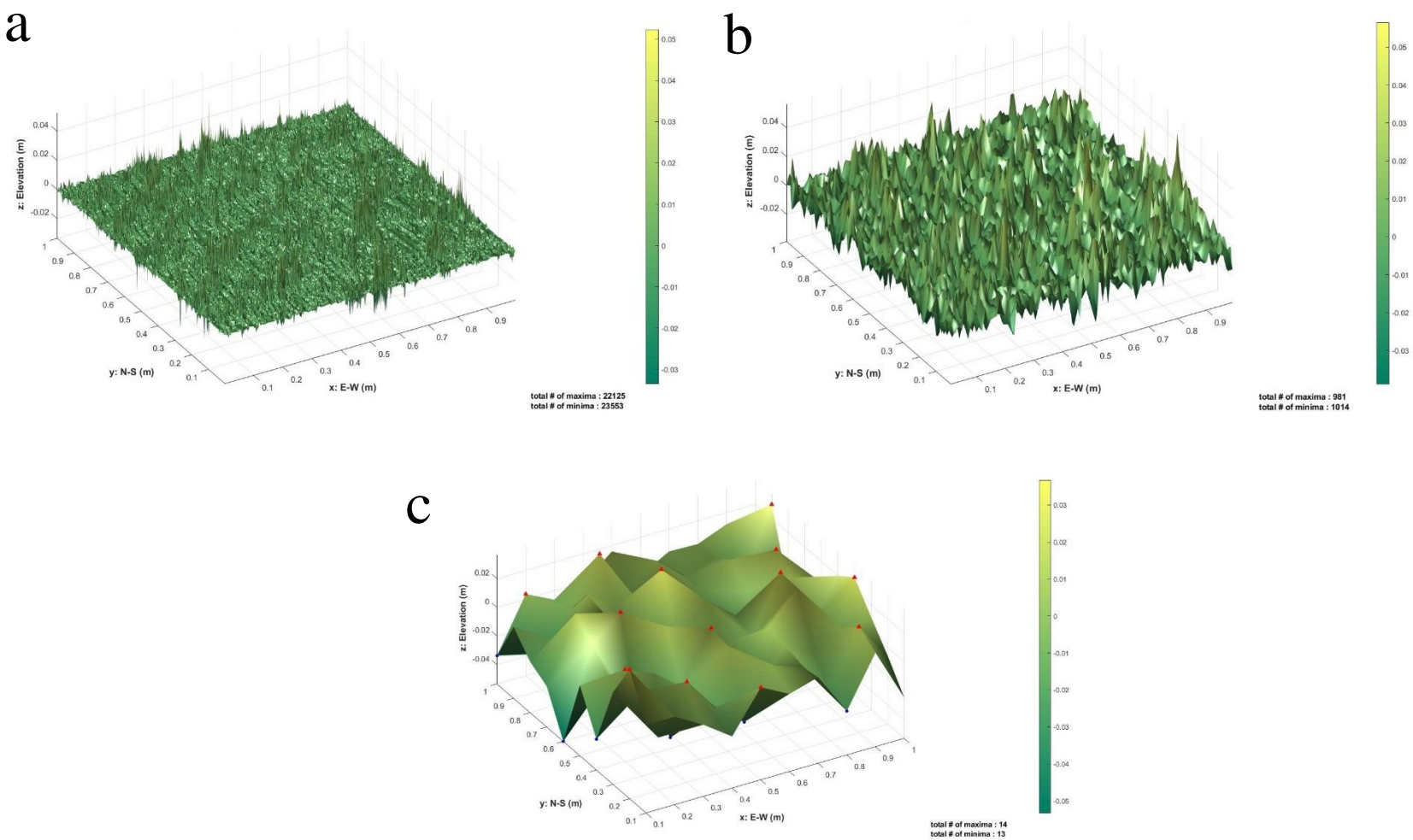

Figure 4.3. Interpolated surfaces from the Elm Street study site of a) 0.001 meters, b) 0.01 meters, and c) 0.1 meters.

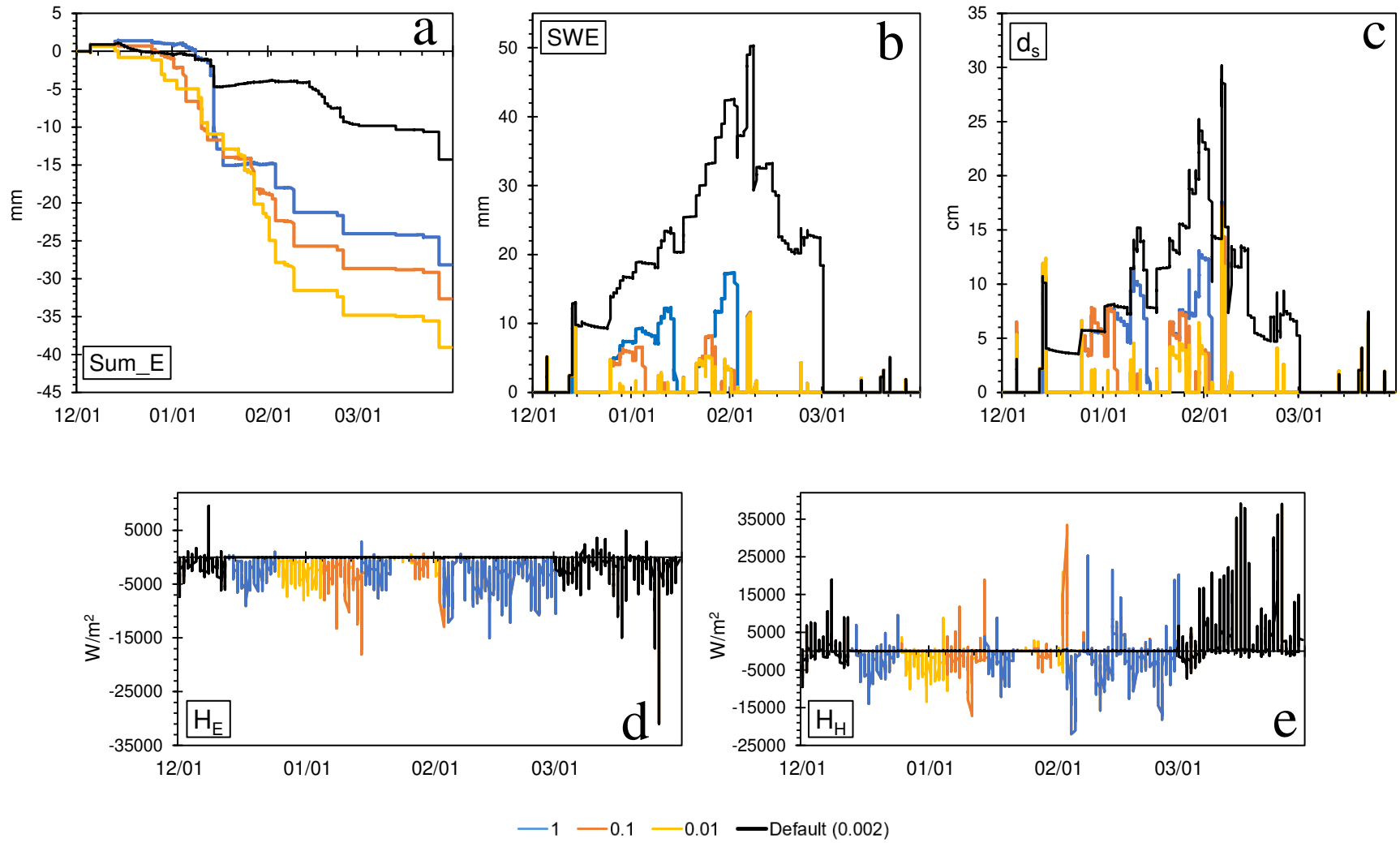

Figure 4.4. SNOWPACK results from the Trout Farm site using z_0 values computed from varying resolution interpolations which resulted in z_0 values of 0.259 meters (0.01 meter resolution), 0.08 meters (0.1 meter resolution), and 0.01 meter (1 meters resolution). The SNOWPACK outputs are from a) cumulative sublimation, b) SWE, c) snow depth, d) latent heat, and e) sensible heat.

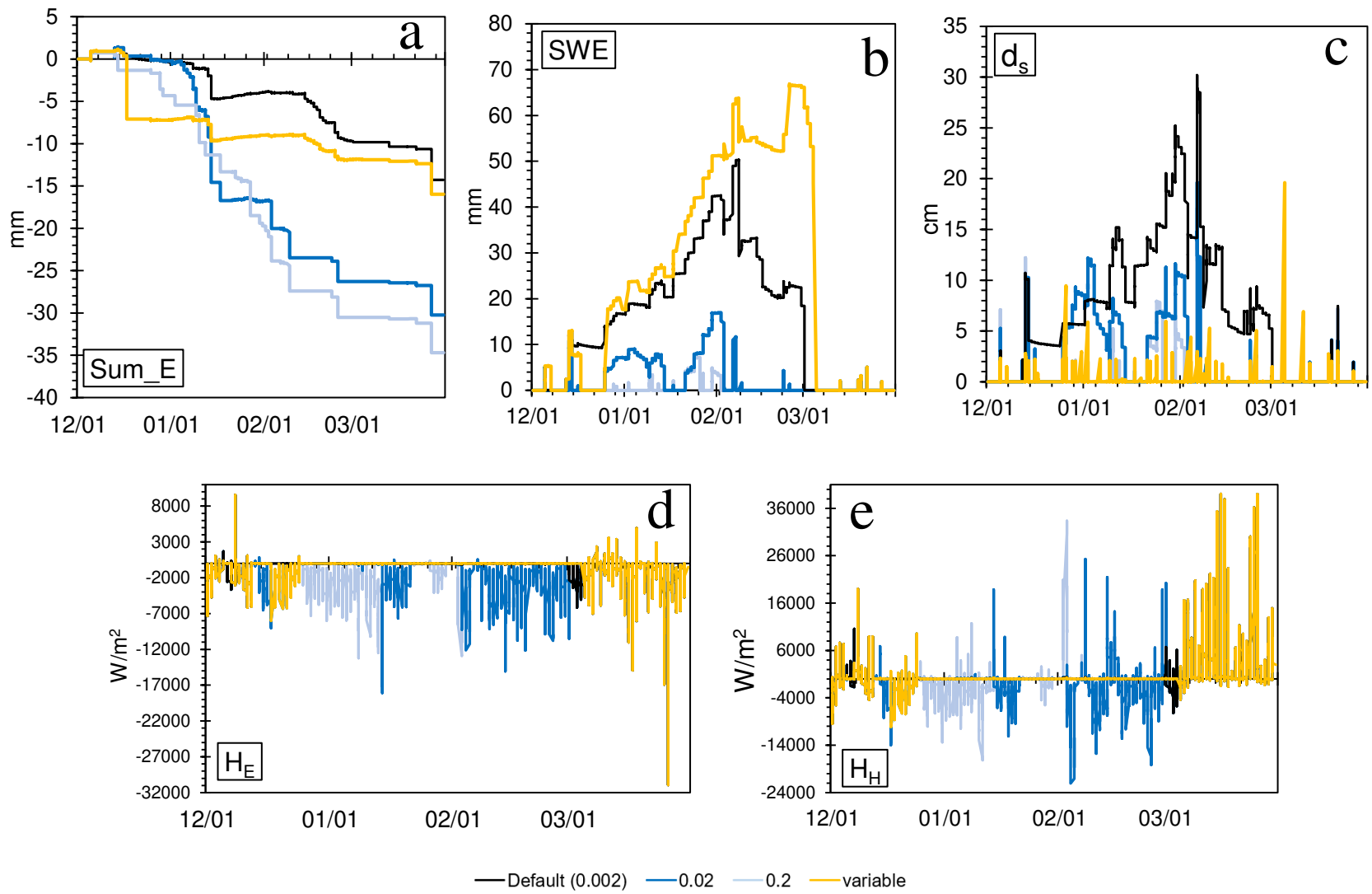

Figure 4.4. SNOWPACK results from the Trout Farm site using 0.002, 0.02, 0.2 meters, and a dynamic z_0 values from the outputs of a) sum of sublimation, b) SWE, c) snow depth, d) latent heat, and e) sensible heat.

5.0 DISCUSSION

5.1 Study overview and objectives

The primary goal of this research was to examine the spatial and temporal variability of the aerodynamic roughness length and the relevance thereof to hydrological processes. The inclusion of a variable as opposed to a static z_0 within climate, snowpack, and hydrologic models will improve model representation of processes (Fassnacht, 2010; Gromke, 2011; Miles et al, 2017; Hultstrand and Fassnacht, 2018). Chapters 2 through 4 examined how to measure z_0, the variation of z_0 as a function of snow depth, and the implications of incorporating a dynamic z_0 into a snow model rather than the current use of a static z_0.

The values of z_0 computed from surface geometry were found to be similar to those computed from the anemometric method (Figure 2.2). Out of 30 correlating LiDAR and anemometric wind profiles, the $z_{0\text{-}G}$ values underestimated in 12 out of 30 profiles, overestimated in 14 out of the 30 profiles and were almost exact in 4 out of the 30 profiles. The Nash-Sutcliffe Coefficient of Efficiency was 0.75, the r^2 was 0.96, the linear regression best fit slope of 0.98, and a Root Mean Square Error of 8.9 millimeters. However, the anemometric method requires a meteorological tower and primarily uses wind speed data from anemometers, temperature, and relative humidity sensors. Four or more anemometers are required to create a proper wind profile, though they are subject to over estimating the speed during gusty events (Gromke, 2011). Sonic anemometers and eddy covariance are preferred for wind profile studies (Sexstone *et al*., 2016), but are more expensive. This elaborate set up limits the uses to locations where the necessary measurements exist or a tower can be established with no obstacles upwind from the placement of the tower (Lettau, 1969). The geometric method has greater spatial applicability as is identifies surface roughness elements from surface geometry (Lettau, 1969); measurements of the surface are becoming much more available. Airborne and terrestrial LiDAR measurement of the Earth's surface, specifically of

the snowpack surface, have become more readily available over the past two decades (Hopkinson et al., 2004; Deems *et al.*, 2013; Harpold *et al.*, 2014; Revuelto et al., 2014; López-Moreno *et al.*, 2015). More recently photogrammetry from camera in aircraft (Nolan et al., 2015), unmanned aerial vehicle (Bühler *et al.*, 2016), or satellite imagery (Shaw *et al.*, 2019) have been used to map the snow surface. Interestingly, all these applications (in the aforementioned citations) have mapped snow depth, by differencing the snow surface from the snow off, or ground, surface. Here, terrestrial (and in chapter 4 airborne) LiDAR was used to map the snow surface. Thus, using maps of the snow surface enables application the geometric method to estimate z_0 over much larger areas than are available with the anemometric method, further enhancing the ability to capture the spatial and temporal of z_0. There is much variability in the snowpack (Bales *et al.*, 2006; Deems *et al.*, 2013; López-Moreno *et al.*, 2015), among various scales (Blöschl, 1999), including for snow roughness (Figure 3.3) (Brock et al., 2006; Fassnacht et al., 2009b; Sanow et al., 2018). Due to the strong correlation between the anemometric and geometric derived z_0 values, the geometric method was used throughout the remainder of this study.

The snowpack is not homogenous throughout the winter season and the snowpack depth and surface will vary (Niu and Yang, 2007; Kukko *et al.*, 2013; Smith, 2014). The spatial and temporal variability of the snow surface can be characterized using z_0. Thus, the correlation between z_0 and snow depth needs to be further explored (Niu and Yang, 2007; Fassnacht *et al.*, 2009a; Fassnacht *et al.*, 2009b). Once the geometric method was established as an effective method to measure z_0, the correlation between z_0 and snow depth (d_s) was examined. This correlation was observed at all unaltered study sites, and varied both spatially and temporally. The initial roughness of the sites and the primary roughness feature influenced the z_0-d_s correlation with the slope ranging between -0.05 to -0.32 and the initial z_0 values to range between 0.005 to 0.57 meters (Table 3.1; Figure 3.3). This was likely due to land cover and underlying topography, reducing z_0 as the snowpack developed (Niu and Yang, 2007; Fassnacht *et al.*, 2009a; Fassnacht *et al.*, 2009b). If the land cover, i.e., snow-free z_0, is known, then the z_0-d_s correlation could be applied as dynamic variable with the minimum z_0 occurring when max snow depth envelopes all

roughness features. These relations can be developed for areas with similar land cover, snowpack cover, and depth. However, where possible, the correlation should still be determined for any specific study area (Fassnacht, 2010). The z_0- d_s correlation can be disrupted in the presences of external factors, such as the altering of the snow surface due to anthropogenic and ecological influences such as recreational activities, wildlife tracks, vegetation snow loading, etc. (Figure 3.4, 3.8). Overall, the inclusion of a dynamic z_0 will improve process representation in hydrologic models since it is currently considered a static parameter (Manes *et al.*, 2008; Fassnacht *et al.* 2009a; DeBeer and Pomeroy, 2017; Sanow *et al.*, 2018).

Periods of accumulation and to periods of melt were compared at Julie Circle. This affected the z_0-d_s correlation by altering the slope of the trendlines by -0.01 (Figure 3.5). This further highlights the existence of hysteresis in snowpack processes (Davidson, 2004; Luce and Tarboton, 2004; Swenson and Lawrence, 2012; Magand *et al*., 2014). During snowmelt, the surface of the snowpack tends to be rougher, implying a larger z_0, (Fassnacht et al., 2009a), especially with the presence of various melt features, such as meltwater rills at the surface or sun cups (Mitchell and Tiedje, 2010). This variation between melt and accumulation indicate that it should be included in hydrologic, snowpack, climate, and meteorological models to estimate z_0. Further, other snow roughness features form, especially in the presence of wind, such as sastrugi (Kochanski et al., 2018), and these can dramatically alter z_0. While not addressed in this research, wind-induced snow roughness features tend to recur in similar locations (Filhol and Sturm, 2015) and thus their evolution in terms of z_0 could be estimated.

Snowpack processes occur over large and small scales (Blöschl, 1999; Luce *et al*., 1999; Manes *et al*., 2008; Quincey *et al*., 2017). Current hydrologic models rarely represent the spatial and temporal variability of the snowpack, and consequently, z_0 (Quincey *et al*., 2017). Using a static z_0 value for snow, instead of a dynamic value, can lead to over or underestimations in model outcomes (Figures 1.6, 4.4 and 4.5) (Luce et al. 1999; Manes et al., 2008; DeBeer and Pomeroy, 2017). To better understand the limitations of using a static z_0, several model runs were completed using SNOWPACK at varying scales and resolutions. The interpolation resolution was found to have a substantial effect on the z_0 value. As

resolution values increased, the z_0 decreased (Table 4.1). Changing z_0 by just an order of magnitude (or less) led to varying SNOWPACK output results of sublimation, peak SWE, snow depth, sensible, and latent heat values (Figure 4.4). The trends show that a lower z_0 value produced smaller sublimation and latent heat values, and larger peak SWE, cumulative snow depths, and latent heat values compared to larger z_0 values. These results indicate that the resolution of the measurement and of the post-processing needs to be considered when applying z_0 in a hydrologic model.

5.2 Implications of findings

Globally, up to 66% of area is covered in a shallow, seasonal snowpack (Sturm and Liston, 2021). These snowpacks vary spatially and temporally, based on local, regional, and global weather and climate (Sturm and Liston, 2021). As of now, these snowpacks are modeled as static and homogenous, as opposed to a dynamic, accurate representation (Liston, 2004; Debeer and Pomeroy, 2017). Not all physical properties and processes of these snowpacks are being represented, which cause these models to be less accurate (seDebeer and Pomeroy, 2017; Quincey *et al.*, 2017). For example, Hulstand *et al.* (2018) found sublimation uncertainty rates can vary 1-29%, and z_0 was one of the top three variables accounting for this uncertainty. Sexstone *et al.* (2018) found that simulated sublimation rates can vary between 15-35% based on the land cover type. Sublimation, energy fluxes, snowpack properties and metamorphism, etc., are all connected to the surrounding topography and land cover, and should be modeled as such.

The implications of this research have potential uses for several aspects of the hydrologic cycle. The z_0 is one metric to represent the surface-atmospheric interface, which is necessary when modeling the snowpack. Using a developed, robust z_0, we can enhance model outputs of the heat exchanges at the snowpack surface. This improves the accuracy of all aspects of the model which are controlled by this air-snow heat transfer within the energy budget (Lacroix et al., 2008; Manes et al., 2008). Sublimation is one variable that is highly dependent on accurate latent and sensible heat fluxes (Fassnacht, 2010). Most

studies involving sublimation are limited to point scale measurements (Sexstone *et al*., 2018). Additionally, many of these studies, such as SNOTEL locations, are in open areas within forest, as opposed to open areas or areas above tree line (Landry *et* al., 2014; Sexstone *et al*., 2018). SNOTEL stations are underrepresented at high elevations and over-represented in forested environments (Fassnacht *et al*., 2012; Harpold *et al.,* 2012; Sexstone and Fassnacht, 2014). Open, alpine sites have increased wind speeds which enhances redistribution and sublimation rates (Hock *et al*., 2017). Exclusion of these areas that are highly susceptible to increased sublimation rates can underestimate total sublimation loss. Sublimation is an important factor within water balance models and has been found to contribute to an average of 28% loss in the Colorado Rocky Mountains (Sexstone *et al*., 2018). A spatially and temporally based z_0 value will aid in these calculations as it is a necessary variable within the sublimation computation (Fassnacht, 2010).

The snowpack directly affects all aspects of the hydrologic cycle and is crucial as a freshwater reservoir (Clow, 2010; Dutra *et al*., 2010; Magand *et al*., 2014; Huss et al., 2017; Wayand et al., 2018). The need for understanding and quantifying every aspect of the hydrologic cycle is increasingly important due to global climate change (Bales *et* al., 2006; Harpold *et al*., 2012). The spatial and temporal variability of the snowpack highlights the variability of the mass and energy balance, which is key to predicting possible impacts on water resources (Harpold et al., 2012). Bathurst and Cooley (1996) varied z_0 from 0.001 to 0.003 meters and found a 30% increase in total runoff volume due to increased snowmelt related to the turbulent exchange.

Small scale roughness features (<1 km) have had limited studies, and the resulting sub-grid variability within models has been ignored (Manes et al, 2008; Magand et al, 2014). The sub-grid variability is critical when modeling the turbulent heat fluxes (Magand et al, 2014). One reason for the lack of inclusion in models is because of the difficult nature of measuring roughness and the limitations of access throughout the winter season (Lacroix *et al*., 2008). The addition of a z_0-d_s correlation within the land surface scheme could enhance these predictions, even with limited temporal data. Models use 100%

coverage as opposed to snow covered fraction, even in complex terrain (Debeer and Pomeroy, 2017). This study showed that the snowpack melt rates are different than the accumulation. Additionally, melt and accumulation rates are also affected by the initial roughness value due to topography and land cover. Ignoring this variability will decrease the accuracy of the model (Liston, 2004; Debeer and Pomeroy, 2017).

Spatial and temporal variability have been discussed within this research, both have notable implications, however, spatial variability in the context of a shallow, seasonal snowpack may be slightly more consequential. The snowpack will be impacted by the land cover of the surface. For example, the type of forest (boreal, montane, etc.) and its density will impact the amount of intercepted snowfall (Pomeroy *et al*., 1998). This study was conducted primarily on open, arid plots with little interference by large trees (with the exception of Julie Circle). It was shown that the variation in land cover impacted the amount of snow on the ground and the ability to capture z_0 using a LiDAR. Within a dense forest setting, a terrestrial or airborne LiDAR may not be able to capture all the variations within the snowpack due to the interference from the trees. The snowpack tends to exhibit some amount of temporal repeatability (Pflug and Lundquist, 2020), and therefore once a site has been observed, even for a limited amount of time (1-2 seasons), temporal characteristics can still be incorporated into a study.

Surface roughness has been explored within other fields of hydrology, such as glaciology (Munro, 1989; Brock *et al.*, 2006; Miles *et al*., 2017; Quincey *et al*., 2017). During the summer, or melt season, glaciers are typically rough with exposed crevasses. These large scale roughness features enhance the turbulent heat exchanges between the air and the glacier which drive melt rates (Smeets and van den Broeke, 2008; Quincey *et al*., 2017). During the winter season, these rough areas are covered in fresh snow and roughness decreases (Brock *et al.*, 2006). Understanding and measuring glacier mass balance is becoming more critical as glacier retreat is more prominent, especially during the melt season (Brock *et al.*, 2006; Smeets and van den Broeke, 2008; Quincey *et al*., 2017).

Another field of the hydrologic processes affected by z_0 is calculated albedo measurements. Using the results from the SNOWPACK model within this study albedo was calculated for the 2019-2020 winter season at Trout Farm (Figure 5.1). The albedo was calculated for each of the varying resolution runs as well as the variable z_0 run. The 0.01 resolution run had the highest of all calculated incoming shortwave radiation. This run also produced the highest z_0 value of 0.259 meters. The variable run produced the lowest albedo, and also had the lowest z_0 values ranging between 0.019-0.00006 meters. As climate change progresses, the snowpack duration (and resulting albedo) is getting shorter (Anttila *et al*., 2014; Minder *et al*., 2018). Proper modeling of this process using z_0 is necessary to understand the full extent of potential warming due to reduction in snowpack depth and duration that is being observed (Minder *et al*., 2018).

5.3 Limitations and future opportunities

Weather and location were limitations in this study. The ARDEC data were collected for two years and rarely was there much snow (deeper than 15 centimeters) with correlating high wind (>4 m/s). Data collection was attempted during storm events; however, the high wind speeds blew away most of the snow resulting in a lack of measurable accumulation rates. Data collection during calm snow events, returned no correlating high wind speeds, i.e., reducing the data available for chapter 2 (Figure 2.2). The meteorological tower was then moved to Northwest Colorado for the remainder of the study. Wind there also stayed very low due in part to the placement in a farm field near a large sandstone wall ~0.4 kilometers away. The location was chosen based on land owner permission. Other fields were active with livestock during the winter. Ideally, future studies could place a tower in a location where wind speeds reach >4 m/s and also received enough snow that immediate wind caused redistribution is less of an issue. The anemometers in this study were also a limitation throughout data collection. At ARDEC two of the five anemometers stopped working, one was able to be fixed, the other was not. A similar problem occurred at the Trout farm site, one of the anemometers stopped working mid-season and it was

unfixable. Since funding was very limited in this study, sonic anemometers were not used; in future work, these could be deployed for better reliability during concurrent scans.

Field data collection in this study only used snow surface data from one short-distance TLS unit; other TLS units can collect much more data (López-Moreno et al., 2017). Future studies could use other three-dimensional surface scanning methods, such as ALS and photogrammetry, to recreate the z_0-d_s correlation. ALS can cover much larger study areas. Study sites can be divided in land cover types and larger swaths could be recorded during ALS flights (Bühler *et al*., 2016; Painter et al., 2016). Future studies could increase the scan frequency to improve the temporal coverage of scans. Another potential for increased temporal coverage is with the use of unmanned aerial systems (UASs). UASs are able to capture snowpack variability in areas not accessible from the ground, are cost-effective, and can cover larger areas (Bühler *et al*., 2016). At easily accessible study sites, especially during snowfall events, scanning several times a day would be improve quantifying the z_0-d_s correlation. Frequent scans would also improve the hysteresis correlation between melt and accumulation. Future studies would build on the data collected during this study (Table 5.1).

Inclusion of spatial and temporal z_0 within models does not have to be limited to the snowpack surface. It could be used for any surface that is the ground-atmosphere boundary. Future studies could observe z_0 in relation to evapotranspiration in agriculture and ecological processes (Harpold *et* al., 2012). For example, water yield in post-disturbance watersheds (i.e. burn scars) are critical for modeling flood quantities and determining flood mitigation strategies (Goeking and Tarboton, 2020). Having pre- and post- z_0 values of these watershed can improve the hydrologic models. Another opportunity to apply this method involves winter recreation. Winter activities are becoming more popular and this trend will likelihood increase (Bowker *et al*., 2012). This is having an effect on the disturbance of the snowpack with both motorized and non-motorized recreationists, near and far from road access (Olson *et al.,* 2017). This wide-spread disturbance of the snowpack effects ecological, hydrological, and meteorological

processes (Olson *et al*., 2017, Goeking and Tarboton, 2020). Modeling z_0 throughout these highly trafficked areas can improve understanding of the effects recreation on the snowpack.

The resolution aspect of the study showed variable z_0 values as post processing resolution changed (Table 4.1). Future studies could explore this farther using more meteorological monitoring equipment. By comparing high quality in-situ measurements of the study site to model results, an optimum post processing resolution could be explored. The current study had limited financial resources to determine the resolution necessary to sample the snow surface to achieve the most accurate heat fluxes.

Uncertainty potential should be considered when estimating hydrologic processes (Sexstone *et* al., 2016; Hulstrand and Fassnacht, 2018). For example, sublimation has been found to vary spatially and temporally by 10-35% of snowpack losses (Hulstrand and Fassnacht, 2018). Future studies could examine the uncertainty within this research using the Monte Carlo framework and the estimated z_0 values. This process could be completed for each chapter. In Chapter 2, the addition of meteorological variables could also be assed that were used to compute $z_{0\text{-}A}$. In Chapter 4, further resolution interpolations and resulting z_0 values could be explored. Additionally, these values could be applied to the SNOWPACK model to assess the model outputs.

As climate change develops, there has been an observed decrease in snowpack duration and earlier snowmelt timing (Harpold *et al*., 2012; Lopez-Moreno *et al*., 2017). Therefore, it is more critical than ever to have properly calibrated models with a dynamic z_0 value to quantify the rate of change in these hydrologic processes (Gromke *et al.*, 2011; Debeer and Pomeroy, 2017). Warmer temperatures will enhance sublimation, which is directly affected by z_0 (Chapter 1) (Harpold *et al*., 2012). The increase in temperature is also leading to earlier melt rates, and once the snowpack begins to melt, the sensible and latent heat fluxes will further enhance that rate (Harpold *et al*., 2012). Future studies should explore all aspects of the snowpack energy and mass balance and the contribution of z_0 within these processes.

5.4 References

Bales, R.C., Molotch, N.P., Painter, T.H., Dettinger, R.R., Dozier, J., 2006. Mountain hydrology of the western United States. Water Resources Research, 42(8) [doi: 10.1029/2005WR004387].

Bathurst, J.C., Cooley, K.R., 1996. Use of the SHE hydrological modeling system to investigate basin response to snowmelt at Reynolds Creek, Idaho. Journal of Hydrology, 175(1-4), 181-211 [doi: 10.1016/S0022-1694(96)80011-4].

Blöschl, G., 1999. Scaling issues in snow hydrology. Hydrologic Process, 13, 2149-2175 [doi: 10.1.1.709.499].

Bowker, J.M., Askew, A.E., Cordell, K.H., Betz, C.J., Zarnoch, S.J., Seymour, L., 2012. Outdoor recreation participation in the United States - projections to 2060: a technical document supporting the Forest Service 2010 RPA Assessment. Gen. Tech. Rep. SRS-160. U.S. Department of Agriculture Forest Service, Southern Research Station [doi: https://doi.org/10.2737/SRS-GTR-160].

Bühler, Y., Adams, M.A., Bösch, R., Stoffel, A., 2016. Mapping snow depth in alpine terrain with unmanned aerial system (UASs): potential and limitations. The Cryosphere, 10, 1075-1088 [doi: 10.5194/tc-10-1075-2016].

Clow, D.W., 2010. Changes in the timing of snowmelt and streamflow in Colorado: a response to recent warming. Journal of Climate, 23(9), 2293-2306 [doi: 10.1175/2009JCLI2951.1].

Davison, B.J., 2004. Snow Accumulation in a distributed Hydrological Model. Unpublished M.A.Sc. thesis, Civil Engineering, University of Waterloo, Canada, 108pp + appendices.

Debeer, C. M., Pomeroy, J.W., 2017. Influence of snowpack and melt energy heterogeneity on snow cover depletion and snowmelt runoff simulation in a cold mountain environment. Journal of Hydrology, 553, 199–213 [doi: 10.1016/j.jhydrol.2017.07.051].

Deems, J.S.; Painter, T.; Finnegan, D., 2013. Lidar measurement of snow depth: a review. Journal of Glaciology, 59(215), 467–479 [doi: 10.3189/2013jog12j154].

Dutra, E., Balsamo, G., Viterbo, P., Miranda, P. M. A., Beljaars, A., Schar, C., Elder, K., 2010. An improved snow scheme for the ECMWF land surface model: description and offline validation. Journal of Hydrometeorology, 11(4), 899–916 [doi: 10.1175/2010jhm1249.1].

Fassnacht, S. R., Williams, M. W., Corrao, M. V., 2009a. Changes in the surface roughness of snow from millimetre to metre scales. Ecological Complexity, *6*(3), 221–229 [doi: 10.1016/j.ecocom.2009.05.003].

Fassnacht, S.R., Stednick, J.D., Deems, J.S., Corrao, M.V., 2009b. Metrics for assessing snow surface roughness from digital imagery. Water Resources Research, 45, W00D31 [doi: 10.1029/2008WR006986].

Fassnacht, S. R., 2010. Temporal changes in small scale snowpack surface roughness length for sublimation estimates in hydrological modelling. Cuadernos De Investigación Geográfica, 36(1), 43 [doi: 10.18172/cig.1226].

Fassnacht, S.R., Dressler, K.A., Hultstrand, D.M., Bales, R.C., Patterson, G., 2012. Temporal inconsistencies in coarse-scale snow water equivalent patterns: Colorado River Basin snow telemetry-topography regressions. Pirineos, 167, 167-186 [doi: 10.3989/Pirineos.2012.167008].

Filhol, S., Sturm, M., 2015. Snow bedforms: A review, new data, and a formation model, Journal of Geophysical Research of Earth Surface, 120, 1645–1669 [doi:10.1002/2015JF003529].

Goeking, S.A., Tarboton, D.G., 2020. Forests and water yield: a synthesis of disturbance effects on streamflow and snowpack in western coniferous foersts. Journal of Forestry, 172-192 [doi: 10.2737/SRS-GTR-160].

Gromke, C., Manes, C., Walter, B., Lehning, M., Guala, M., 2011. Aerodynamic roughness length of fresh snow. Boundary-Layer Meteorology, 141(1), 21–34, [doi: 10.1007/s10546-011-9623-3].

Harpold, A., Brooks, P., Rajagopal, S., Heidbuchel, I., Jardine, A., Stielstra, C., 2012. Changes in snowpack accumulation and ablation in the intermountain west. Water Resources Research, 48 [doi: 10.1029/2012WR011949].

Harpold, A.A., Guo, Q., Molotch, N., Brooks, P.D., Bales, R., Fernandez-Diaz, J.C., Musselman, K.N., Swetnam, T.L., Kirchner, P., Meadows, M.W., Flanagan, J., Lucas, R., 2014. LIDAR-derived snowpack data sets from mixed conifer forests across the Western United States. Water Resources Research, 50, 2749-2755 [doi: 10.1002/2013WR013935].

Hock, R., Hutchings, J.K., Lehning, M., 2017. Grand challenges in Cryospheric sciences: toward better predictability of glaciers, snow, and sea ice. Frontiers in Earth Science, 5(64), 1-14 [doi: 10.3389/feart.2017.00064].

Hultstrand, D.M., Fassnacht, S.R., 2018. The sensitivity of snowpack sublimation estimates to instrument and measurement uncertainty perturbed in a Monte Carlo framework. Frontiers of Earth Sciences, 12(4), 728-738 [doi: 10.1007/s11707-018-0721-0].

Huss, M., Bookhagen, B., Huggel, C., Jacobsen, D., Bradley, R.S., Clague, J.J., Vuille, M., Buytaert, W., Cayan, D.R., Greenwood, G., Mark, B.G., Milner, A.M., Weingartner, R., Winder, M., 2017. Toward mountains without permanent snow and ice. Earth's Future, 5(5), 418-435 [doi: 10.1002/2016ef000514].

Kochanski, K., Anderson, R. S., Tucker, G. E., 2018. Statistical classification of self-organized snow surfaces. Geophysical Research Letters, 45, 532–6541 [doi: https://doi.org/10.1029/2018GL077616].

Kukko, a., Anttila, K., Manninen, T., Kaasalainen, S., Kaartinen, H., 2013. Snow surface roughness from mobile laser scanning data. Cold Regions Science and Technology, 96, 23–35 [doi: 10.1016/j.coldregions.2013.09.001].

Lacroix, P., Legrésy, B., Langley, K., Hamran, S. E., Kohler, J., Roques, S., Dechambre, M. 2008. In situ measurements of snow surface roughness using a laser profiler. Journal of Glaciology, 54(187), 753-762 [doi: 10.3189/002214308786570863].

Landry C.C., Buck, K.A., Raleigh, M.S., Clark, M.P., 2014. Mountain system monitoring at Senator Beck Basin, San Juan Mountains, Colorado: A new integrative data source to develop and evaluate models of snow and hydrologic processes. Water Resources Research, 50, 1773–1788 [doi: 10.1002/2013WR013711].

Lettau, H. 1969. Note on aerodynamic roughness-parameter estimation on the basis of roughness-element description. Journal of Applied Meteorology, 8, 828-832 [doi: 10.1175/1520-0450(1969)008<0828:NOARPE>2.0.CO;2]

Liston, G.E., 2004. Representing sub-grid snow cover heterogeneities in regional and global models. Journal of Climate, 17(6), 1381–1397 [doi: 10.1175/1520-0442(2004)0172.0.co;2].

López-Moreno, J.I., Revuelto, J., Fassnacht, S.R., Azorín-Molina, C., Vicente-Serrano, S.M., Morán-Tejeda, E., Sexstone, G.A., 2015. Snowpack variability across various spatio-temporal resolutions. Hydrological Processes, 29(6), 1213-1224 [doi: https://doi.org/10.1002/hyp.10245].

López-Moreno, J.I., J. Revuelto-Benedí, E. Alonso-González, A. Sanmiguel-Vallelado, S.R. Fassnacht, J.E. Deems, and E. Morán-Tejeda, 2017. Using very long-range terrestrial laser scanner to analyze the temporal consistency of the snowpack distribution in a high mountain environment. Journal of Mountain Science, 14(5), 823-842 [doi: https://doi.org/10.1007/s11629-016-4086-0].

Luce, C.H., Tarboton, D.G., Cooley, K.R., 1999. Sub-grid parameterization of snow distribution for an energy and mass balance snow cover model. Hydrological Processes, 13(12-13), 1921–1933 [doi: 10.1002/(sici)1099-085(199909)13:12/133.0.co;2-s].

Luce, C. H., Tarboton, D.G., 2004. The application of depletion curves for parameterization of subgrid variability of snow. Hydrological Processes, 18(8), 1409–1422 [doi: 10.1002/hyp.1420].

Magand, C., Ducharne, A., Le Moine, N., 2014. Introducing hysteresis in snow depletion curves to improve the water budget of a land surface model in alpine catchment. Journal of Hydrometeorology, 15(2), 631–649 [doi: 10.1175/jhm-d-13-091.1].

Manes, C., Guala, M., Löwe, H., Bartlett, S., Egli, L., Lehning, M., 2008. Statistical properties of fresh snow roughness. Water Resources Research, 44(11), 1–9 [doi: 10.1029/2007WR006689].

Miles, E.S., Steiner, J.F., Brun, F., 2017. Highly variable aerodynamic roughness length for a hummocky debris-covered glacier. Journal of Geophysical Research: Atmospheres, 122, 8447-8466 [doi: 10.1002/2017JD026510].

Minder, J.R., Letcher, T.W., Liu, C., 2018. The charter and causes of elevation-dependent warming in high-resolution simulations of Rocky Mountain climate change. Journal of Climate, 31 (6), 2093-2113 [doi: https://doi.org/10.1175/JCLI-D-17-0321.1].

Mitchell, K.A., Tiedje, T., 2010. Growth and fluctuations of suncups on alpine snowpacks. Journal of Geophysical Research, Earth Surface, 115, F4 [doi: 10.1029/2010JF001724].

Niu, G., Yang, Z.L, 2007. An observation-based formulation of snow cover fraction and its evaluation over large North American river basins. Journal of Geophysical Research, 112(D21) [doi: 10.1029/2007jd008674].

Nolan, M., Larsen, C.F., Strum, M., 2015. Mapping snow-depth from manned-aircraft on landscape scales at centimeter resolution using structure-from-motion photogrammetry. The Cryosphere Discussions, 9(1), 333–381 [doi: 10.5194/tcd-9-333-2015].

Olson, E.L., Squires, J.R., Roberts, E.K., Miller, A.D., Ivan, J.S., Hebblewhite, M., 2017. Modeling large-scale winter recreation terrain selection with implications for recreation management and wildlife. Applied Geography, 86, 66-91 [doi: 10.1016/j.apgeog.2017.06.023].

Painter, T.H., Molotch, N.P., Cassidy, M., Flanner, M., Steffen, K., 2007. Contact spectroscopy for determination of stratigraphy of snow optical grain size. Journal of Glaciology, 53(180), 121-127 [doi: 10.3189/172756507781833947].

Pflug, J.M., Lunquist, J.D., 2020. Inferring distributed snow depth by leveraging snow pattern repeatability:investigation using 47 LiDAR observations in the Tuolumne Watershed, Sierra Nevada, California. Water Resources Research, 56 (9) [doi: https://doi.org/10.1029/2020WR027243].

Pomeroy, J.W., Parviainen, J., Hedstrom, N., Gray, D.M., 1998. Coupled modelling of forest snow interception and sublimation. Hydrological Processes, 12, 2317-2337 [doi: https://doi.org/10.1002/(SICI)1099-1085(199812)12:15<2317::AID-HYP799>3.0.CO;2-X].

Quincey, D., Smith, M., Rounce, D., Ross, A., King, O., Watson, C., 2017. Evaluating morphological estimates of the aerodynamic roughness of debris covered glacier ice. Earth Surface Processes and Landforms, 42, 2541-2553 [doi: 10.1002/esp.4198].

Revuelto, J., Lopez-Mureno, J.I., Azorin-Molina, C., Zabalza, J., Arguedas, G., Vicente-Serrano, S.M., 2014. Mapping the annual evolution of snow depth in a small catchment in the Pyrenees using the long-range terrestrial laser scanning. Journal of Maps, 10(3), 379-393 [doi: 10.1080/17445647.2013.869268].

Sanow, J.E., Fassnacht, S.R., Kamin, D.J., Sexstone, G.A., Bauerle, W.L., Oprea, I., 2018. Geometric versus anemometric surface roughness for a shallow accumulating snowpack. Geosciences, 8(12), 463 [doi: 10.3390/geosciences8120463].

Sexstone, G.A., Fassnacht, S.R., 2014. What drives basin scale spatial variability of snowpack properties in the Front Range of Northern Colorado? The Cryosphere, 8, 329-344 [doi: 10.5194/tc-8-329-2014].

Sexstone, G.A., Clow, D.W., Stannard, D.I., Fassnacht, S.R., 2016. Comparison of methods for quantifying surface sublimation over seasonally snow-covered terrain. Hydrologic Processes, 30, 3373-3389 [doi: 10.1002/hyp.10864].

Sexstone, G.A., Clow, D.W., Fassnacht, S.R., Liston, G.E., Hiemstra, C.A., Knowles, J.F., Penn, C.A., 2018. Snow sublimation in mountain environment and its sensitivity to forest disturbance and climate warming. Water Resource Research, 54(2) 1191-1211 [doi: 10.1002/2017WR021172].

Smeets, C.J.P.P., van den Broeke, M.R., 2008. Temporal and spatial variations of the aerodynamic roughness length in the ablation zone of the Greenland ice sheet. Boundary Layer Meteorology, 128, 315-338 [doi: 10.1007/s10546-008-9291-0].

Smith, M.W., 2014. Roughness in the earth sciences. Earth Science Reviews, 136, 202-225 [doi: 10.1016/j.earscirev.2014.05.016].

Shaw, T.E., Gascoin, S., Mendoza, P.A., Pellicciotti, F., McPhee, J., 2019. Snow depth patterns in a high mountain Andean catchment from satellite optical tristereoscopic remote sensing. Water Resources Research, 56(2) [doi: 10.1029/2019WR024880].

Sturm, M., Liston, G.E., 2021. Revisiting the global seasonal snow classification: an updated dataset for Earth system applications. Journal of Hydrometeorology, 22, 2917-2938 [doi: 10.1175/JHM-D-21-0070.1].

Swenson, S.C., Lawrence, D.M., 2012. A new fractional snow-covered area parameterization for the Community Land Model and its effect on the surface energy balance. Journal of Geophysical Research, 117(D21) [doi: 10.1029/2012JD018178].

Wayand, N.E., Marsh, C.B., Shea, J.M., Pomeroy, J.W., 2018. Globally scalable alpine snow metrics. Remote Sensing of Environment, 213, 61-72 [doi: 10.1016/j.rse.2018.05.012].

Tables

Table 5.1 New datasets collected for this research

Name	Data Type	Year	Description
ARDEC Met	Met Data	2017-2019	All meteorological data collected at the ARDEC study site
Trout Farm Met	Met Data	2019-2020	All meteorological data collected at the Trout Farm study site
19-20 Met	Met Data	2019-2020	All meteorological data collected at snow sites in Northwest Colorado (Trout Farm, Julie Circle, CR11, Lost Creek, Yellow Jacket, Upper Piceance Creek, Piceance, Cathedral Creek, and Spring Creek)
ARDEC LiDAR	LiDAR	2017-2019	All LiDAR scans taken at the ARDEC study site
19-20 LiDAR	LiDAR	2019-2020	All LiDAR scans taken at NW Colorado study sites

Figures

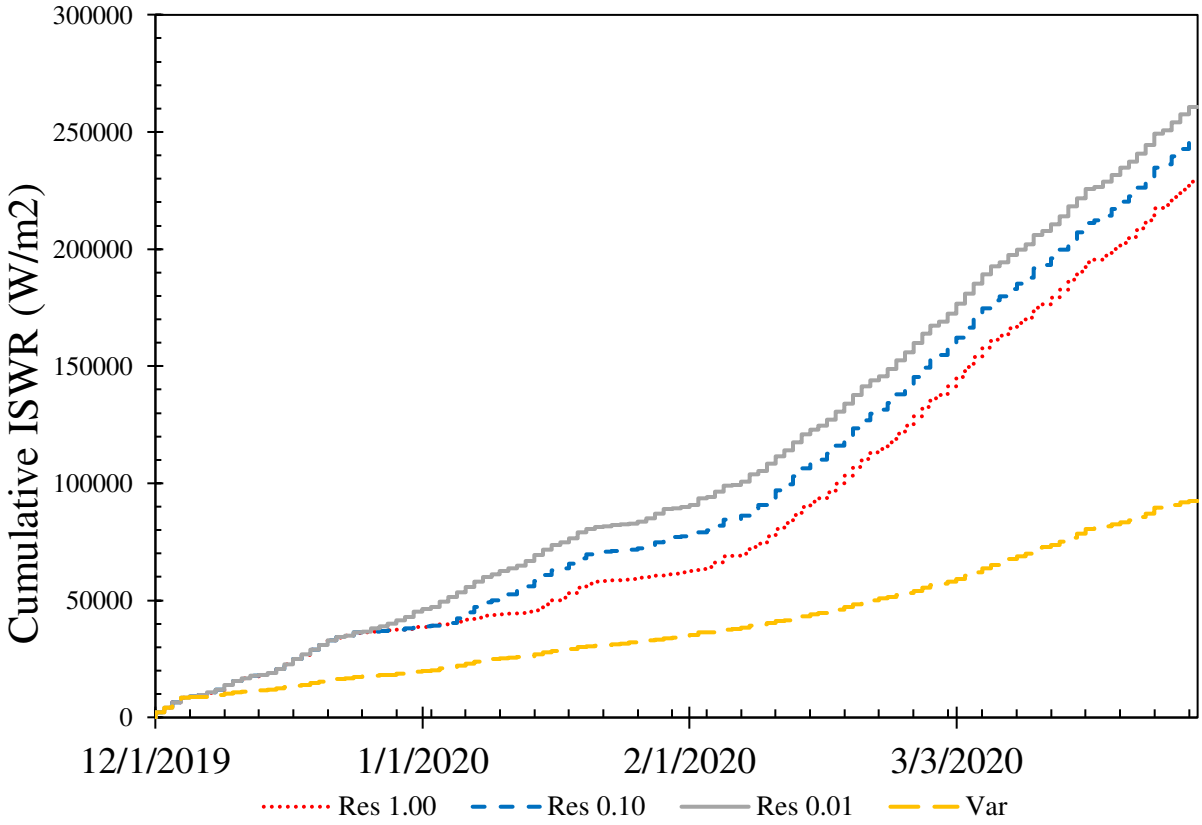

Figure 5.1. Results from the SNOWPACK model with varying z_0 values applied to calculate albedo throughout the 2019-2020 winter season at Trout Farm.

6.0 REFLECTION

As I began as a PhD student, I assumed the process would be rigid and outlined, and I was immediately proven incorrect. Throughout school, I played by the rules, thinking from class to class, from point A to point B. Upon reaching grad school, I realized that this is a deceptively simplified view of the path to becoming a scientist and that assuming anything within a research project is a linear process is laughably naïve. I am proud of the finished product that I have produced, but even more proud of the skills and abilities I learned along the way.

First, when using scientific instruments, their ability to function throughout a cold winter is not always constant. Checking their readings, not just initially, but every single field visit is imperative. This is the basis for the 'great anemometer debacle' on which I look back with overwhelming frustration. I didn't download the data every time I went to the meteorological tower for a LiDAR scan (usually because of the bitter cold and snow falling and potentially ruining my laptop), but worse, I only checked the data at the end of the year. One of the biggest lessons in fieldwork is to look over the data immediately, is it working? Are you collecting it correctly? Where is there room for improvement? Even if the end results and methodology in which the data is used is changed over the course of the project, at least you know what you have is accurate data.

One thing that I did start doing early on was keeping detailed notes of my LiDAR processing methodology. This was very useful when I would stop processing for a month or more. When I came back to it, I was able to avoid making mistakes, leaving out steps, etc. This process was also helpful in passing along guidance to newer graduate student who were also working with similar data. After the first year of data collection, I learned to also keep detailed notes of site visits. This included photos, weather, time, LiDAR scan numbers, etc. which I then kept very organized with folders and backups. Organization of data and processes proved to be one of the most valuable tools for future research and field work.

Beginning my PhD, I read a lot of background paper for my literature review. I referred back to this literature review and all notes I took from my readings any time I was writing a piece of the dissertation. I also kept hard copies that were highlighted with notes in the margin to refer back to, eventually I ended up digitizing these highlighted passages and notes which was helpful to search through when trying to find certain citations throughout my writing. Looking back, I should have kept this process going; but with most papers I read in the latter years, I just kept digital copies to search through instead of adding them to my notes. If I were to do it again, I would add the literature notes every 6 months or so, as my topics became more robust.

Time management was crucial throughout my time working towards this degree. From my second semester until graduation 4.5 years later, I held a full-time government job. I started off with the USGS in Fort Collins as an Operations Research Analyst. My field research at this time took place at the ARDEC field outside of Fort Collins, and I'd have to rush out to the field during any period when snow might occur. I had to use annual leave or work extra hours to make up for my erratic vacancies. During the winter of 2018-2019, I added sites at Cameron Pass and Rabbit Ears Pass, which were 3 hours away from Fort Collins, one way. This filled my weekends with long car rides and cheap gas station burritos for the entire winter, and kept me up late into the night reading papers and catching up on schoolwork that I didn't have time for during the week. My second federal job was working with the Bureau of Land Management's White River Field Office in Meeker, CO as their only hydrologist. Meeker is 5 hours from Fort Collins, so I had to pick up and move away from the original study sites and come up with an entire new plan. Here, I was able to 'double-dip' work and school. The study sites I set up around the field office for snow monitoring were of great value to everyone in the office. In this position, a lot of NEPA analysis was done and having snow depths and on/off dates was very valuable when writing grazing permits, oil and gas leases, and water right analyses. It was very helpful to conduct these site visits during working hours and I will be forever grateful to the White River Field Office for their support. This also freed up my night and weekends to spend more time analyzing LiDAR scans taken over the past few

years. My final job during my PhD program, was as a hydrologist for the National Weather Service – Alaska Pacific River Forecast Center, in Anchorage, Alaska. So once again, I had to abandon my study sites and move far north. At this point, my data collection was mostly done, so I was once again back to writing, data-processing, and analyzing on nights and weekends. Throughout this process, some days, weeks, and months were more difficult than others; however, I ultimately found a lot of joy in it all. It gave me the freedom to advance my federal career and experience and finish a degree I had been longing to get. My ability to manage my time, expectations, and responsibilities for myself and others developed to a new level of which I am very proud.

This research started off as a 'thing to check off my to do list' but by the end it became so much more. I find myself incredibly engaged with the snowpack when snowboarding, cross-country skiing, or just driving around town. I have almost as many photos of surface hoar and sublimation on my phone as I do of my cats! Surface roughness has become a surprisingly interesting topic to discuss at work, with friends, and even during my weekly curling game with teammates. I feel the research I conducted will truly enhance the way we use hydrologic models going forward. At my current position with the National Weather Service, I have already begun to implement more dynamic variables in our forecast models. Our current hydrologic models use static z_0 and ET values, which I intend to modify.

I'd be remiss if I didn't mention one of the most important people throughout this whole process, my husband Luke. He acted as a field technician, an editor, a sounding board, a mover, and a psychologist. His dedication even resulted in the loss of an entire thumbnail to a mild field work accident. I never could have done any of this without him making dinner on late nights, walking our dog when I couldn't get away, feeding the cats when I was at the office late, or one of the other innumerable responsibilities that pop up in everyday life. I wish I could give him an 'Assistant PhD, because he earned it. I should also mention that we got married just 1 month into this process, so I imagine he is looking forward to my graduation even more than I am!

Throughout the jobs, research, moving around, etc., I have discovered something very unexpected: joy for the unknown. Most people hear the history of my past 5 years and think I am insane, but what they don't understand is the thrill of a deadline, the pressure to get things done, and the happiness when the new destination has been reached. My resume is wildly un-traditional, but I think that's what makes who I am a fierce candidate for any job. This entire process was critical in shaping the researcher, scientist, and person that I feel I was supposed to become. At the beginning, I thought I was trying to prove to everyone else I could do this, but by the end, I realized the only one really needing convincing was me. As Taylor Swift so eloquently said, 'haters gonna hate, hate, hate.' Just make sure the hater isn't yourself!